Synthesis and bioassay of rationally designed DXR inhibitors as potential anti-malarial lead compounds

A thesis

submitted in fulfilment of the requirements for the degree of

Master of Science

Of

Rhodes University

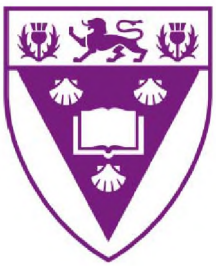

By

Iviwe Cwaita Nokalipa

B.Sc.Hons (Rhodes University)

This is dedicated to my late parents; Z Nokalipa and N.H Jombile

Never be afraid to reach for the stars, because even if you fall, you'll always be wearing a Parent-chute™ – Phil Dunphy [Phil's-osophy]

Abstract

Globally, the eradication of malaria has been challenging due to the problem of resistance that past and currently available drugs exhibit. This is exacerbated by the inherent need for anti-malarial drugs to be affordable to the poverty-stricken majority that is primarily affected by this burden.

This research has focused on the development of potential inhibitors of 1-deoxy-D-xylulose-5-phosphate reductoisomerase (DXR), an essential enzyme in the mevalonate-independent pathway for the biosynthesis of isoprenoids in *Plasmodium falciparum*. DXR mediates the isomerisation and reduction of 1-deoxy-D-xylulose-5-phosphate into 2-*C*-methyl-D-erithrytol 4-phosphate.

This enzyme has been determined to be a target for the development of novel anti-malarial agents and extensive molecular modelling has been undertaken to develop inhibitors that fit into the DXR active site. The *in silico* docking data have been used to inform the design and synthesis of various *N*-benzyl-substituted phosphoramidate ligands that were determined to have potential as novel substrate mimics of fosmidomycin, a known DXR inhibitor.

Synthesis of the *N*-benzyl-substituted phosphoramidate ligands involved a nine-step sequence commencing from diethyl phosphoramidate. In all, some 40 compounds have been prepared, some of them new, and were fully characterized using NMR. Attention has also been given to the mass spectrometric fragmentation patterns exhibited by selected intermediates. Four of the final products were evaluated for *in vitro* antimalarial activity using a PLDH assay and exhibited IC50 values < 100 μM.

Acknowledgements

Firstly I would like to thank my supervisors Prof P.T Kaye and Dr Lobb for their never ceasing support throughout this project including the times where I was highly frustrated by the work, their support and motivation allowed me to keep going. Prof Kaye has the ability to show patience, wisdom even when things look gloomy and for that I am thankful. Without Dr Lobb allowing me to experience NMR and molecular modelling, allowing me to express my own interpretation of the data taught me a real appreciation for docking studies as a whole.

The Chemistry department at Rhodes University is a community full of such helpful individuals; academic staff, technical staff as well as students who are always willing to assist anywhere they can; hopefully I remember everyone, a special thank you to Michelle Isaacs the bioassay technician who conducted the *Pf*DXR inhibition assays, Colin Mkhize for the statistics data analysis, Dr R Klein, Dr C Veale, Dr X Nondou, Dr Faridoon, Christina and many others in labs S3, S4 and F22. To Alicia Singh, my friend and lab mate, we spend so many days together discussing everything from chemistry to travelling the world, thank you and you inspire me.

I owe so much to my family that took me under their wings; my grandmother who raised me and taught me everything I know about God and life, Nonokazi Nokalipa who has showed me a mother's love from the beginning, Nozuko Jombile whose relationship goes beyond that of a step-mother, I truly appreciate your love and support. To my brothers Thabo, Loyiso and Zakhe Jombile who I pray for to be inspired and live their best lives. To my 2 sisters Anamhla and Khanya; making us the "3 sisters" you make me want to be the best version of myself I can be because of how special you always hold me in your hearts and prayers.

Last but certainly not least, to my best friend, Yogendran Arunachellan who has literally been my rock whenever I'm exhausted and frustrated, you've shown me kindness and

prayed for me constantly. I appreciate the constant support, motivation, truly unconditional love and your family, could have not done this without you.

Finally I am extremely grateful to Rhodes University, NRF and MRC for the financial support over the years that allowed me to undertake these studies.

Philippians 4: 13. *I can do all things through Christ who strengthens me.*

Abbreviations

ACT: Artemisinin combination therapy

ATP: Adenosine triphosphate

CDP-ME: 4-Diphosphocytidyl-2-C-methyl-D-erythritol

CDP-ME2P: 4-(Diphosphocitidyl)-2-C-methyl-D-erythritol-2-phosphate

CTP: Cytidine triphosphate

DDT: Dichlorodiphenyltrichloroethane

dhfr: Dihyrofolate reductase

dhps: Dihydropteroate synthase

DMAP: Dimethylaminopyridine

DMAPP: Dimethylallyl pyrophosphate

DNA: Deoxyribonucleic acid

DOXP/DXP: 1-Deoxy-D-xylulose-5-phosphate

DXS: 1-Deoxy-D-xylulose-5-phosphate synthase

GDP: Gross domestic product

HIV: Human immune virus

AIDS: Acquired immune deficiency syndrome

Hsp: Heat shock protein

HTS: High throughput screening

IC_{50}: Half maximal inhibitory concentration

IPP: Isopentenyl pyrophosphate

iRBC: Infected red blood cell

mdr: Multi-drug resistance gene

MECP: 2C-methyl-D-erythritol-2,4-cyclodiphosphate

MEP: Methylerythritol phosphate; 2-C-methyl-D-erythritol 4-phosphate enzyme

NADPH: Nicotinamide adenine dinucleotide phosphate

NMR: Nuclear magnetic resonance

P. falciparum: *Plasmodium falciparum*

P. knowlesi: *Plasmodium knowlesi*

P. malariae: *Plasmodium malariae*

P. ovale: *Plasmodium ovale*

P. vivax: *Plasmodium vivax*

*pf*CRT: *Plasmodium falciparum* chloroquine resistance transporter

PLDH: Malaria parasite lactate dehydrogenase

RBC: Red blood cell

RBM: Roll back malaria

RNA: Ribonucleic acid (as well as mRNA, rRNA, tRNA; messenger RNA, ribosomal RNA and transfer RNA)

TB: Tuberculosis

TBAB: Tetrabutylammonium bromide

WHA: World health assembly

WHO: World health organisation

List of Figures

Figure 10. The non-mevalonate pathway in the production of IPP; fosmidomycin blocks the conversion of substrate DXP to product MEP, a vital reaction in this biosynthesis.[171]

Figure 11. The docked structure of enzyme in *Ec*DXR (2EGH) with co-factor NADPH (green), known inhibitor fosmidomycin (dark-green) and Mg^{2+} ion (blue). The water molecules excluded for clarity. The dashed lines represent hydrogen bond lengths in Å and the neighbouring amino acid residues represented by name and ID number.[163]

Figure 12. The structure of DXR inhibitor fosmidomycin; essential structural features for anti-malaria activity, the phosphonate group (orange), the methylene spacer (green) and the hydroxamate moiety (blue). Fosmidomycin drawing constructed using Symax draw 3.2 tools, atom type colour. [175]

Figure 13. Synthesis of phosphonate esters and phosphonic acids.

Figure 14. Synthetic routes explored in the synthesis of the dihydroxy-amido phosphonate esters and their corresponding acid derivatives.

Figure 15. Reported and proposed *N*-benzylated fosmidomycin analogues

Figure 16. The synthetic pathway of the *N*-benzyl derivatives.

Figure 17. Furan derivatives with varying R groups, showing the expected regioisomer (**a**), in each case.

Figure 18. The various substituents in the docked ligands where n= 2, 3 or 4, R^1= **a** (CH_3), **b** (CH_2CH_3) or **c** (CH_2OH) and R^2= CH_2Br, SH, OH, NH_2 etc.

Figure 19. Structure of ligand **2a_Br** benzyl substitution CH_2-Br at R group which contains variation of the 2 methylene spacer and terminal methyl with water molecules, Crystal structure of ligand 2a_Br shown in ball and stick with atom type colour.[178]

Figure 20. The structure of *P. falciparum* DXR protein subunit A with NADPH co-ordinated in active site, natural ligand DXP removed from active site, protein colour by secondary type with ligand NADPH in ball and stick with atom type colour.[163]

Figure 21. Protein **1Q0L** subunit A with the distribution of 63 ligands; majority of the ligands falling outside the binding cavity/site of the enzyme. The protein colour by secondary type with ligands and NADPH in ball and stick with atom type colour.

Figure 22. The ligand **2a_H** interacts in the *Ec*DXR active site **(1Q0L)** with the conserved amino acids that are observed with fosmidomycin with additional interactions with the auxiliary groups that the analogues contain and 2 water molecules. The crystal structure of fosmidomycin and 1a_H are in ball and stick with atom type colour. The hydrogen atoms are not shown and dashed lines represent H-bond distance in Å.[178]

Figure 23. Docked conformation of ligand **2b_SH** in the in the *Ec*DXR active site **(1Q0L)**. With expected interactions with adjacent amino acids. The crystal structure of fosmidomycin structure in ball and stick with atom type colour.[178]

Figure 24. Docked conformation of ligand **4c_SH** in the in the *Ec*DXR active site **(1Q0L)**. With expected interactions with adjacent amino acids. The crystal structure of fosmidomycin structure in ball and stick with atom type colour.[178]

Figure 25. Protein **1Q0Q** subunit A showing the distribution of 63 ligands; majority of the ligands falling outside the binding cavity/site of the enzyme. The protein colour by secondary type with ligands and NADPH in ball and stick with atom type colour.[178]

Figure 26. The ligand **2c_OH** interacts in the *Ec*DXR active site **(1Q0Q)**. The crystal structure of **1c_OH** and DOXP are in ball and stick with atom type colour. The hydrogen atoms are not shown and dashed lines represent H-bond distance in Å.[178]

Figure 27. Proteins **3AU9** and **3AUA** subunit A showing the distribution of 63 ligands; majority of the ligands falling outside the binding cavity/site of the enzyme for **3AU9** and **3AUA** while all are excluded in binding site for **3AU8**. The protein colour by CPK with ligands and NADPH in ball and stick with atom type colour.[178]

Figure 28. The protein **3AU9** The DXR crystal structure with ligands in active site; **2a_NH** and fosmidomycin (yellow) are in ball and stick with atom type colour. The hydrogen atoms are not shown and dashed lines represent all interactions in distance in Å.[178]

Figure 29. The protein **3AUA** The DXR crystal structure with ligands in active site; **2a_NH** and FR9000089 (yellow) are in ball and stick with atom type colour. The hydrogen atoms are not shown and dashed lines represent all interactions in distance in Å.[178]

Figure 30. The average Ki values (μM) across the *Ec*DXR and *Pf*DXR protein

Figure 31. The average Ki values (μM) across the *Ec*DXR and *Pf*DXR protein for increasing methylene spacer

Figure 32. 600MHz ^{1}H NMR spectrum of compound **26** in $CDCl_3$.

Figure 33. 600MHz ^{1}H NMR spectrum of compound **28** in $CDCl_3$.

Figure 34. 600MHz ^{1}H NMR spectrum of compound **40** in DMSO-d_6.

Figure 35. 600MHz ^{1}H NMR spectrum of compound **41** in $CDCl_3$.

Figure 36. 400MHz ^{13}C NMR spectrum of compound **29d** in $CDCl_3$.

Figure 37. 600MHz ^{1}H NMR spectrum of compound **29a** in $CDCl_3$.

Figure 38. 600MHz ^{1}H NMR of compound **30e** in $CDCl_3$.

Figure 39. HRMS of compound **30f**

Figure 40. HRMS of compound **31e**

Figure 41. 400MHz NMR of compound **32e** in $CDCl_3$.

Figure 42. ^{1}H NMR of compound **34d** in D_2O.

Figure 43. 600MHz DEPT135 NMR spectrum of compound **34a** in D_20.

List of Tables

Table of Contents

1. Introduction

1.1. History of malaria

The *Homo sapiens* species has been infected with hundreds of parasites some of which have been responsible for serious diseases and illnesses throughout its evolution. The origins of these diseases were often misunderstood or unknown as knowledge of microorganisms was limited. However, the symptoms described in many ancient texts can be linked to diseases we know today. Malaria is among one of the oldest human diseases in recorded history and it continues to be the cause of death for millions of people all over the world.[1] The existence of this parasitic disease can be traced far back in history in various parts of the world, where documented evidence confirms the presence of malaria throughout the millennia.

Written records about malaria can be dated for thousands of years to the period of Egyptian medicine (3000 – 400) BC as well as in some sub-continent writings.[1,2] There are literature references to malaria from many countries; in India, ancient scriptures as well as songs contain references to fever–like symptoms that are considered to have been about malaria,[3] while in China, malaria had been discovered and described in the *Nei Ching* as fevers.[3] Even though knowledge about malaria was limited, it is evident that this disease has been a medical concern for many years. Numerous occurrences of epidemic fever–related deaths have been attributed to malaria; these include the hypothesis that Alexander the Great died from malaria on his way to India.[3]

Competition for research attention and funding for diseases such as acute lower respiratory infection, TB (tuberculosis), HIV/AIDS (human immune virus/ acquired immune deficiency)[4] has grown, but malaria continues to be prevalent and remains a challenging illness in many parts of the world. Recently, the WHO (world health organisation) has classified HIV/AIDS, TB and malaria as priority diseases in the world,[5] posing the highest risk to human health. Resistance has emerged to currently available medicines for all these diseases and no vaccine has yet been developed for any of them.[5] There are promising malaria vaccines such

the RTS.S candidate but these have yet to completely eliminate the parasite.[6] Major research efforts are clearly essential if we are to eradicate these epidemic illnesses.

In the early stages of research there was minimal knowledge about malaria and it required years of investigation to finally establish the cause of the infection and link the symptoms displayed by the host with the vector of the parasite. Malaria was explained in ancient times as an evil spirit and by the well–known miasma theory,[7] which led to the Italian name of *Malaria* meaning "bad air". The theory was conceptualised when malaria reached epidemic proportions in Greece by the Greek physician, Hippocrates.[8] It was believed that the illness arose from contaminated air. After the discovery of bacteria by Antonie van Leeuwenhoek in 1676,[9] as well as the experimental evidence demonstrated by Louis Pasteur that diseases are not spontaneously generated but are caused by certain microorganisms and bacteria,[9] research in microorganisms accelerated. Human parasites such as trematodes, nematodes and pathogenic protozoa are responsible for many diseases[10] and it is essential that we understand their entire function and life cycles. Increased knowledge of parasites, in general, has promoted further research on the malaria parasite, in particular. Initial research was based mainly on observations with no scientific understanding, notions such as the initial connection of the illness to mosquitoes by Patrick Manson[9] which opened the opportunity to the provision of scientific evidence.

The discovery of the *Plasmodium* parasite in the red blood cells of infected patients by a French physician Charles Laveran in 1880[1] sparked initial interest in the malaria parasite by researchers. Laveran was working as a surgeon in Algeria in 1878[11] when he noticed a black pigment on dead soldiers in the mortuary. He then started examining the bodies of soldiers who were suffering from this unknown disease.[11] In 1897, Ronald Ross then discovered the parasite vector to be a certain species of mosquito, a fact which he demonstrated by deliberately infecting birds with malaria and then isolating the parasite from the salivary glands of the mosquitoes which had fed on the infected birds.[12,13] This information narrowed the species of interest which was essential for a more specific or targeted approach. Various researchers assisted in understanding the malaria parasite after Laveran;

these include Camillo Golgi, a neurophysiologist who identified the merozoite stage of the parasite, William MacCallum who, while working as a medical student at John Hopkins, discovered the reproductive stages of the malaria parasite.[11]

Once some knowledge on the biological and cellular level of the parasite become available, scientists looked towards analysing the parasite`s lifecycle in its entirety. In order to move toward a drug treatment plan, extensive research was conducted on the parasite as well as those affected by it. Malaria is an intracellular protozoan parasite from the genus *Plasmodium*[14] that is carried by the female *Anopheles gambiae* mosquito as the vector; the mosquito then infects the human host.[15,16] There are over 400 species of the *Anopheles* mosquitos and only approximately 30–40 of these can transmit malaria.[15-17] Four of these species are commonly involved in the infection of human hosts, namely *Plasmodium vivax*, *P. ovale*, *P. malariae* and *P. falciparum*,[16] with *P. falciparum* being the most deadly. In 2008, the WHO identified a fifth species of malaria parasite; *Plasmodium knowlesi*, which originally infected primates and which also caused malaria in humans.[18] The origin of *P. falciparum* in humans can be traced back to cross-species transmission through *Anopheles* mosquitos which were able to infect apes and then transfer this strain of malaria to humans.[19]

The different malaria parasite species pose health threats to humans in various and unique ways. These differences include the incubation period that the parasite has in both the vector and the host, the haemazoin structures that each species forms during haemoglobin intake[20] (sometimes used as a mechanism to diagnose the species of infection), and the genetic make-up of each species,[21] which opens other channels for gene therapy where drugs can be developed specifically for each *Plasmodium* species. *P. vivax* is the most common species of malaria parasite and can be found in far more parts of the world[22] than the other species. However, this species is believed to be more benign than other *Plasmodium* parasites and is often neglected in most research laboratories even though it is responsible for up to 80 million infections almost every year in Africa.[23] The shape and size of the *P. vivax* haemozoin crystals were found to differ slightly from those of *P. falciparum*,

with the *P. vivax* appearing to be cubic.[20] In a study conducted in 29 villages in Papua New Guinea evaluating the relationship between parasitic density and age dependent clinical tolerance, it was found that *P. vivax* was the second most deadly *Plasmodium* species and more prevalent in younger patients.[24] The parasite target erythrocytes that each species prefers also differ significantly. *P. vivax* parasites prefer to invade immature RBCs while *P. falciparum* invades mostly mature RBCs (red blood cells).[23] Both *P. vivax* and *P. ovale* species have the ability to remain inactive or dormant in the liver stage while *P. malariae* and *P. falciparum* do not;[25] this allows the former species to re-appear and cause infection relapses months after treatment of the first infection.

The majority of research efforts are focused on the *P. falciparum* species but it is important to note that, in most of Sub-Saharan African countries, 1% to 7% of malaria cases can be attributed to *P. ovale* and *P. malariae*.[26] The *P. falciparum* haemazoin is similar, in some respect, to all the human-infecting species but significantly different to the bird-infecting *Plasmodium* species.[20] Haemazoin structures of human-infecting species are still different enough to be distinguishable for diagnoses. In many high risk areas in the world, co-infection across *Plasmodium* species is common,[27] and the treatment of one species significantly affects another.

According to the WHO, 99 countries in the world were confronted with ongoing malarial infections in 2011.[28] The malaria burden covers some parts of South America and Asia, but the majority of malaria deaths are occurring in sub-Saharan Africa.[29] Efforts to reduce these mortality rates have been put in place by the WHO with 55 countries approaching WHA and RBM targets, which aim to reduce malaria cases by 75 % by the year 2015.[28] These initiatives have been established to monitor progress in the fight against malaria.

Malarial infections are more common amongst young children and pregnant women.[30] It is therefore important that new drugs are highly pure and safe. The parasite is more prevalent in poverty-stricken areas of the world;[31] this can be seen by the correlation of high malaria rates with developing as well as third-world countries,[28] with countries with low GDP (gross domestic product) growth being at particularly high risk whereas high GDP growth rates

generally experience low malaria risk.[32] It is therefore very important that new drugs are prepared from affordable starting materials in order to allow for affordable drug treatment. Even with such gloomy statistics there is hope, as there has been a 25 % global decrease over the three years since 2010[33] in the number of people who have died due to malarial infections. This indicates a move in the right direction that will, hopefully, lead to the eventual eradication of the disease. Current research is focused on the development of novel drugs with novel modes of action to overcome limitations of current drugs.

The major challenge facing malaria research is the re-occurring issue of anti-malarial resistance.[28] Anti-malarial drugs which were once effective in malaria treatment have been affected by the drug resistance phenomenon which is predominantly exhibited by the *P. falciparum* species.[34,35] Consequently, there is an urgent need for novel drugs that can combat resistance and effectively treat human malaria.

1.1.1. Life-cycle of the malaria parasite

The first step in understanding the *Plasmodium* parasite is to analyse its life-cycle; this allows for an understanding of its functioning and mechanisms of survival. The *Plasmodium* parasite passes through different stages as well as various morphologies and cellular environments.[36] In some ways this is advantageous as it provides numerous potential targets for anti-malarial drug discovery with opportunities for novel modes of anti-malarial action. The parasite passes through six forms during its life-cycle in the malaria vector, namely female or male gametocytes and the corresponding gametes, zygote, ookinete, oocyst and sporozoite.[4] In the human host, the parasite has two stages following infection, the liver stage and the erythrocyte or blood stage.[37] In the mosquito, the parasite undergoes its reproduction stage involving the formation of new parasites capable of infecting a new host during the process of feeding. The stages of the parasite life-cycle can be represented from vector to host or from host to vector. The life-cycle of all *Plasmodium* species is similar with slight differences at each stage of maturation.

Generally, the cycle can be explained beginning from the initial bite of human host, where the parasite is delivered via a blood meal, the sporozites travels to the liver where it matures in the hepatocytes to merozoites which invade RBC and replicate asexually, invading further RBC. The merozoites may develop into gametocytes which are taken up by the a mosquito, from ingestion via a blood meal. These further develop to gametes, which sexually reproduce to produce zygotes, from which there is eventual production of the sporozoites that are transmitted to human host during the next blood meal.

The first stage in the cycle (Figure 1) begins when the female *Anopheles* mosquito penetrates the tissue of the human host and deposits sporozoites[37] through saliva during a blood meal. Sporozoites are slender haploids which enter the blood stream through the mosquito's salivary glands. From the host's bloodstream the sporozoites are transported to the liver.[38] Fewer parasites leave the bite site and enter the human host liver than those present during initial infection.[39] This is an excellent point for targeted termination as the parasite numbers are reduced and might be easier to kill. However, this stage is completed within 48 hours and diagnosis has to be timely.[40] The process by which the parasites leave the bite site and are transported to the liver is not fully understood. There are not many drugs that target this stage of the parasite life-cycle, mainly due to the short time in which infection develops.

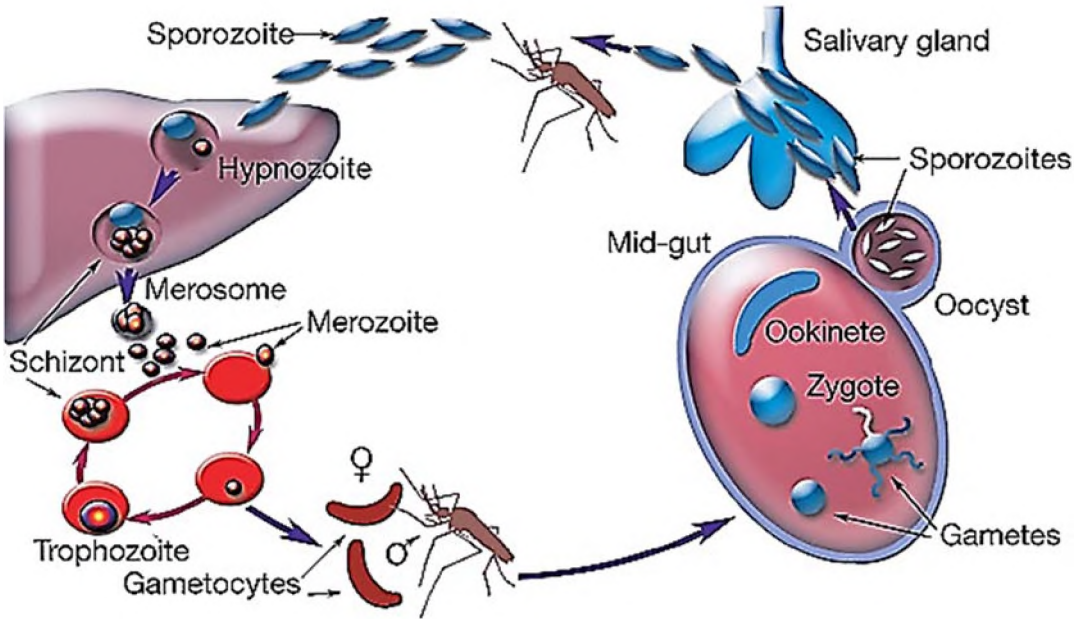

Figure 1. The life-cycle of the *Plasmodium* parasite in the human host.[58]

The parasites then commence a maturation stage in the liver where they go through various stages from the hypnozoite form (Figure 1); this is also known as the hepatic phase[38] in which they either remain dormant or continue maturing over several days.[41] This distribution is significant in some species, such as *P. vivax*, which prefer to remain in the dormant stage for longer periods. The liver stage of the malaria parasite was only discovered in 1948;[42] until then early drug discovery had been mainly targeted at the blood stage of the life-cycle. The newly-evaded hepatocytes then become schizonts as in Figure 1, which when mature continue on to the blood infection stage.[43] The schizonts invade RBCs, preferably mature red blood cells[40] although different species of *Plasmodium* schizonts have different RBC preferences. Since the schizonts are maturing in the liver, diagnosis is impossible as they exhibit masked immunity.[40] This stage of maturation shows no symptoms of illness. Maturation occurs over a few days before the mature schizonts burst out of the liver.[44] When the schizonts mature they become merozoites; this is also known as a pre-erythrocytic or exo-erythrocytic phase.[41] The mature schizonts are then released in large numbers into the blood and begin to interact with the host's red blood cells.[43] Liver-stage drugs would be ideal as these would terminate the parasites prior to their maturation or invasion.

The final stage of maturation known as the intra-erythrocytic or ring stage[45] occurs when the liver bursts and releases merozoites, which at this stage, undergo asexual reproduction and multiply.[46] The production of infected RBCs also known as iRBCs[47] from the initial merozoites is complex and numerous techniques, such as live cell imaging and electron microscopy, have been used to investigate what occurs at this stage of the infection.[41] Once this asexual stage ends (typically 48 hours after infection), the first matured merozoites are produced and released into the bloodstream[40] and go on to infect more RBCs and thus results in the accumulation of iRBC (infected red blood cells) in the host cells. This continuous invasion weakens the host's immune system. The merozoites cannot be detected inside the RBC and are masked to the immune system, allowing them to undergo numerous cycles of asexual cell division which rupture the RBCs,[41] releasing more merozoites into the bloodstream that invade more host cells. The RBC rupturing leads to small waste particles being left in the blood which result in the host displaying symptoms such as fever, chills, headaches, diarrhoea, nausea and body aches.[48] These are the clinical symptoms of malaria.

The malaria parasites use combinations of movement and membrane fusion to attach to and invade the RBCs[41]. These include use of the actin-myosin motor to bind to the surface of the target protein and passive diffusion to enter the host cell. [49] The cleaved merozoites utilise an anchor made from actin-myosin filaments in the membrane to move sporozoites and invade the RBCs.[50] The RBC membrane comprises a lipid bilayer covering a protein network,[45] and the parasite needs appropriate strategies for traversing the cell wall. Binding to the motor is highly selective and only occurs in the *Apicomplexa*[41] where an opportunity for targeted termination arises. All the stages of maturation of the parasite are completely dependent on and facilitated by the host cell.[51] This is why there have been extensive studies on the blood stage of the parasite.

About 1% of the merozoites produced then undergo differentiation and become gametocytes, a process that takes 9–12 days.[51] The newly formed gametocytes develop into microgametocytes and macrogametocytes, which form female and male gametes,

respectively, and which are ingested by a mosquito during a blood meal.[38] This is yet another potential point for targeted termination of the parasite as relatively fewer merozoites undergo maturation into gametocytes. The remaining 99 % of the merozoites produced continue to invade and infect more RBCs, thus multiplying parasites and exacerbating symptoms in the human host,[38] finally leading to death. The next essential stages in the life-cycle of the *Plasmodium* parasite take place in the vector, i.e., in the female *Anopheles* mosquito (Figure 1). After the gametocytes have been ingested by the mosquito through the blood meal, they escape the host RBCs and begin the sexual replication stage.[52] In the female *Anopheles* mosquito, the female and male gametes develop in the mid-gut,[53] where they develop to infect another host during another blood meal. There are various strategies for anti-malarial drugs that target the vector at the stage where sexual replication occurs. The growth or development of the parasite once it enters the vector depends on the temperature and type of parasite species.[54]

The male macrogametocytes emerge from the RBCs that are ingested by the mosquito during a blood meal and go through a 3-step process of maturation; they grow external flagella as seen in Figure 1, after which they fertilize the female microgametocytes.[55] The process of gametocytogenesis which follows is not fully understood,[56] although some studies show that attempts by the mosquito's immune system to fight off the parasite triggers the sexual development stage. The gametocytes travel further up the mid-gut of the mosquito and develop into zygotes which form mature ookinetes[57] which can either remain as they are or develop into oocysts. The oocysts finally produce a large number of sporozoites[57] which travel to the salivary glands of the mosquito and are transferred into a new host when the mosquito obtains its next blood meal.

Relatively little research that focuses on the gametocytes phase appears to have been undertaken,[56] possibly due to the complexity of their maturation in the RBCs, their masked immunity and the fact that this would require vector-based strategies. While various stages of the parasites life-cycle have been targeted with anti-malarial drugs that are specific to a pathway or phase, challenges remain. These include the problem of resistance.

1.2. Past and present anti-malarial drugs

Even though malaria was not fully understood, the fever-like symptoms have been treated using traditional medicines that formed the bases for anti-malarial drug discovery centuries later. Now, each of the known drugs are expected to target a specific pathway, an organelle of the parasite and some the mosquito itself. Since the mosquito was known to be the vector for malaria,[57] the first anti-malaria strategy was to eradicate the mosquito larvae as these would be easier to locate than the mobile adults[59] using insecticides such as Pyrethrum.[60] These were used until it became apparent that the cost and the inconvenience of having to continuously spray[61] would be problematic. Malaria was wide-spread during the time of the Second World War (1940–1945)[62] and many soldiers died from the disease as fighting extended the malaria-endemic to many parts of the world. After the war, a new malaria insecticide was discovered; known as DDT (dichlorodiphenyltrichloroethane), it would come to be one of the greatest weapons against malaria.[63]

The initial research for insecticides included natural-occurring derivatives such as chrysanthemic acid which was isolated from a flower[38] and DDT. While initial attention had been on attacking the vector, scientists began to focus on the human host and research on anti-malarial vaccines began during 1912.[64,65] However, this approach has proved challenging due to the complexity of the parasite's lifecycle.[66] The vaccines were expected to target various stages of the malaria parasite's maturation in the host[65] and to be cheap as majority of infections occur in poverty-stricken areas in the world in which storage of vaccines in air tight or cold containers would be difficult.[66]

Use of insecticides as anti-malarial prevention methods was finally introduced by the WHO in 1973,[67] but DDT as an insecticide was discovered in 1939 by a Swiss chemist, Paul Muller.[38] Its ability to kill mosquitoes was exploited as a means of eradicating the vector. DDT was originally synthesised in 1874. However it was only used as an insecticide in 1939.[67] The insolubility of DDT in water and its solubility in fat[68] were expected to preclude certain organisms and humans from being affected by DDT. During and after World War II, DDT was distributed to many parts of the world. This led to DDT being a cheap and effective way to

treat and prevent malaria.[69] However, there were health risks that were suspected and unknown. While exclusion of humans as a DDT target was based on its inability to transverse the skin membrane as well as its insolubility in aqueous media, DDT was detected in plants which humans then ingested, and small amounts of DDT were thus absorbed into the human body.[70]

The advantageous properties of DDT negated its persistence in the environment as well as in other living organisms. Human cells, for example, are made of many fat tissue cells. DDT, being soluble in such media, is able to dissolve and bind to these cells. Obvious health risks are associated with such occurrences and the one disease researchers were most worried about was cancer. Research conducted on rodents showed DDT to be retained within the organism with a very long lifetime, as well as to cause cancer.[67] In 1972, the use of DDT in the majority of the world was banned.[67] However, some countries continue to produce and use DDT even today. DDT was sprayed indoors or outdoors in areas where mosquitos and mosquito larvae persisted and it was discovered to act by affecting the peripheral nervous system sodium and potassium (Na^+/K^+) channels when an insect came in contact with the insecticide.[68] This leads to muscle spasms which then leads to the paralysis of the insect which finally results in death.[38]

The idea that DDT was a serious health hazard was evoked by Rachel Carson, a marine biologist, when she published her book "Silent Spring".[71] Even though the book was lacking in scientific evidence, it led many researchers to investigate her allegations. It became clear that the use of insecticides pose both health and environmental threats and that DDT was able to persist in the environment for a long time and thus move up the food chain to affect all living organisms.[67] These developments highlighted the need for effective anti-malarial drugs. The synthesis of new anti-malarial drugs was initially based on natural-occurring compounds as well as some known inhibitors of various organelles and pathways in other organisms, illustrated in (Figure 2).

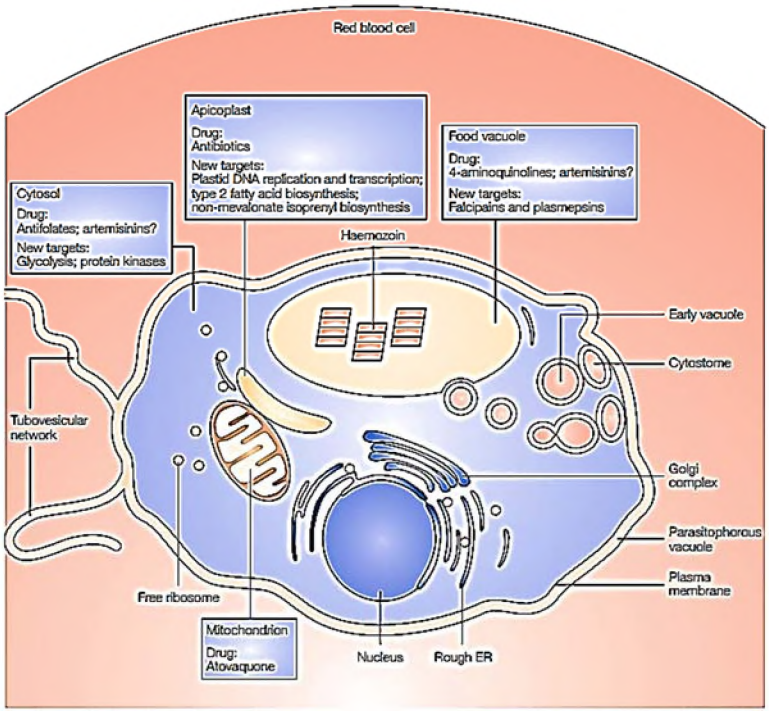

Figure 2. The various *Plasmodium* parasite cellular organelles that are essential for parasite survival and continued invasion of host RBC,[72] which represent current and potential drug targets and relevant drug classes.

The first class of compounds to be developed as anti-malarial drugs were synthetic quinoline analogues of the natural product quinine.[73] Synthetic quinolines have a 4-oxo-1,4-dihydroquinoline backbone and many are utilised as effective antibiotics or anti-malaria drugs today.[81] These compounds are considered to target the food vacuole, an organelle (Figure 2) with a large number of enzymes that degrades and hydrolyses molecules that an organism no longer needs.[74] Various models have been hypothesized as to how the food vacuole collects and degrades the unwanted haemoglobin[75] and to understand the mechanisms which the various quinolines exploit. Theories on the role of quinolines as anti-malarials include haemazoin polymerisation, their effect on lipids membranes,[76] the generation of free radicals[77] and many others. Quinolines have been used to treat malaria for over 300 years[76] and, in spite of their limitations, they are still used today. The quinoline motif occurs in many naturally-occurring compounds and is known to exhibit anti-bacterial, anti-malarial and anti-inflammatory properties[78] as well as many other biologically important activities. The first of these compounds to be used was the alkaloid, quinine,

obtainable from *Cinchona* bark.[73] This compound is suggested to have been discovered by a Peruvian Indian when he accidentally drank from water that had come in contact with the *Cinchona* bark and found his malarial symptoms alleviated. Once the news spread, missionaries who visited Peru exported the knowledge to parts of the Western world during the 17th century.[80] Since then, numerous medically active derivatives of quinine have been synthesised.

Quinine was initially used as a crude extract. In 1820, however, Pelletier and Caventou were able to extract and isolate it as a pure compound.[82] Early attempts to synthesise quinine failed due to its structural complexity;[73] this meant that it needed to be extracted from the *Cinchona* bark daily. This was time-consuming and threatened the survival of the *Cinchona* species. Another limitation with the use of quinine is its toxicity; side effects include cinchonism, tinnitus, impairment of hearing, headache, nausea, vertigo, vomiting, abdominal pain, diarrhoea, loss of vision and, sometimes with higher doses, hypotension.[80] There was also poor patient compliance due to the unpleasant taste of the orally-ingested quinine.[83] It became clear that new and improved anti-malarial drugs had to be developed, a challenge which was spurred by limited access to quinine itself during World War II.

Quinine and its stereoisomer quinidine have been used as first line drugs for malaria in many parts of the world; in fact, it is still used in countries like the United States.[83] During World War II, major research efforts led to the synthesis of various analogues of quinine, which include the 4-aminoquinolines, amodiaquine and chloroquine.[73] Chloroquine, as seen in (Figure 3), is a derivative of quinine that has been used for many years and its mechanisms of action has been the topic of considerable research.[84] Chloroquine was an ideal drug being cheap, readily available and fairly easy to synthesise.[83]

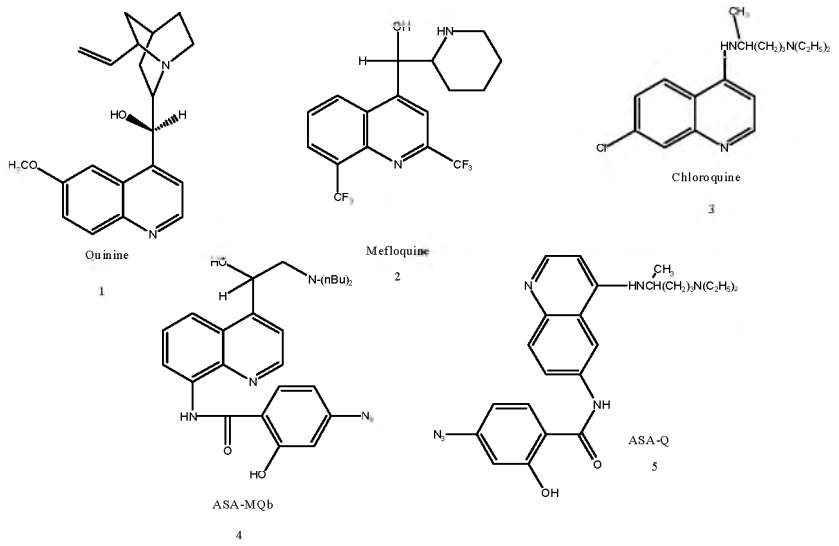

Figure 3. The structures of various quinoline-derived anti-malarial drugs: quinine, mefloquine, chloroquine, ASA-MQb and ASA-Q.[82]

The discovery of the formation of the "brown pigmentation" in parasite cells by Giovanni Lancisi[85] was the initial step in understanding the mechanism of action for chloroquine and other quinoline-derived anti-malarial drugs (Figure 3). The dark particles were found to accumulate in the food vacuole, an acidic lysosome-like organelle which is responsible for degrading haemoglobin and discarding toxic haeme as dark, crystalline haemazoin.[86] The prevailing theory is that chloroquine interferes with haeme detoxification which is a strategy for survival utilised by the parasite.[85] The parasite takes up haemoglobin from the host in order to provide itself with essential nutrition for cell survival.

Another targeted mechanism that occurs in the food vacuole is haemoglobin hydrolysis,[77] a process which is interrupted by protease inhibitors and artemisinins. Proteases are commonly-occurring enzymes present in most living organisms, and are responsible for the degradation of proteins into amino acids in various catalytic and regulatory pathways.[87] In the malaria parasite, these proteases (plasmepsin I, palsmepsin II and falcipain) are responsible for the degradation of haemoglobin[77] and for the rupture of RBCs. Research on protease inhibitors has been constricted by their ubiquitous nature,[88] but cysteine protease inhibitors have shown potential as anti-malarial drugs.[88] Protease inhibitors such as fluoromethyl ketones and vinyl sulfones[77] have been seen to exhibit anti-malarial activity

but are toxicity towards the human host.[89] During the Vietnam War, quinoline derivatives had been used so commonly that their efficiency was rapidly eradicated and, moreover, resistance was rising in other parts of the world.[91] Sometimes, it is essential that we look to the past to change the future, and this approach led to the discovery of the artemisinins. Artemisinin (Figure 4), also known as *qinghaosu*, is a natural extract from the plant Artemisia (or *qinghao*) which has been used in China to cure common fevers and pain for decades.[90]

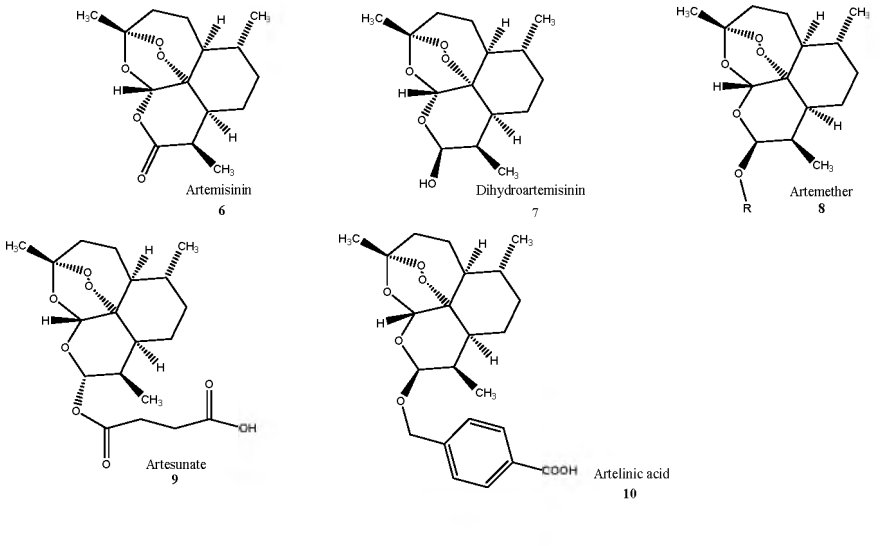

Figure 4. The structure of *qinghaosu* or Artemisinin as well as the various synthetic analogues that contain different R-substituents which allow for the solubility that artemisinin lacks.[96]

In 1967, the Chinese government assembled a group of researchers, known as the 523 research programme,[92] who were instructed to extract and test various Chinese herbs and plants for anti-malarial activity.[93] Artemisinins was then identified to be the active component in the extracts that were evaluated. Although artemisinin was active against malaria, it was discovered to be highly insoluble in both water and oil media[94] and had a short half-life;[95] these short-comings prompted the synthesis of various analogues, as seen in (Figure 4).

Artemisinins have proved to be effective against all *Plasmodium* species[96] and it is vital that its mechanism for inhibition be fully understood. However, the mode of action of these

compounds has been a source of controversy amongst researchers. The prevailing theory involves the generation of free radicals.[97] Artemisinin has a 1,2,4-trioxane backbone containing a peroxide group[93] which is essential for anti-malaria activity; removal of the peroxide moiety yielded an analogue without inhibition activity.[98] It has been proposed that the peroxide binds to haeme Fe^{2+} to produce an oxygen radical which then becomes a carbon-centred radical species,[97] while another proposed mechanism involves the production of hydroxyl radicals.[95] Both of these processes damage molecules that are essential for the parasites' survival and reduce the concentration of haeme ions which are necessary for the degradation of haemoglobin. The Fe^{2+} is thus believed to be responsible for the activation of the pro-drug artemisinin[95] which then produces radical species that are responsible for anti-malaria activity.

Oil- or water-soluble derivatives of artemisinin, such as artemether and artesunate respectively, are now first-line anti-malarial drugs of artemisinin[90] and are used in artemisinin-based combination therapy (ACT), which was developed in 1978 with other known drugs such as piperaquine, mefloquine, amodiaquine, sulfadoxine+pyrimethamine, atovaquone+proguanil, pyronaridine and lumefantrine.[99] These combinations allow for the rapid elimination of the parasite by one drug, combined with the long life-time that the other anti-malarial drug provides. Unfortunately ACT has faced various drawbacks which earlier anti-malaria drugs have also suffered, namely, dangers associated with pregnant patients and, most importantly, anti-malarial drug resistance.[90,100] Numerous studies have determined that use of ACT by pregnant women may result in severe malaria, spontaneous abortion, still birth or premature delivery.[101] The problem is compounded by the fact that pregnant women and children are most vulnerable to malaria infection. The issue of drug resistance to ACT is also an emerging problem that has been detected on the Thai-Cambodian and, more recently, the Thai-Myanmar border.[100]

The lysosome is the site of degradation for biomolecules such as proteins, nucleic acids, carbohydrates and lipids,[74] and is targeted by anti-malarial drugs which mainly disrupt the parasite's haeme degradation cycle. The ability of the parasite to develop mechanisms to

modify this step gives rise to resistance and it has become increasingly important that novel targets are discovered. The targeting biosynthetic pathways (Figure 2) in the cytosol, mitochondria, the plasma membrane and apicoplast are the next logical choices.

The cytosol, also known as the intracellular fluid or cytoplasmic matrix, in which the organelles are compartmentalized, is an aqueous solution containing proteins and polysaccharides.[74] A large number of anti-malarial drugs, such as pyrimethamine, proguanil, sulfadoxine, dapsone, gossypol derivatives, chorproguanil and many others, target various proteins in the cytosol, which are involved in numerous bio-syntheses as well as the regulation of organelle structures.[77] The main target for these drugs has been the folate pathway, which is essential for the synthesis of nucleic acids and methionine,[102] vital molecules for *Plasmodium* parasite DNA replication.

The anti-folates take advantage of the ability of the *Plasmodium* parasite to produce folates upon invasion of a host cell through the condensation of the host's pteridines, *para*-aminobenzoic acid (PABA) and glutamate.[102] The parasites' inability to utilise host nucleotides[103] means that the biosynthesis of these nucleotides must occur in the parasite. The anti-folates inhibit vital enzymes used by the parasite in this biosynthetic pathway; dihydrofolate reductase can be inhibited by chlorguanide, and dihydropteroate synthetase can be inhibited by dapsone, while pyrimethamine and sulfadoxine are able to inhibit both enzymes[104] and have been used in a combination therapy which is commercially available as Fansidar.[105] Anti-malarial drugs, present and past, have been identified in traditional plants and marine organisms; one such drug is gossypol which inhibits the important glycolysis cycle[106] in the parasite. Gossypol, a toxic extract from cotton seeds was discovered as an anti-malarial drug which inhibits lactate dehydrogenase,[106] and derivatives showing inhibition of chloroquine-resistant strains are being used as anti-malarial drugs.[107] These drugs have shown low toxicity and a reduced number of side effects,[108] but because they compete with the natural substrate, resistance has risen and hence their use has been limited.[106]

Recently, Hsp (heat shock protein), a group of proteins that have been of interest in cancer research, are now being studied as a potential anti-malaria drug targets.[107,109] Cancer as well as *Plasmodia* cells utilise Hsp70 when subjected to cellular threat.[109] The effect of *Plasmodium* parasite Hsp90 has also been studied. Research linking the emergence of resistance to *Pf*Hsp90 (which is over expressed during treatment)[110] has suggested that dual inhibition of these proteins by an anti-malarial drug would yield a highly effective combination therapy without the prospects of resistance. The mitochondria are the main source of producing energy for eukaryotic organisms,[74] and are responsible for the electron transfer chain.[111] The mitochondria are a valid target for anti-malarial agents such as the anti-malaria drug atovaquone (2-[trans-4-(4`-chlorophenyl)cyclohexyl]-3-hydroxy-1,4-hydroxy naphthoquinone). Atovaquone is an analogue of ubiquinone, the natural substrate. It induces competitive inhibition and binds the enzyme dihydroorotate dehydrogenase.[115] The drug is used in combination with proguanil, another anti-malaria drug, to reduce the development of resistance.[114] The x-ray crystal structure of the cytochrome bc_1 complex co-ordinated to atovaquone has not been determined. Research using computational techniques has indicated potential interactions that the inhibitor may have with the complex.[116] This combination therapy of atovaquone+proguanil has proved to be an effective chemoprophylactic for people travelling to high-risk malarial areas.[117]

Another approach in anti-malarial therapy involves the disruption of the plasma membrane/ cell wall. The plasma membrane is essential for the cellular compartmentalization in eukaryotic and prokaryotic cells.[74] The membrane is the layer composed of phospholipids and protein that protects the interior of cells as well as performing functions such as acting as a receptor to stimuli and facilitating transportation of molecules in and out of the cell.[118] The importance of membrane synthesis[119] is evidenced by the increase of 500% of the population of phospholipids in RBC after infection by the parasite.[120] It was discovered that quaternary ammonium choline analogues inhibited this membrane biogenesis; these analogues were designed and evaluated for potency against malaria.[121] An analogue with outstanding inhibition was G25, in (Figure 5), which was able to completely clear malaria when tested using very low doses; its IC_{50} value of 0.9 µM compared very favourably with

that of the known inhibitor chloroquine (0.8 μM). Moreover, G25 is active against strains that show resistance to currently used anti-malaria drugs.[122]

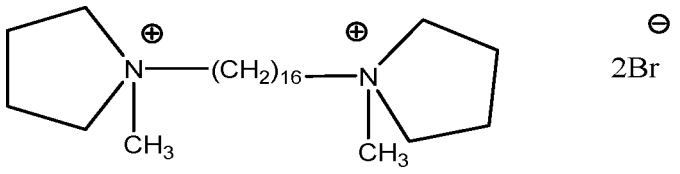

11

Figure 5. The choline analogue, G25.[122]

These anti-malaria drugs are choline analogues; choline is a nutrient that is necessary in the synthesis of membrane phospholipids.[123] This bio-synthesis is vital for the *Plasmodium* parasite's survival during its stage of producing merozoites where large numbers of membrane biogenesis allows for the parasite to continue the infection of RBCs. However, these analogues' bioavailability as oral drugs is low and a solution to the problem has not be obtained.[124] These compounds show potential not only as anti-malaria drugs but as drugs that will address the resistance that some drugs that are commercially available are facing.

Current research in our group focuses on the inhibition of an enzyme in the unique organelle apicoplast.[125] The apicoplast was only discovered in 1996[126] and is a non-photosynthetic plastid from the Phylum *Apicomplexa* occurring exclusively in protozoan parasites[127] which cause diseases such as toxoplasmosis, babesiosis, coccidiosis and, most importantly, malaria.[128] As a uniquely protozoan organelle the apicoplast provides desirable pathways that will exclude the human host. The apicoplast is located close to the mitochondrion and, for a long time, it was believed to be a storage site for mitochondria due to their close proximity and their small size.[127,129] Live cell imaging of the asexual stages of the malaria parasite revealed the apicoplast as a separate organelle that goes through various morphological changes in each step of maturation.[128] The *P. falciparum* apicoplast is essential for the survival of the parasite and therefore a potential target for anti-malaria drugs. Further research on the function, properties, metabolic pathways and genetic make-up has followed.

1.2.1. Drug resistance

The emergence of anti-malaria drug resistance can be traced back to 1986 when resistance to chloroquine and some of its derivatives was reported.[132] Resistance spread from the Thai-Cambodia region to the rest of the world.[133] Resistance to many more drugs began to become apparent and the problem of multi-drug resistance emerged.

The time-span for drugs in clinical use seems to be reducing significantly over the years as illustrated in (Figure 6). This is evidenced by the fact that resistance to quinine only became evident 278 years after its introduction, whereas recent drugs such as proguanil have been faced with resistance only a year after commercial introduction.[134] It is therefore evident that the *Plasmodium* parasite has developed mechanisms to develop resistance faster than it was able to in the past. There are many factors that determine the emergence of resistance including the mode of drug action, natural mutation of the *Plasmodium* genome, the transmission level, patient compliance, host immunity and the drug factors such as half-life, dosing, pharmacokinetics and cross resistance.[134] One such mechanism involves the resistance to anti-folates. Anti-folates prevent DNA (deoxyribonucleic acid) replication, resulting in reduced synthesis of methionine and conversion of glycine to serine, therefore, once the parasite no longer has supplies of methionine and serine cell death occurs.[136] The *dhfr* (dihydrofolate reductase) and *dhps* (dihydropeteroate synthase) are the enzymes that anti-folates inhibit but mutations in the genes of resistant strains of these enzymes [132] prevent the recognition and bonding by the anti-folates.[136]

Chloroquine has been a widely used anti-malaria drug for more than 50 years.[138] Its anti-malarial properties were deemed to be perfect, and the emergence of resistance to it led to panic. There are many theories to explain the chloroquine resistance but the three prevailing possibilities are: i) reduction in the parasite's up-take of the drug; ii) the expulsion of the drug from the food vacuole[135,136] and iii) mutation of *pf*CRT (*Plasmodium falciparum* chloroquine resistance transporter), a transporter in the lysosome,[139,140] which is important since the action of chloroquine is attributed to its ability to accumulate in the lysosome. The first theory is based on the fact that chloroquine is a weak base and when pH levels of the

lysosome are elevated, the neutral and mono-protonated forms of the drugs are able to permeate the membrane and, hence, do not accumulate in the lysosome.[141] The second relies on an expulsion mechanism, mediated by an ATP-dependent transporter; P-glycoprotein, which encodes for the *mdr* (multi-drug resistance gene), in this case *pfmdr*, which reduces the concentration of chloroquine in the lysosome.[136] Finally mutation of *pf*CRT, which facilitates transportation of chloroquine into lysosome, leads to the drug being transferred back into the cytoplasm.[72]

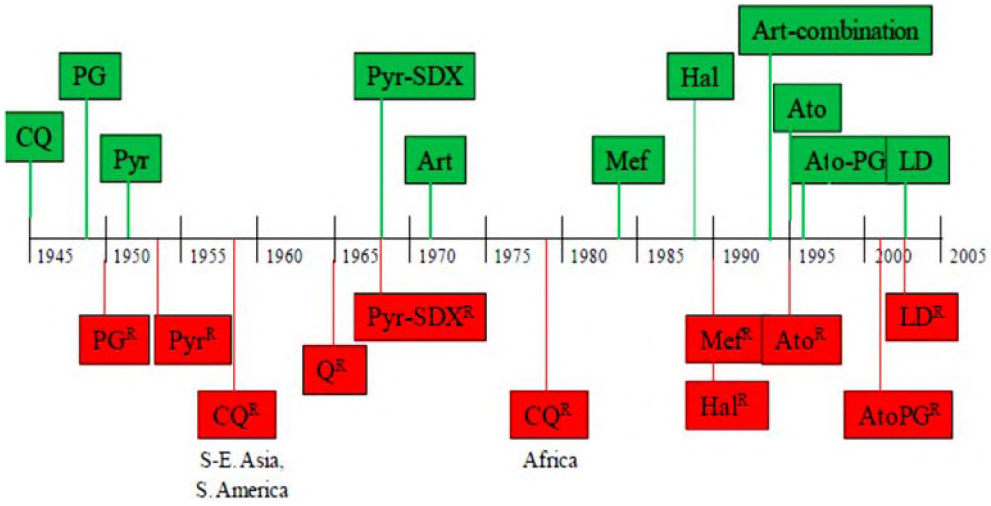

Figure 6. Approximate time-line showing the introduction of anti-malarial drugs (green) and the estimated time-span for the parasite to develop resistance to the particular drug or drug combination (in red) in the indicated continents.[132]

Atovaquone, which acts on the electron transfer chain, experienced resistance rapidly when it was used as a monotherapy, and is now therefore used in combination with proguanil.[114] Resistance is attributed to: i) mutation in the cytochrome *b* gene which results in changes in the amino acid sequence of the parasite rendering atovaquone ineffective; and ii) the slow uptake and high lipophilicity which produces low concentrations of the drug.[137]

The current first-line treatment for *P. falciparum* in endemic areas is ACT.[142] Resistance to the artemisinin-mefloquine combination was recently detected in the Thai-Cambodian region in early 2000,[143] the same region where resistance to chloroquine was first detected.

This is of great concern as there are no drugs in reserve which could be used if this resistance were to spread, reinforcing the need for the discovery of novel drugs.

1.3. Non-mevalonate pathway

Developing research is now focusing on the apicoplast target, specifically the biosynthesis of IPP (isopentenyl pyrophosphate) and DMAPP (dimethylallyl pyrophosphate) through the mevalonate pathways or non-mevalonate pathways.[144] For a long time, it was believed that all living organisms synthesised IPP and DMAPP through the mevalonate pathway.[145] It was only in 1996 that the non-mevalonate pathway was discovered to produce these biosynthetic precursors.[145]

In high eukaryotes, plants and some bacteria, the mevalonate pathway is responsible for the production of: i) farnesyl diphosphate and geranylgeranyl diphosphate which are lipids that can be added to proteins for functionality; ii) isopentenyl adenosine which is essential for tRNA (transfer RNA) modification; iii) coenzyme Q, an antioxidant that is involved in the electron transport chain in mitochondria; iv) dolichol and dolichol-phosphate which are necessary in protein glycosylation; and v) the production of an important molecule for bile acids and steroid hormones such as cholesterol.[146,147] The alternative non-mevalonate pathway has been discovered in the chloroplasts of algae, cyanobacteria, eubacteria, both gram positive and negative bacteria, and apicomplexan.[148] It is the differences in eukaryotic and archaeal non-mevalonate pathway (Figure 7) that can be exploited for the selective anti-malarial drugs in the inhibition of the *P. falciparum*.

The malaria parasite, which falls in the apicomplexa category, utilises this alternative pathway in the biosynthesis of IPP and DMAPP precursors which produce molecules that participate in processes such as protein prenylation, anchoring and degradation, electron transfer, regulation of hormones and *N*-glycosylation,[148,149] processes which are essential for the survival of the parasite in the human host and vector. The apicoplast, as mentioned before, is the plastid in which apicomplexa formation is attributed to cyanobacterial endosymbiosis.[127,129] The non-mevalonate pathway is of medicinal interest because of its

conservation in apicomplexa and absence in the human host. Thus inhibition of the DXOP/ MEP (1-deoxy-D-xylulose-5-phosphate) pathway would lead to the development of treatments for species such as *E.coli*, *M. tuberculosis* and most importantly and specifically for this research, *P. falciparum*. The focus of the current research is specifically on the IPP precursor synthesis and, in particular, the enzymes that are involved throughout the biosynthetic steps.

1.3.1. Isoprenoid biosynthesis

Isoprenoids are derived from IPP and are a diverse class of natural products.[150] They are collectively known as terpenes or terpenoids[151] and also include steroids and carotenoids.[152] These terpenes make up biologically-important molecules such as vitamins, hormones and cytosolic agents.[153] There are a large number of enzymes that take part in the synthesis of various chemical products and therefore inhibition of these key enzymes will result in termination of these processes and finally lead to cell death. The initial research on the non-mevalonate pathway was conducted by Rohmer and co-workers in 1999.[154] Using isotopic-labelled glucose, they traced the formation of hopanoids using NMR (nuclear magnetic resonance) data.[151,155] The difference between the eukaryotic and archaeal MVA pathways led to the target enzymes such as DXR being discovered.

The synthetic pathway begins with the catalysed decarboxylation and condensation of pyruvate and D-glyceraldehyde 3-phosphate by, first, the enzyme DXS (1-deoxy-D-xylulose-5-phosphate synthase), which requires thiamine diphosphate and Mg^{2+} or Mn^{2+} ions[152] for enzymatic activity, yielding DOXP/ DXP as a product.[156] The DXS enzyme is involved in the synthesis of vitamins B_1 and B_6 with an inhibitor being reported for Mycobacterium tuberculosis with IC_{50} value of 10.6 µM.[156]

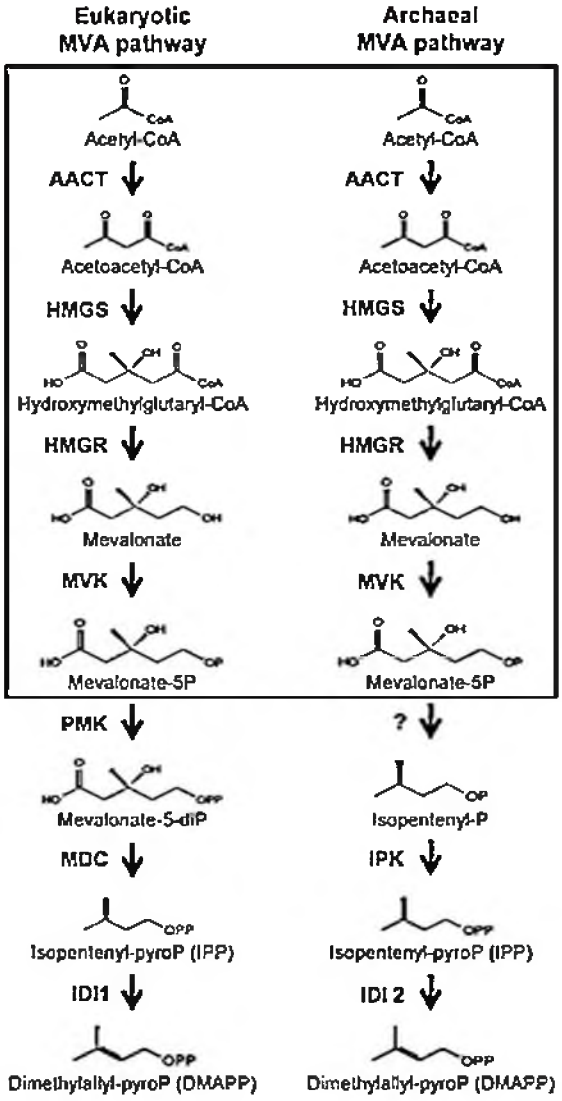

Figure 7. The eukaryotic and archaeal pathways for the synthesis of IPP and DMAPP; these are different in the last 4 steps and this diversity is exploited in the design of anti-malarial drugs.[149]

1.3.2. DXR-catalysed mechanism

The second step in the synthesis is the conversion of DXP to MEP (**Figure 8**) by enzyme DXR or IspC which require a co-factor NADPH and a divalent cation such as Mg^{2+}, Mn^{2} or Co^{2+} ions.[156,157] The enzyme DXR uses NADPH as hydride source for intramolecular isomerisation and reduction of DXP to MEP.[156] This is the target enzyme in the current research as crystallographic data is readily available and an opportunity exists for development of

inhibitors because currently known inhibitors of this pathway are faced with challenges. The produced MEP is converted into CDP-ME (4-diphosphocytidyl-2-C-methyl-D-erythritol) by the enzyme CTP (cytidine triphosphate) by transfer of the diphosphocytidal group.[158] The enzyme requires Mg^{2+} for activity. CTP has been fully characterised as a homo-dimer which is potentially druggable by suitable ligands.[156] The next step in the synthesis is the phosphorylation of CDP-ME to CDP-ME2P by CDP-ME kinase enzyme.[154] The enzyme transfers the ɤ-phosphoryl group from ATP in the presence of Mg^{2+} with promising lead compounds determined by *in silico* HTS for this kinase,[156] as illustrated in (Figure 8).

The final 2 steps involve the conversion of CDP-ME2P to MECP, a cyclic diphosphate, in the presence of Mn^{2+} and Zn^{2+} ions[156] by monomeric enzyme MECP synthase.[148] The final reaction, catalysed by MECDP synthase, is the least understood where the cyclised diphosphate undergoes reduction followed by elimination which yields IPP[148] and, from some of the IPP, DMAPP is made.[151]

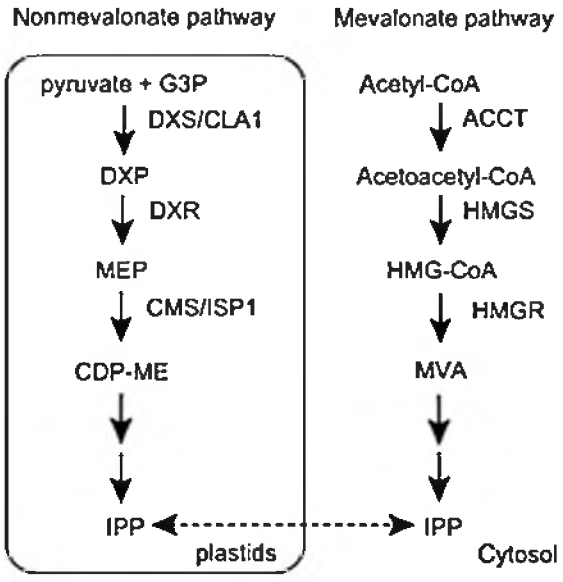

Figure 8. The non-mevalonate biosynthesis of IPP with required enzymes that form the catalytic site for reaction, with products essential for the survival of organism. The difference in the environment i.e. plastid vs cytosol of synthesis between the pathways is essential between the cells.[158]

This complex synthesis and cascade of enzymes reveals a large number of potential anti-malaria drug targets. The majority of known inhibitors are analogues of natural substrates therefore a start would be optimisation of properties of these analogues with the optimisim that a potent inhibitor can be discovered.

1.4. Target enzyme: DXR

1.4.1. Crystal structure

The target enzyme DXR's crystallographic structure has been determined and illustrated in (Figure 9), and this allows computational studies to be conducted readily on the structure as well as to deduce data about the active site. The target DXR is the second enzyme in the catalytic synthesis of IPP, and it is a critical enzyme for the production of vital molecules that the *Plasmodium* parasite requires. It is therefore important that the DXR structure is fully characterised and analysed.

The DXR enzyme is a homo-dimer of 42–45 kD that requires the presence of a divalent cation such as Mg^{2+} and a co-factor NADPH (nicotinamide adenine dinucleotide phosphate) for activity.[158] The first published crystal structure of the DXR enzyme was the apoenzyme[158] and, since then, many crystal structures have been published and with each further understanding of the enzyme has been achieved. The DXR is made up of 3 domains: the largest N-terminal domain bind co-factor NADPH comprises of 150 residues[160] while the small C-terminal domain of 1–150 residues binds natural substrate DOXP.[161] These 2 domains are joined by a linker domain that is 312–398 residues long[160] forming a V-shaped structure that is flexible to allow the opening and closing of the active site (**Figure 9**).[160,162]

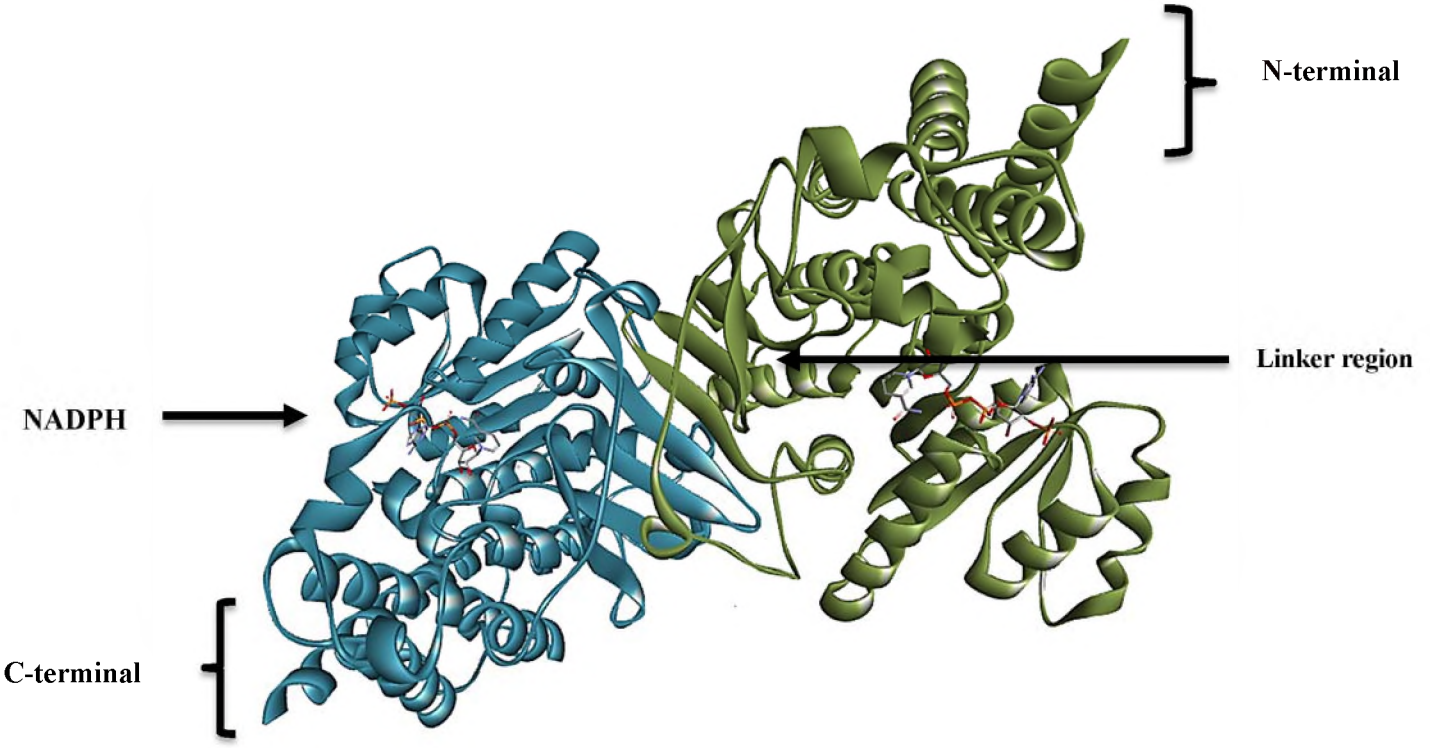

Figure 9. The crystallised structure of *Ec*DXR enzyme (1Q0Q) with co-factor NADPH in each of the homo-dimer's binding cavity; contains no ligand bound in the active site; water molecules are excluded for clarity. The protein coloured by chain: blue represents subunit A, green represents subunit B and the NADPH structure is in ball and stick representation, coloured by atom type.[163]

1.4.2. Binding mechanism

The mechanism of *pf*DXR begins with the deprotonation of the C-4 hydroxyl group of natural ligand DXP which results in bond C3 and C4 to be cleaved producing the enolate of hydroxyacetone the presence of Mg^{2+} stabilises this co-ordination along with glycolaldehyde phosphate.[164] Then via an aldol reaction a C-C bond is formed between C2 and C4 which leads to the production of intermediate 2-methyl-D-erythrose 4-phosphate which is further reduced by NADPH yielding the product MEP.[165] The (Figure 10) shows the enzymes as well as inhibitors that interact in the pathway.

The natural substrate DXP enters the active site and binds to conserved amino acid residues Ser199, Ser235, Asn240, Lys241 and Glu244.[166] The *Ec*DXR has similar residues. The crystal structure of *Ec*DXR, *mt*DXR and *pf*DXR with natural substrate DOXP, a known inhibitor fosmidomycin and its acetyl derivative FR900098, have been determined. These ligands'

crystal structures that are readily available bind DOXP analogues which aim to inhibit malaria parasite through competitive inhibition with natural substrate. Upon entering the binding site, the phosphonate group induces the flexible loop to open, the hydroxamate co-ordinates to the Mg^{2+} ion, and groups along the ligand interact with surrounding residues through hydrogen bonds, ionic bonds, π-π interactions and various other bonds.[167]

1.4.3. Known DXR inhibitors

The search for novel drugs with novel modes of action is the focus of many research studies. This has been the communication that the WHO has been conveying to all scientists as resistance hinders all efforts to eradicate malaria. The discovery of fosmidomycin and its acetyl derivative,[168] natural antibiotics produced by *Streptomyces lavendulae*, in the 1970's as inhibitors of the DXR enzyme[169]. They provided the basis for the search of new ligand structures with novel modes of action. These antibiotics were evaluated for anti-bacterial infections but were abandoned due to limitations.[170] These bind to the DXR enzyme mimicking the natural substrate, blocking the conversion of DOXP to MEP (**Figure 10**).[168-169]

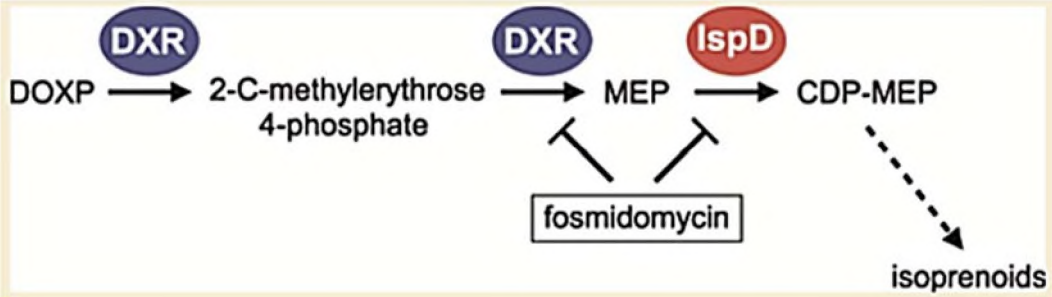

Figure 10. The non-mevalonate pathway in the production of IPP; fosmidomycin blocks the conversion of substrate DXP to product MEP, a vital reaction in this biosynthesis.[171]

The binding of fosmidomycin in the active site of *pf*DXR has been extensively studied and more analogues have been developed that attempt to enhance activity. Fosmidomycin and its acetylated derivative FR900098 were evaluated as potential drugs. However, they had limitations such as absorption, recrudescence and half-life.[172] Fosmidomycin has also been used in combination with Clindamycin, another apicoplast-targeting inhibitor, and these

show promising results as anti-malarial drugs.[169] The potential exists that this combination may be a new class of anti-malaria drugs.

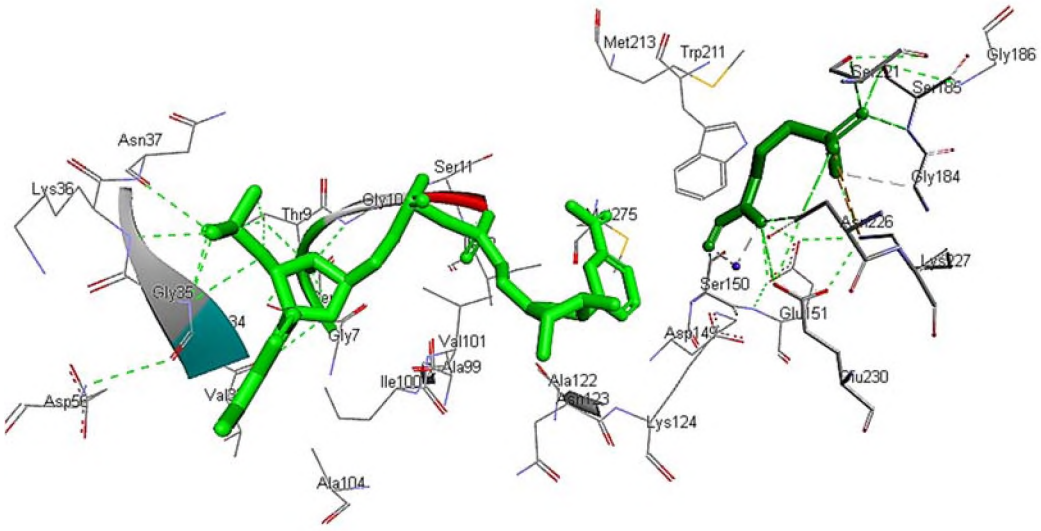

Figure 11. The docked structure of enzyme in *Ec*DXR (2EGH) with co-factor NADPH (green), known inhibitor fosmidomycin (dark-green) and Mg^{2+} ion (blue). The water molecules excluded for clarity. The dashed lines represent hydrogen bond lengths in Å and the neighbouring amino acid residues represented by name and ID number.[178]

The binding mechanism of fosmidomycin (Figure 11) is similar to the DXP substrate. Therefore analogues have to contain structural features that are conserved in both DXP and inhibitors for activity to be observed. The essential SAR (structure activity relationship) contains the particular necessary structural features in the inhibitor for activity to be observed.[173] The analysis has been conducted by many research studies is illustrated in Figure 12 finding that the substitution of the phosphonate head group, which is responsible for forming tight hydrogen bonds with various residues as well as the water molecules in the DXR binding cavity,[174] resulted in no activity. Therefore the phosphonate group is essential for binding DXR by increasing the methylene spacer or hydrophobic patch. Reduction in activity was observed and thus the two methylene spacer is necessary to permit the simultaneous binding of hydroxamate and phosphonate groups. The presence of an electron withdrawing group near the phosphonate decreases its pKa which enhances phosphonate–DXR interaction. Finally, the use of a pro-drug approach yields good inhibition.[174]

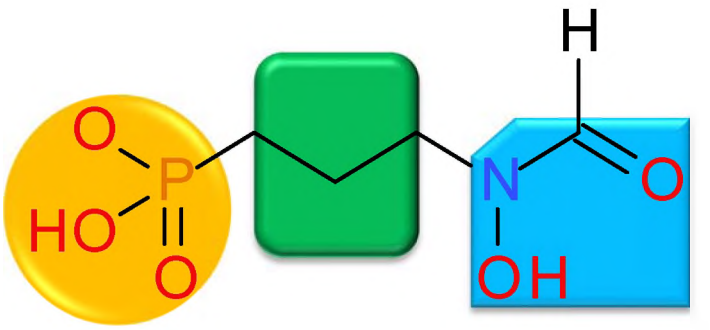

Figure 12. The structure of DXR inhibitor fosmidomycin; essential structural features for anti-malaria activity include the phosphonate group (orange), the methylene spacer (green) and the hydroxamate moiety (blue). Fosmidomycin drawing constructed using Symyx Draw 3.2 tools with atom type colour. [175]

The indicated SAR, in Figure 12, has been determined to be crucial for activity and therefore analogues that will have potential as anti-malaria drugs will require maintaining this SAR, or alternatively involve the incorporation of yet-to-be-determined groups that have the ability to enhance these properties. For the current research the conserved structures were preserved and structural changes that will hopefully enhance activity were introduced.

1.5. Aims of current studies

1.5.1 Past research

The previous research focused primarily on the exploration of the DXR binding cavity and the synthesis of a potential DXR inhibitor.[176,177] The series of DXR inhibitors was based on fosmidomycin and DOXP analogues which Conibear synthesised, *viz.*, phosphonate esters and their phosphonic acid salts, by using heterocyclic amino derivatives which were reacted with chloroacetyl chloride or 3-chloropropionyl chloride to produce chloroamides. These had minimal inhibitory activities. Furthermore, Mutorwa also synthesised 3-substituted anilines using the same route while using different acid chlorides (chloroacetyl chloride, 3-chloropropionyl chloride, 4-chlorobutanoyl chloride and 5-chloropentanoyl chloride). These compounds provided access to analogues containing 1, 2, 3, and 4 methylene groups in the hydrophobic patch (Figure 13).

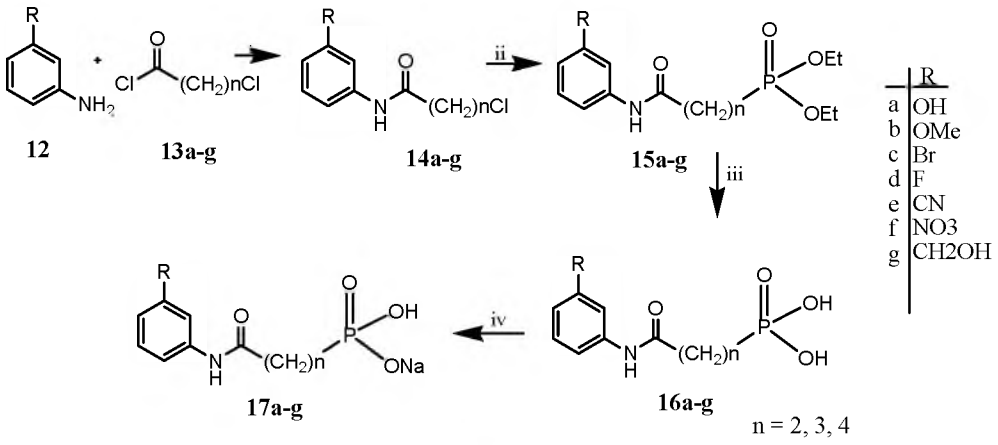

Figure 13. Synthesis of phosphonate esters and phosphonic acids.

Another compound series was the synthesis of dihydroxy-amido esters (Figure 14) which are mimicking the alkyl backbone of DOXP to retain enzyme-ligand binding specificity and modifying the phosphonate and hydroxamate moieties to obtain analogues with improved inhibitory activity. The saturation transfer difference NMR (STD) experimental data showed that some of the dihydroxy-amido phosphonic acid derivatives bind to *Ec*DXR, whilst others did not; however, these compounds were not tested using *Ec*DXR or *Pf*DXR bioassays.

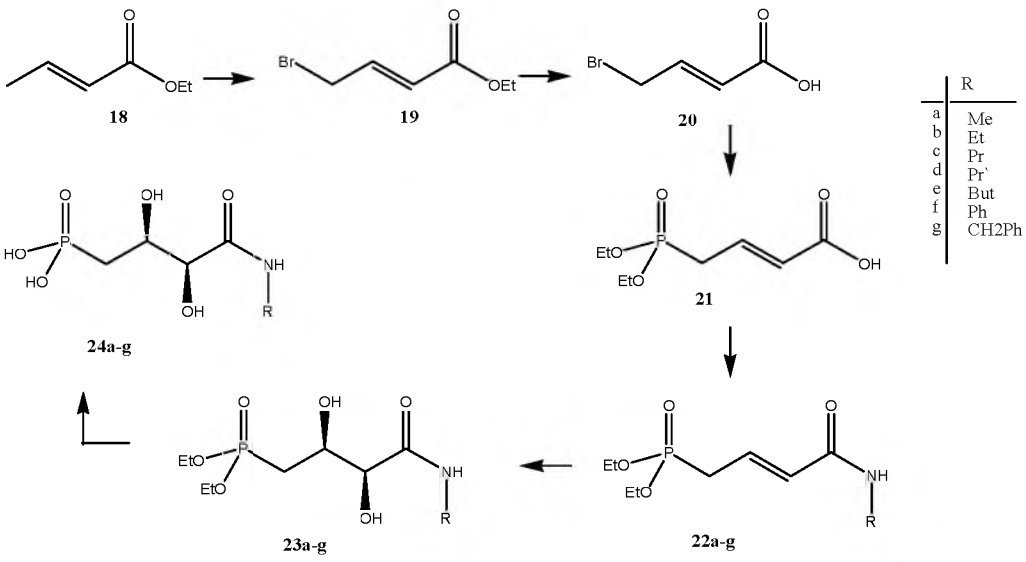

Figure 14. Synthetic routes explored in the synthesis of the dihydroxy-amido phosphonate esters and their corresponding acid derivatives.

1.5.2 Current research

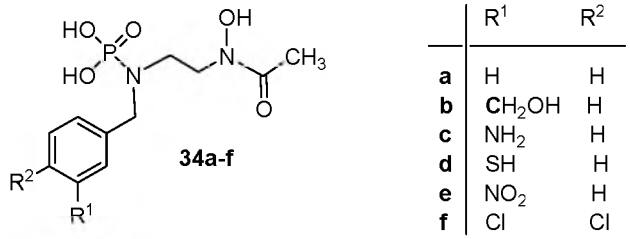

Figure 15. Reported and proposed *N*-benzylated fosmidomycin analogues.

Further quantities of the *N*-benzyl-substituted phosphoramidic acids **34a-f** (Figure 15), obtained *via* this 9-step pathway outlined in Figure 16, these were required for bioassay purposes. Moreover, since Haemers *et al.*[194] observed that the introduction of a 3,4-dichlorobenzyl moiety, in the DXR inhibitors which they were researching, increased inhibition activity significantly, we decided that it would be useful to prepare the 3,4-dichlorobenzyl analogue of our series of potential DXR inhibitors **34a-f.** We also considered that introduction of the strongly electronegative 3-nitrobenzyl moiety might prove to be

worthwhile. Here the introduction of the dichlorobenzyl derivative showed increased inhibition. The nitrobenzyl derivative is deactivating and therefore it is interesting to observe the effects of its presence in the effect on inhibition.

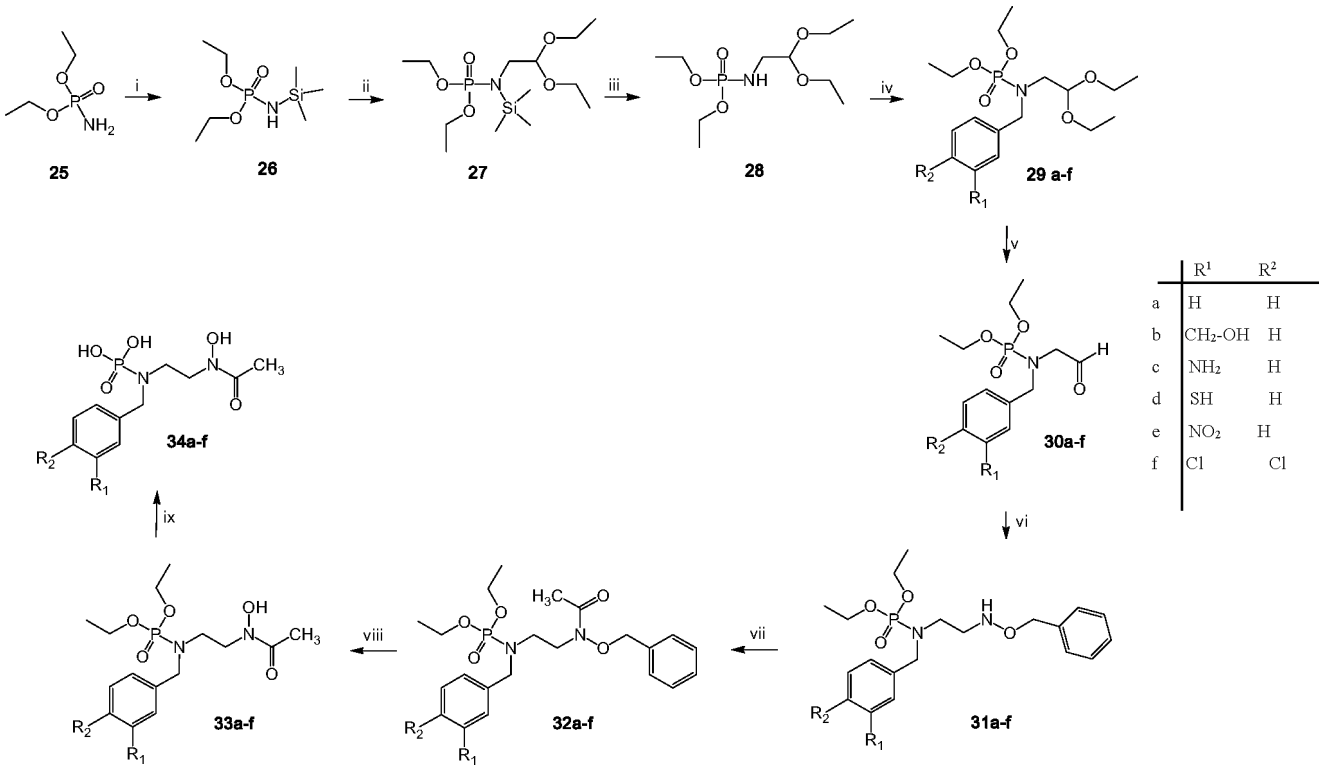

Figure 16. The synthetic pathway of the *N*-benzyl derivatives.

Access to the furan derivatives (Figure 17), as conformationally constrained fosmidomycin analogues has already been developed in our group, but the conformation of the regioselectivity of the second step (acylation of the *O*-tritylated intermediate **36**) was required. Regiosiomers are obtained in these reactions and the structures drawn in Figure 16 represent what we expect the favoured products to be (**37a**, **37b**, **37c**).

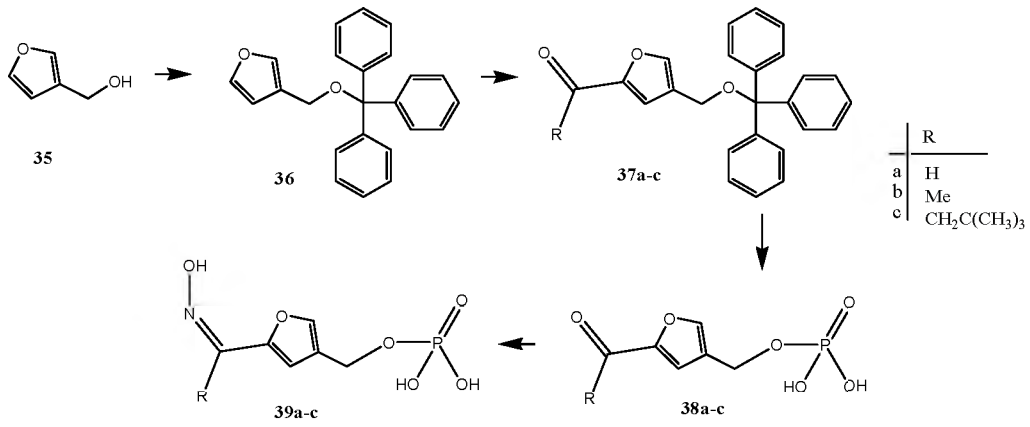

Figure 17. Furan derivatives with varying R groups, showing the expected regioisomer (**a–c**), in each case.

The aims of this research project have thus included the following.

1. A detailed and extensive computer-modelling analysis of the docking of a range of potential ligands in the *Pf*DXR active site.
2. The preparation of further quantities of the *N*-benzylated phosphoramidic acids **34a-d**, for bioassay purposes, *via* the established 9-step pathway.
3. An extension of this method to access the novel 3,4-dichloro- and 3-nitrobenzyl analogues **34e** and **34f**.
4. A repetition of the acylation of the *O*-tritylated intermediate **36** to establish the regioselectivity of the acylation in each case (for R = H, CH_3, *t*-butyl).

2. Discussion

2.1. Molecular modelling

Docking simulations were performed in order to explore the DXR enzyme binding site in order to predict the binding affinity of the generated ligands and to identify and evaluate hydrophobic binding regions. The enzyme receptor pocket may be exploited by the introduction of large hydrophobic groups for increased binding and inhibition. This investigation was conducted as an extension of previous work on examining the *Pf*-DXR binding cavity.[176] The research aimed to assess the limitations and properties that determine effective binding of the ligands in the active site.

Docking studies were conducted using a series of 63 structures modelled on fosmidomycin analogues. The 63 ligands were constructed using Discovery Studio Visualizer 4.0,[173] while the enzyme structures were obtained from the protein data bank. Six protein x-ray crystal structures were found to contain the natural ligand DXP with fosmidomycin or FR900098 in their binding cavity.[163] To validate the reliability of the docking study, the natural ligand DXP and the known inhibitors, fosmidomycin and FR900098, were removed from the binding site and re-docked along with the constructed putative ligands shown in (Figure 18).

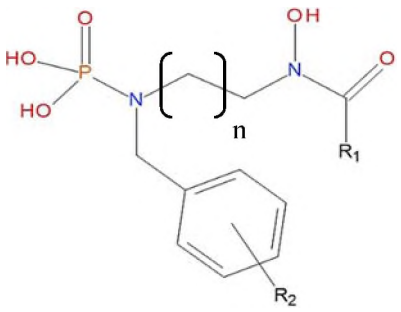

Figure 18. The variation of substituents in the modelled ligands, where n= 2, 3 or 4, R^1= **[a]:** CH_3, **[b]:** CH_2CH_3 or **[c]:** CH_2OH and R^2= H, CH_2Br, SH, OH, NH_2, amongst others.

Table 1. Summary of the ligands constructed *in silico*; **n** is the number of methylene groups in the spacer chain, while the variations in the terminal carbonyl group and the benzyl substituents are indicated by $\mathbf{R^1}$ and $\mathbf{R^2}$, respectively.

Ligand	n	R^1	R^2		n	R^1	R^2		n	R^1	R^2
2a_H	2	CH_3	H	3a_SH	3	CH_3	SH	4a_OH	4	CH_3	CH_2OH
2a_SH	2	CH_3	SH	3a_OH	3	CH_3	CH_2OH	4a_Cl	4	CH_3	Cl
2a_OH	2	CH_3	CH_2OH	3a_Cl	3	CH_3	Cl	4a_Br	4	CH_3	CH_2Br
2a_Cl	2	CH_3	Cl	3a_Br	3	CH_3	CH_2Br	4a_CH3	4	CH_3	CH_2CH_3
2a_Br	2	CH_3	CH_2Br	3a_CH3	3	CH_3	CH_2CH_3	4a_NH_2	4	CH_3	NH_2
2a_CH3	2	CH_3	CH_2CH_3	3a_NH_2	3	CH_3	NH_2	4b_H	4	CH_2CH_3	H
2a_NH_2	2	CH_3	NH_2	3b_H	3	CH_2CH_3	H	4b_SH	4	CH_2CH_3	SH
2b_H	2	CH_2CH_3	H	3b_SH	3	CH_2CH_3	SH	4b_OH	4	CH_2CH_3	CH_2OH
2b_SH	2	CH_2CH_3	SH	3b_OH	3	CH_2CH_3	CH_2OH	4b_Cl	4	CH_2CH_3	Cl
2b_OH	2	CH_2CH_3	CH_2OH	3b_Cl	3	CH_2CH_3	Cl	4b_Br	4	CH_2CH_3	CH_2Br
2b_Cl	2	CH_2CH_3	Cl	3b_Br	3	CH_2CH_3	CH_2Br	4b_CH3	4	CH_2CH_3	CH_2CH_3
2b_Br	2	CH_2CH_3	CH_2Br	3b_CH3	3	CH_2CH_3	CH_2CH_3	4b_NH_2	4	CH_2CH_3	NH_2
2b_CH3	2	CH_2CH_3	CH_2CH_3	3b_NH_2	3	CH_2CH_3	NH_2	4c_H	4	CH_2OH	H
2b_NH_2	2	CH_2CH_3	NH_2	3c_H	3	CH_2OH	H	4c_SH	4	CH_2OH	SH
2c_H	2	CH_2OH	H	3c_SH	3	CH_2OH	SH	4c_OH	4	CH_2OH	CH_2OH
2c_SH	2	CH_2OH	SH	3c_OH	3	CH_2OH	CH_2OH	4c_Cl	4	CH_2OH	Cl
2c_OH	2	CH_2OH	CH_2OH	3c_Cl	3	CH_2OH	Cl	4c_Br	4	CH_2OH	CH_2Br
2c_Cl	2	CH_2OH	Cl	3c_Br	3	CH_2OH	CH_2Br	4c_CH3	4	CH_2OH	CH_2CH_3
2c_Br	2	CH_2OH	CH_2Br	3c_CH3	3	CH_2OH	CH_2CH_3	4c_NH_2	4	CH_2OH	NH_2
2c_CH3	2	CH_2OH	CH_2CH_3	3c_NH_2	3	CH_2OH	NH_2				
2c_NH_2	2	CH_2OH	NH_2	4a_H	4	CH_3	H				
3a_H	3	CH_3	H	4a_SH	4	CH_3	SH				

The 63 ligands, summarised in Table 1 and illustrated in Figure 18 differ in: i) the number of methylene groups (CH_2)present [$(CH_2)_n$: n= 1, 2, or 3]; ii) the nature of the terminal metal-chelating group [R^1= **a** (CH_3); **b** (CH_2CH_3) or **c** (CH_2OH) and iii) the nature of the benzyl substituent (R^2= CH_2Br, NH_2, OH, SH etc.). Thus for ligand **2a_Br** (Figure 19), n = 2, R^1= CH_3 and R^2= Br.

The constructed ligands retain the polar phosphonate moiety, which is present in both fosmidomycin and FR900098 and which is important for hydrogen bonding to nearby amino acid residues, and the polar hydroxamate group which is essential for coordinating to the metal cation.

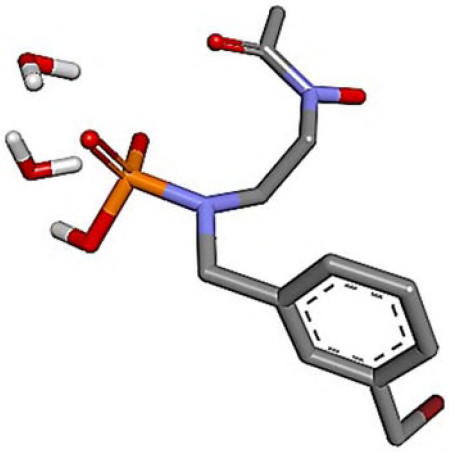

Figure 19. Structure of ligand **2a_Br** in which n = 2, R^1=CH_3 and R^2=Br with water molecules, the crystal structure of ligand **2a_Br** is shown stick representation with atom-type colour.[178]

The six *Pf*- or *E.Coli*- DXR protein structures which were used are; 1Q0L, 1Q0Q, 2EGH, 3AU8, 3AU9 and 3AUA which are from *Pf* and *E.coli* species. The DXR protein **1Q0L** (Figure 20) is a *Ec*DXR protein with the known inhibitor fosmidomycin bound in the active site; **1Q0Q** is a selenomethionine-labelled protein from *E.coli* which contains the natural substrate DXP bound in the active site; **2EGH** from *E.coli* has no ligand; **3AU8** is another *Pf*DXR protein with a bound fosmidomycin ligand; **3AU9** is *Pf*DXR protein with bound fosmidomycin in the active site and **3AUA** is a *Pf* DXR protein and has FR900098 bound in the active site. All of these structures contain the NADPH co-factor and the divalent metal cation Mg^{2+}, and were completely desolvated (2 water molecules on the polar phosphonate moiety of ligands was included in the docking process) prior to docking/modelling studies.

Each sub-unit of the DXR 86-kDa homodimer consists of a large N-terminal NADPH-binding domain (77 – 230 amino acid residues) adjacent to a large catalytic domain (231 – 269 amino acid residues) which provides the groups necessary for catalysis (metal + substrate binding). This catalytic domain is connected to a small C-terminal domain (396 – 486 amino acid residues) with a linker region (370 – 395 amino acid residues) which constitutes a

flexible 'lid' that closes the active site once a substrate is bound. For the purpose of the current docking simulations, the sub-unit A binding site was used as the docking site with both NADPH molecules in the same orientation. The 63 ligand variations along with the 6 protein structures (Figure 20) and 3 known ligands (DOXP, fosmidomycin and FR9000098) made up the collection for molecular modelling in this docking study.

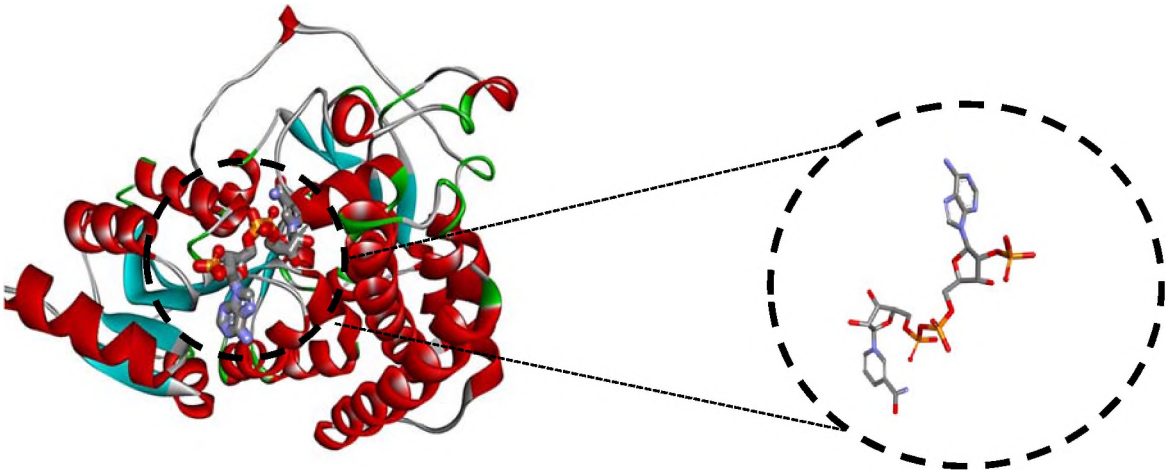

Figure 20. The structure of *Pf* DXR protein subunit A from 1Q0L with NADPH co-ordinated in the active site. The protein is coloured by secondary structure type with ligand NADPH in ball and stick with atom-type colours.[163]

The docking of the phosphoramidate derivatives began with the removal of the solvating water molecules that are present in the crystal structures of the proteins as well as the removal of the bound substrate i.e. fosmidomycin, FR9000000 or DOXP. The NADPH as well as the divalent Mn^{2+} cation were left in at their original positions. The +2 charge was manually assigned to the manganese and the two water molecules that are normally coordinated to the bound phosphonate group in fosmidomycin were added near the phosphonate groups of each of the ligands, thus facilitating evaluation of the correct alignment or orientation of the docked ligand in the active site. To validate the reliability of the docking study, the natural ligand DXOP and the known inhibitors fosmidomycin and FR900098 were removed from the binding site, their dihydrated structures were optimised and they were successfully re-docked. The structures of the 63 dihydrated model ligands

were similarly optimised and docked into the various enzymes. The best docking conformation, in each case, was then analysed and selected, based on the binding affinity, calculated from the binding free energy of each atom in the ligand – an indication of the fit of the ligand in the active site. The docked ligands were then overlaid with other docked ligands to allow for meaningful comparison of ligand and receptor cavity.

For each of the protein models, certain residues within the active site were assigned as flexible. This permits dynamic movement within the active site to reproduce the flexibility that the protein might exhibit *in vivo*. The same residues, although numbered differently (there are variations in the residue number due to the protein sequence and numbering system differences) in the X-ray structures were chosen to be flexible in docking to the six crystal structures. These residues correspond in all six proteins and are in direct proximity to the active site. For the **2EGH** protein, Ser 221, Ser 185, Asn 226, Lys 227 and Glu 230 were the flexible residues, for **1Q0Q** and **1Q0L**, these were Ser 222, Ser 151, Asn 227, Lys 228 and Glu 231, while for proteins **3AU8**, **3AU9** and **3AUA** the same residues, Ser 270, Ser 306, Asn 361, Lys 312 and Glu 315 were selected as flexible. These flexible residues within the active site were chosen since they correspond in all 6 proteins with slight differences in the residue number in the various DXR crystal structures.

Using Windows Secure Copy (WinSCP),[179] the constructed ligands and the unbound, desolvated protein were transferred to a linux cluster. WinSCP, free software available programme readily from the internet created by Martin Prikryl in 2000,[179] is used to transfer data from a personal computer to a remote computer – commonly a supercomputer that will process the data. A terminal (putty) was used to control and access the submission scripts on the cluster while Autodock Vina,[180] an open-source program was used for the docking simulations of the constructed ligands and modified proteins. The ligands and protein were prepared using Autodock tools; Autodock Vina has proved to be significantly more accurate in the prediction of binding affinity as well as exhibiting other features, such as ease of use, speed and assignment of flexible side chains.[180] The anhydrous and dihydrated ligands were used in docking studies conducted.

Docking in the active site was first evaluated for EcDXR enzyme, using the **1Q0L**[168] enzyme structure which contains fosmidomycin, NADPH and the Mg^{2+} cation (Figure 21). Each of the 63 ligands were evaluated for:- i) their ability to bind to the active site; ii) the accuracy of their alignment with fosmidomycin and, finally iii) their binding orientation relative to fosmidomycin. These aspects were considered to be important in identifying the inhibition potential of the various ligands. Ligands with active site interactions similar to that of fosmidomycin are expected to have similar binding abilities, possibly with enhanced penetration of the active site and increased inhibition. The orientation of the designed ligands in comparison to fosmidomycin is essential as the critical ligand moieties need to align with the appropriate amino acid residues to accommodate binding in the active site. This does not preclude other binding interactions from being involved but ensures the conservation of established interactions.

The two connected binding pockets in the protein active site should be occupied by the co-factor NADPH, the Mg^{2+} cation and the docked ligand. Fosmidomycin and 25 of the 63 ligands appear to occupy the same binding pocket (Figure 21). However, only 17 of these ligands were both correctly docked and well orientated and, of these, only those ligands whose binding energy was also favourable will be evaluated further in detail. A general trend with **1Q0L** was an increase in the length of the methylene spacer (n=3–4) led to ligands being extended beyond the active site although some exceptions were encountered when R^2 groups were small (e.g H, SH and NH_2) but when R^2 = CH_3Br or CH_3, the ligand was actually excluded from the binding site. The presence of the terminal ethyl group such as n=2 and R^2 = SH resulted in SH (and in some cases NH_2) being retained in the active site. When the terminal group was the hydroxymethyl moiety, the ligand remained in the active site when R^2 was SH, NH_2 and H.

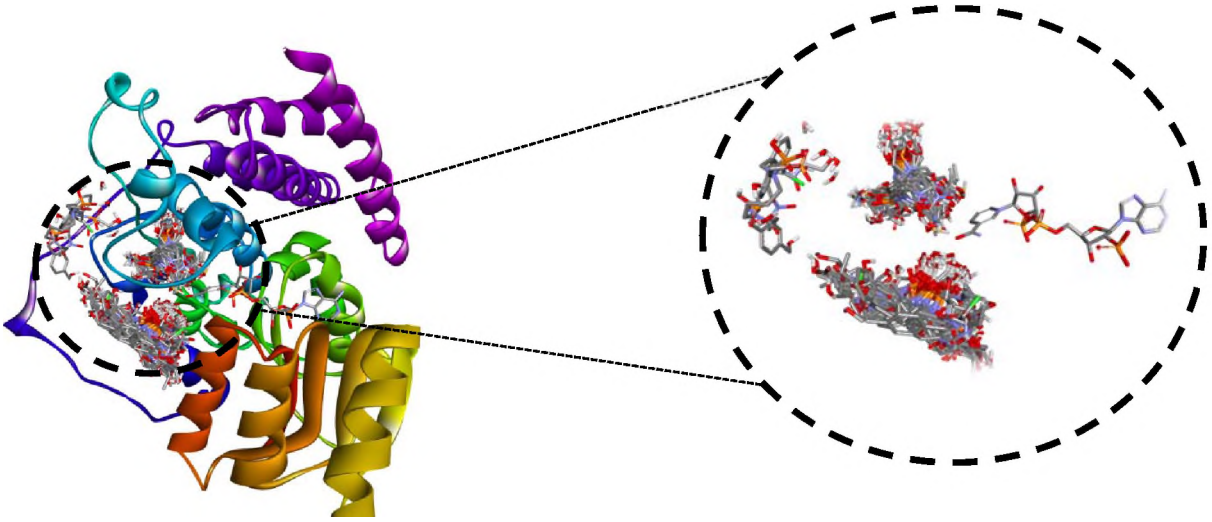

Figure 21. *Ec*DXR Protein **1Q0L** subunit A showing the distribution of 63 modelled ligands; majority of the ligands cluster outside the binding cavity of the enzyme, some near NAPDH while the rest excluded from the active site cavity. The cartoon of the protein is coloured using a rainbow type format with ligands and NADPH in ball and stick format with atom type colour.[178]

The docked ligand **2a_H** (Figure 22) interacts mainly with the DXR active site, the phosphonate group interacts with Lys228 and is bound to water molecule hydrating the active site, the dihydrogen groups interact with Asn227, Ser186, Ser222 and the water molecules, the hydroxide interacts with Met214, the terminal carboxylic groups interacts with Ser151 with methyl binding to Trp212. The additional interactions are the aromatic ring electrons interacting with Trp212, Glu152 and Lys228. The known inhibitor fosmidomycin (yellow) is included as a comparison for conformation and orientation in the active site. The added groups give rise to the new interactions observed with fosmidomycin. The same interactions as the **2a_H** are observed for **2a_Cl** with the additional chlorine interaction with His251 and Ser254. This was seen for **2a_NH$_2$** and **2a_SH** as well (where this interaction is now with the NH_2 or the SH). This was promising as the addition of the phenyl R groups did not exclude the ligands from binding to the active site but further enhanced the interaction of the ligand with the conserved amino acids as well as introducing new interactions.

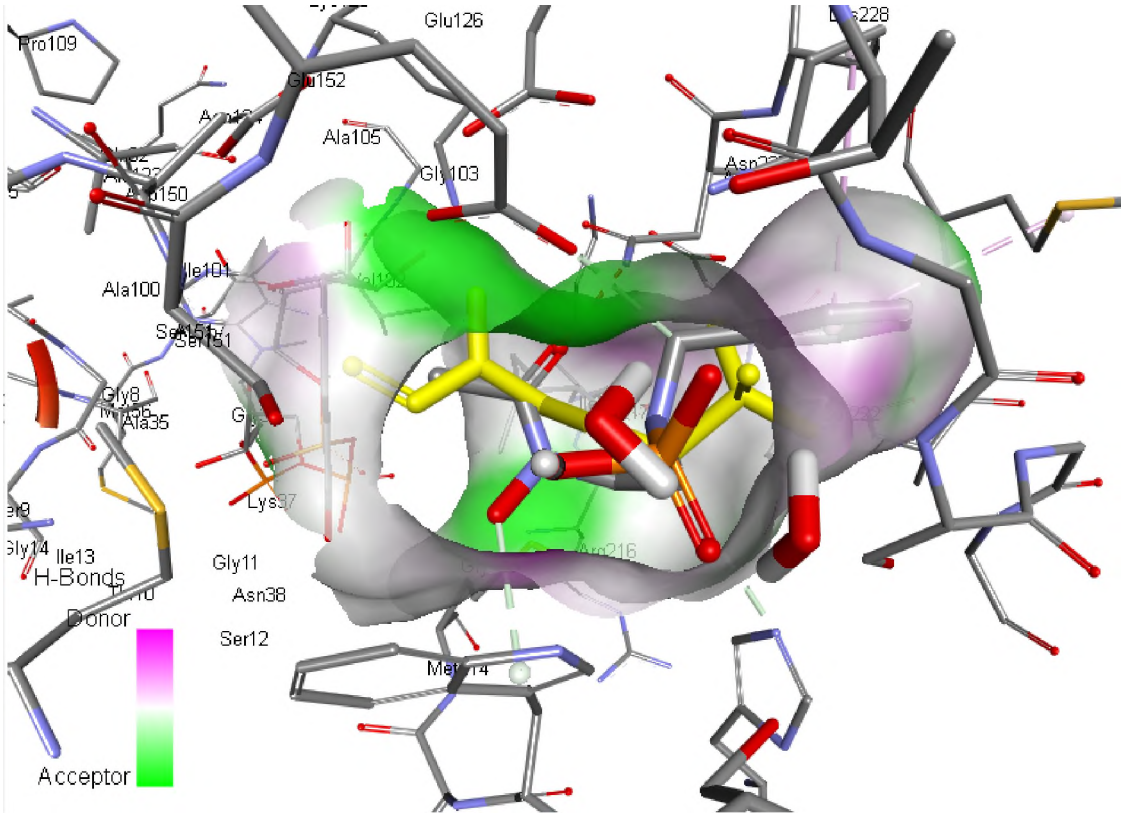

Figure 22. The ligand **2a_H** interacts in the *Ec*DXR active site **(1Q0L)** with the conserved amino acids that are observed with fosmidomycin with additional interactions with the auxiliary groups that the analogues contain and 2 water molecules. The crystal structure of fosmidomycin and 1a_H are in ball and stick with atom-type colour. The hydrogen atoms are not shown and dashed lines represent H-bond distance in Å.[178]

The next aspect explored was the substitution of the terminal methyl on the ligand with an ethyl group to evaluate the change of geometry of docking as a result of increasing the size of the terminal group while keeping the methylene spacer the same. The addition of this ethyl terminal group resulted in all ligands excluding **2b_H** and **2b_SH** preferring to bind outside the active site as well as resulted in **2b_H** "reverse" binding relative to fosmidomycin. In the best docking conformation, the terminal ethyl group interacted with amino acids that originally were proximal to the phosphonate group in fosmidomycin and vice versa. The ligands exhibiting "normal" binding were analysed as these interactions proved favourable for fosmidomycin and therefore potential analogues should aim to secure binding similar to that of a known inhibitor.

The ligand **2b_SH** (Figure 23), has all the interactions which are observed in the methyl analogue but with further interaction between the terminal ethyl group and Trp212. The R group **SH** has further interactions with Ile256 and Thr184. Fosmidomycin (yellow) compares favourably with ligand **2b_SH** in both interactions and orientation.

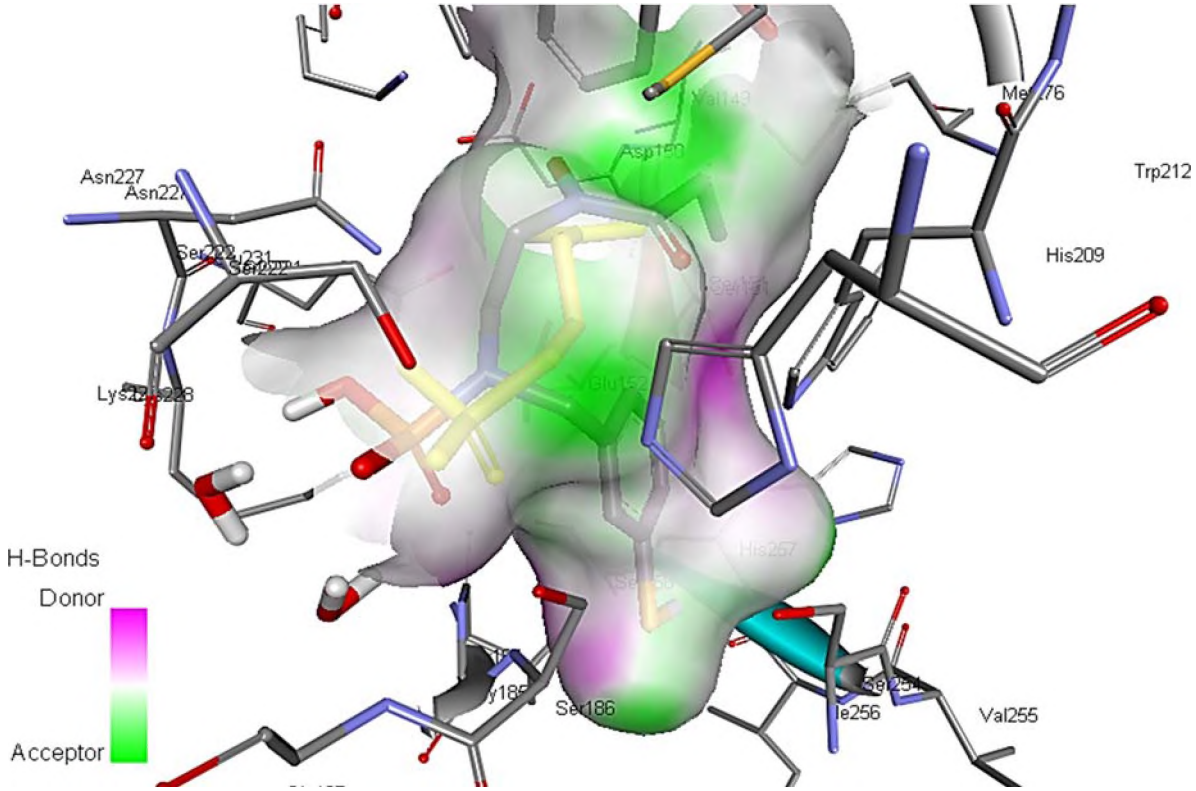

Figure 23. Docked conformation of ligand **2b_SH** in the *Ec*DXR active site **(1Q0L)** showing interacting residues. The crystal structure of fosmidomycin structure in ball and stick format in yellow, while 2b_SH has atom-type colour.[178]

This large terminal group was further investigated by the addition of a terminal hydroxymethyl **(c),** while keeping the methylene spacer length constant. For this series of terminal hydroxymethyl models, only **2c_SH** was retained in the active site during docking; all other ligands docked external to the active site. The presence of the terminal hydroxymethyl group **(c)** resulted in unique orientation and interaction of the **2c_SH** ligand with Trp212 and the co-factor NADPH. These interactions have not been observed with any of the ligands, and their presence is interesting for how far the ligand is able to interact directly with NADPH and potential for synthesis of a ligand bound to NADPH analogues that

might enhance binding in both binding domains and activity. In this binding there is an apparent reversal of the roles of the aromatic and hydroxylamine portions of the ligands, with the aromatic side orienting toward the NADPH while the hydroxylamine portion (with the terminal hydroxymethyl group) occupying the lower pocket.

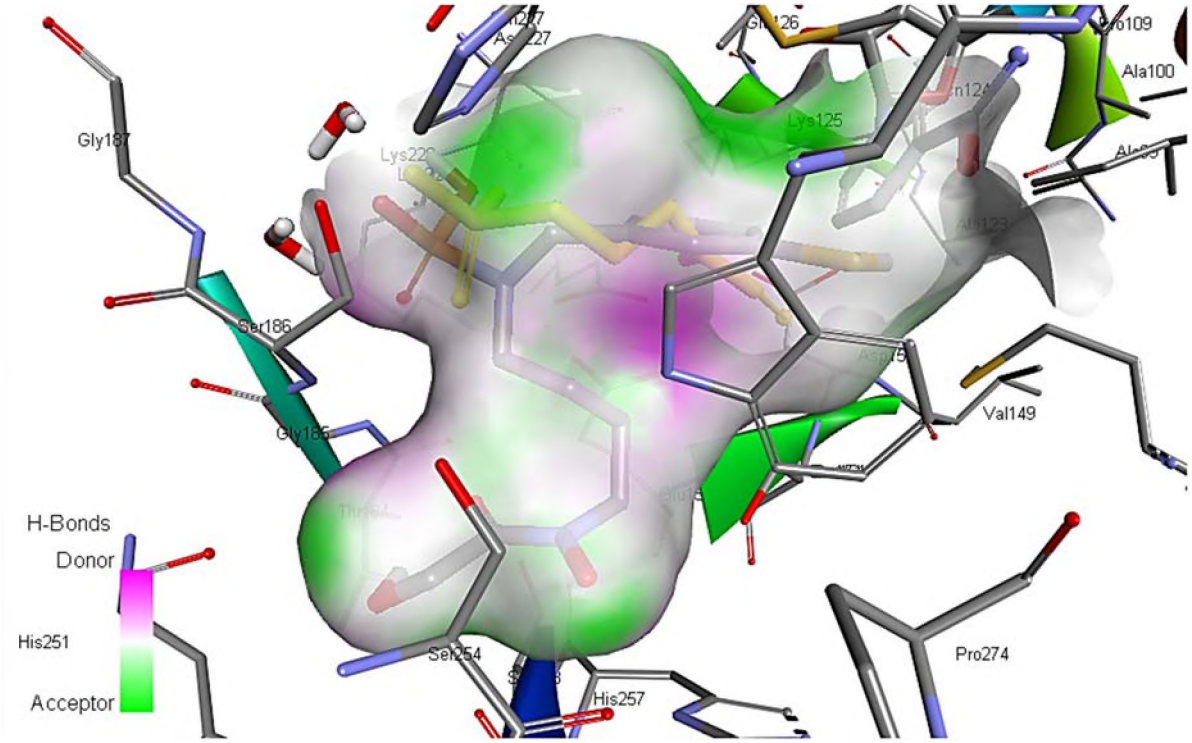

Figure 24. Docked conformation of ligand **4c_SH** in the in the *Ec*DXR active site **(1Q0L)**, with expected interactions with proximate residues. The crystal structure of fosmidomycin structure in broader stick representation with atom-type colour.[178]

Finally, increasing the methylene spacer from 2 to 3 methylene groups resulted in exclusion of R^2 (such as OH, CH_3 and Br) in the binding site as well as the presence of the larger terminal ethyl **(b)** and hydroxymethyl **(c)**. However, this increase in the methylene spacer length did not affect NH_2 and SH interaction in the active site for the appropriate compounds. The ligands **2a_CH$_3$**, **2a_Cl** and **2a_H** bound directly on top of NADPH while ligands **2b_SH**, **2c_SH**, **2a_NH**, **2b_NH**, **2c_NH** and **2a_Cl** were the only models that docked in the correct conformation and orientation as fosmidomycin. When the methylene spacer was increased yet again to 4 methylene groups while keeping orientation and substitution constant, this resulted in the majority of the ligands not binding in the DXR active site with

the exception of **4a_NH**, **4b_H**, **4c_H** and **4c_SH**. These ligands, when in the binding site, align the phenyl group along with fosmidomycin (yellow) and the long methylene chain occupies a different pocket in the active site (Figure 24). This explores different binding during docking, and these interactions with additional pockets could potentially provide novel leads.

The *Ec*DXR enzyme **1Q0Q** is a selenomethionine-labelled DXR protein from *E.coli* with natural substrate DOXP bound in the active site. The protein crystal structure is a homodimer and thus subunit A was used for docking studies. This protein is the same protein as **1Q0L** but with a different template ligand in the active site and therefore the interaction of the ligands should be similar to that of **1Q0L** but the binding interactions are compared to DOXP and exceptions will be reported.

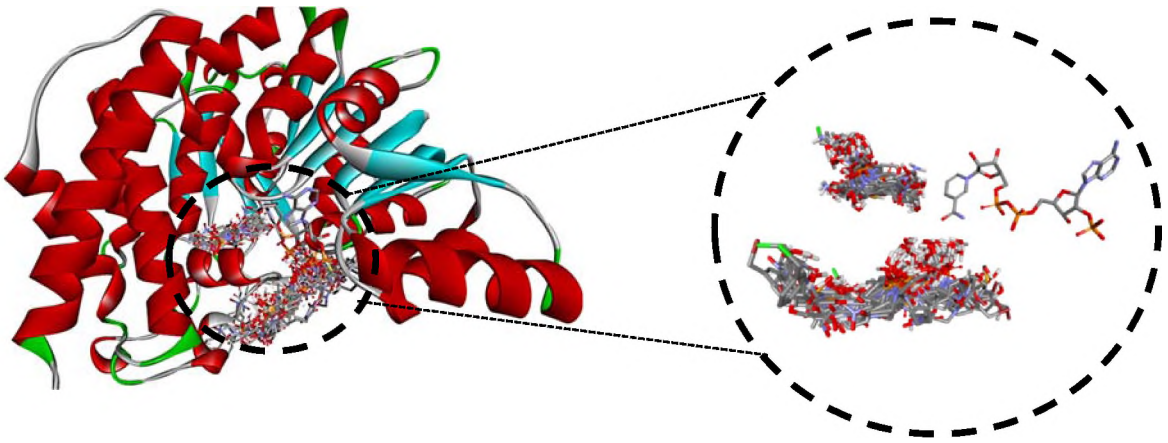

Figure 25. Protein **1Q0Q** subunit A showing the distribution of 63 ligands; the majority of the ligands fall outside the binding cavity/site of the enzyme. The protein colour by secondary type with ligands and NADPH in ball and stick with atom-type colour.[178]

The DOXP and 17 of the 63 ligands appear to be in the same binding pocket (Figure 25). The ligands that were both correctly docked and well orientated, i.e. where the phosphonate group orientated similarly to DOXP, were only 9. The ligands bind in two conformations, **2a_OH**, **2b_NH**, **2b_OH**, **2c_Cl**, **2c_NH** and **2a_NH** had the phenyl group aligned with DOXP while the orientation of **2a_H**, **2a_NH**, **2a_SH**, **2b_H**, **2b_SH**, **2c_OH**, **2c_SH**, **4a_H** and **4c_NH**

was identical to that of DOXP. Evidently the large R^2 group as well as the majority of the increased methylene spacer **(2–3)** and large terminal groups **(b–c)** contributed to exclusion from the active site.

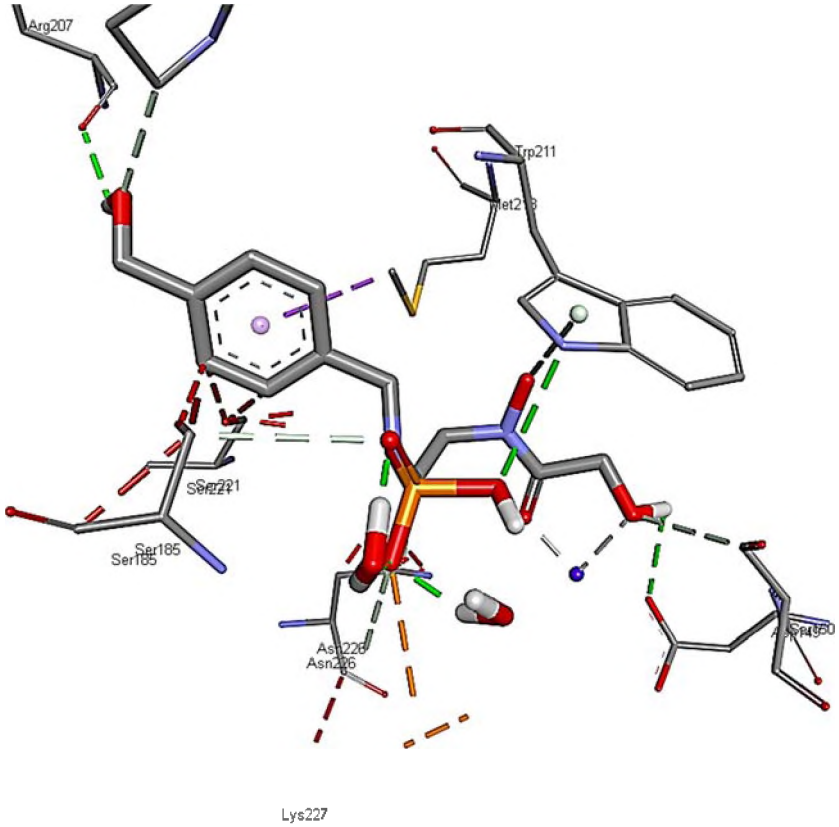

Figure 26. The ligand **2c_OH** interacts in the *Ec*DXR active site **(1Q0Q)**. The crystal structure of **2c_OH** and DOXP are in ball and stick with atom type colour with Mg^{2+} ion (blue). The hydrogen atoms are not shown and dashed lines represent H-bond distance in Å.[178]

In Figure 26, ligand **2c_OH** shows interactions in the DXR active site *via* the phosphonate group interacting with Ser221 and is also bound to a water molecule hydrating the active site. The hydroxyl group on the phosphate moiety interacts with Asn226, Lys227 and the water molecules. The hydroxide interacts with Trp211 and Met218, and the phenyl hydroxyl group interacts with residue Arg207. The additional interactions are the aromatic ring electrons interacting with Ser185, Ser221 and Met218.

Docking in the active site was then evaluated for the *Pf*DXR enzyme; the remaining proteins, **3AU8**, **3AU9** and **3AUA** are all DXR crystal structures from *P. falciparum.* **3AU8** has no

inhibitor such as fosmidomycin and FR9000089 in the active site. All the structures contain a divalent cation and NADPH, and docking to this enzyme was mainly to study the interactions of the potential ligands in this *Pf*DXR. The reproducibility of binding for the **3AU8** under the docking method used could not be ascertained for validation due to this absence of a ligand in the crystal structure. However, the docking proceeded under the conditions described earlier which were validated. In Figure 27, the distribution of the ligands are compared between the proteins **3AU9** and **3AUA**. It is therefore essential for docking studies to include a known ligand template. From **3AU9** it was observed that only 5 ligands appear in the active site in the correct orientation as the crystal structure fosmidomycin while for **3AUA** there are 12 ligands that align with FR9000089.

Figure 27. Proteins **3AU9** and **3AUA** subunit A showing the distribution of 63 ligands; the majority of the ligands fall outside the binding cavity/site of the enzyme for **3AU9** and **3AUA**. The protein colour is by rainbow format and the structure with ligands and NADPH in stick representation with atom-type colour.[178]

Figures 28 and 29 details the results of docking one ligand; the interaction of **2a_NH** is analysed as docked in both proteins **(3AU9 and 3AUA)** against fosmidomycin and FR900089 respectively. As illustrated, the ligand (**2a_NH**) interacts with the same residues in both proteins and is oriented along with the template ligands (yellow). The ligand **2a_NH** exhibits

a “reverse” binding relative to fosmidomycin. The terminal carboxylic group is interacting with amino acids that interacted with phosphonate group in fosmidomycin. The compound has some inhibition of 82.11 nM, as per Ki value, which indicated that, although they bind differently to fosmidomycin, they have the potential to be inhibitors, which can be further researched. The ligands exhibiting “normal” binding were further analysed as these interactions are by the original design for specificity of this series of ligands. Since these interactions match those observed for a ligand with good binding and specificity, *viz* fosmidomycin, the potential analogues should aim to secure binding in a similar manner.

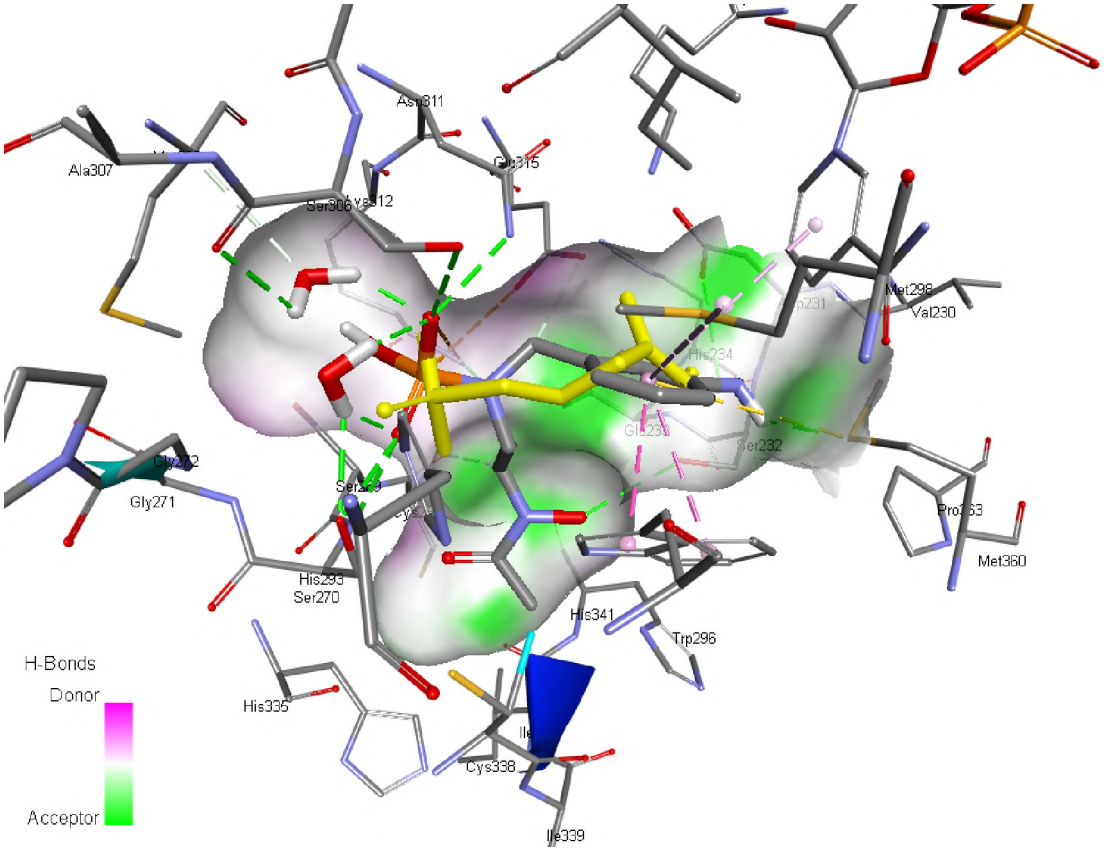

Figure 28. The protein **3AU9** DXR crystal structure with ligands in the active site; **2a_NH** and fosmidomycin (yellow) are in ball and stick with atom-type colour. The hydrogen atoms are not shown and dashed lines represent all interactions in distance in Å.[178]

Several other ligands also interact in docking with the active site residues in much the same way. The main difference is however that certain groups such as the terminal hydroxymethyl (**b**) or OH R group introduce further interactions with residues. The terminal

hydroxymethyl (**b**) was retained in the active site for smaller R groups regardless of methylene spacer length. Both Figures 28 and 29 reiterate how essential the template ligand is for the evaluation of potential ligands as the orientation and conformation is vital for the formation of known interactions.

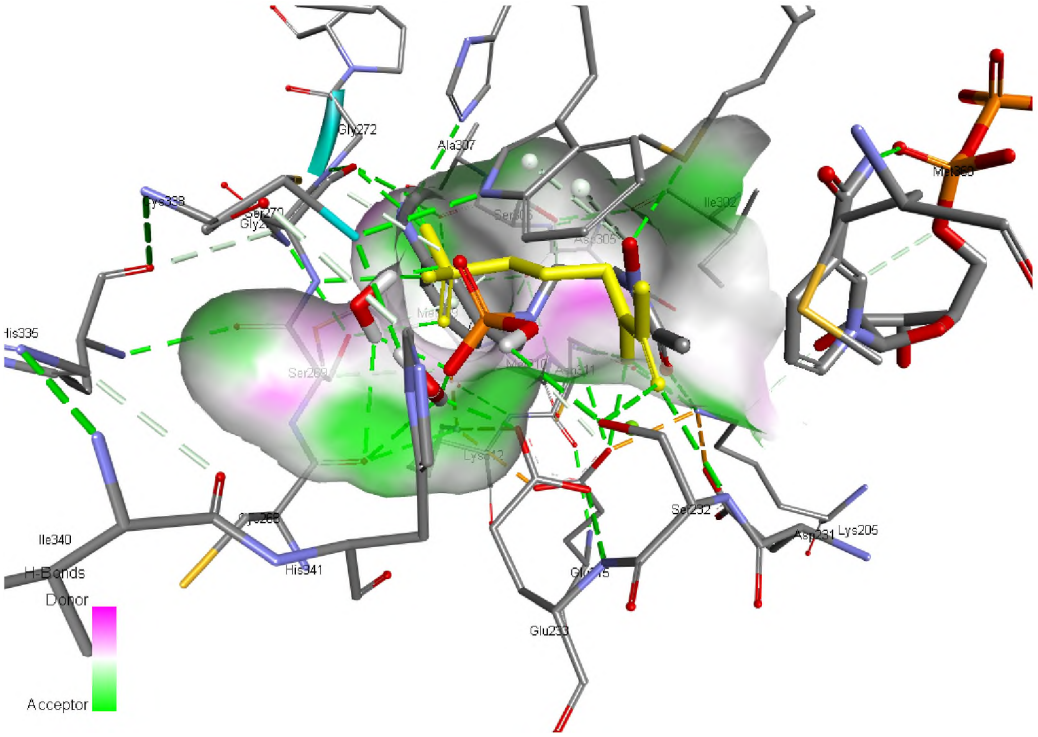

Figure 29. The protein **3AUA** DXR crystal structure with ligands in the active site; **2a_NH** and FR9000089 (yellow) are in ball and stick with atom type colour. The hydrogen atoms are not shown and dashed lines represent all interactions in distance in Å.[178]

A comparison of the calculated Ki values reveals some interesting information (Table 2). The inhibition constant (Ki) is the concentration of the inhibitor necessary for reducing the rate of the enzyme activity by half. This analysis was conducted to determine the various changes in the theoretical Ki that are observed for each of the proteins when the ligands were varied. The results which can be inferred from this data is that certain changes in R groups (R^1 or R^2) affect Ki and hence potentially exhibit inhibition.

Determining the Ki experimentally, although more accurate, can be time-consuming and tedious and thus, more frequently, theoretical calculations of inhibition constants are conducted. The calculations involve the plotting of fractional enzyme activity in the

presence of an inhibitor as a function of a constant enzyme and inhibitor concentration.[186] These values compare well with experimental values (on test cases that were used to calibrate the software) and therefore can be a good indicator of potentially potent inhibitors. In Figure 30 are the average Ki values (µM) for each protein is represented in a graph. The experimentally (computationally) acquired Ki values for fosmidomycin and FR900098 are 0.251 µM and 0.101 µM respectively, 187 therefore values closer or less than these show potential as lead compounds.

Table 2. The average Ki values and standard deviations for docked ligands for each of the six proteins.

Protein	Mean Ki (µM)	Ki St Dev (µM)
1Q0Lp	34,78	85,68
1Q0Qp	10,75	20,44
2EGHp	0,1539	0,6649
3AU9p	29,23	125,40
3AUAp	23,29	120,70

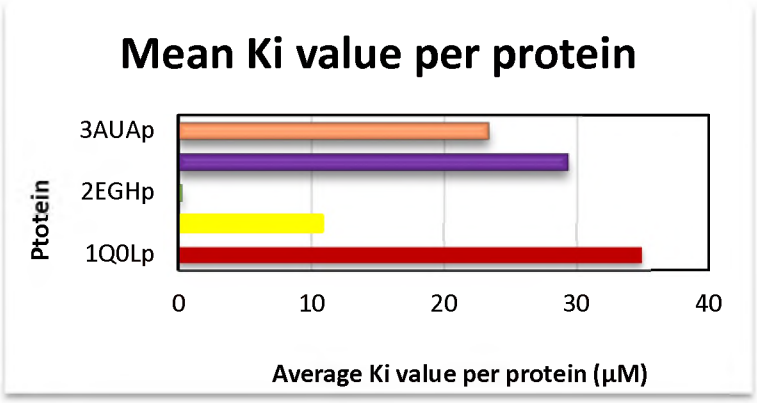

Figure 30. The average Ki values (µM) across the *Ec*DXR and *Pf*DXR protein.

The protein with the lowest average Ki is **2EGH** at 0.15 µM, while proteins **3AUA**, **3AU9**, **1Q0Q** and **1Q0L** have average Ki of 23.29, 29.23, 10.75 and 34.24 µM, respectively. Another analysis was of the average Ki value as the methylene spacer increases (Table 3 and Figure 31) for each of the ligands. The expectation is that the longer the methylene spacer **(2–4)**,

the higher the average Ki. However, due to the effect of phenyl group interactions aligning with the template ligand and allowing the rest of the chain to occupy a different pocket as well as the terminal hydroxymethyl **(c)** forming additional interactions in the protein cavity, the Ki values vary for each protein.

Table 3. The average Ki value for each of the proteins by length of methylene spacer i.e. 2–4 methylene groups in chain.

Ki mean per chain length (µM)	1Q0Lp	1Q0Qp	2EGHp	3AU9p	3AUAp
2	59,7581215	14,85521	0,132197	0,039902	34,13813
3	24,1891424	11,87607	0,049761	65,15088	34,60815
4	20,9232165	5,241746	0,285917	22,1587	0,030747

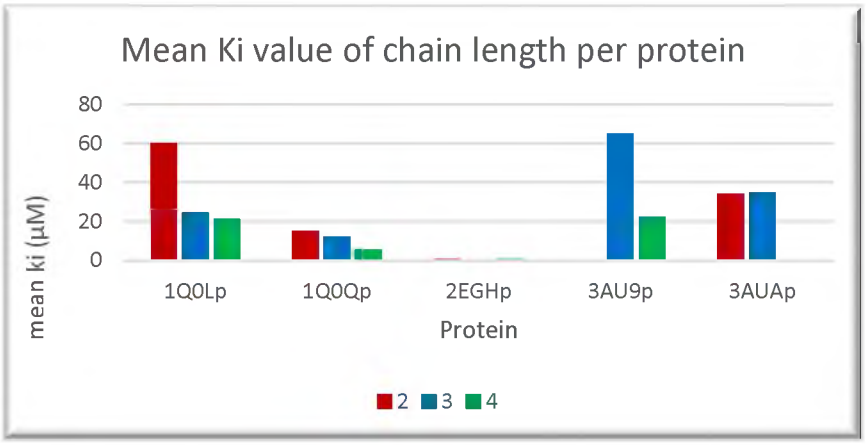

Figure 31. The average Ki values (µM) across the *Ec*DXR and *Pf*DXR protein as the length of the methylene spacer increases.

The studies conducted were to evaluate the binding site of *Ec*DXR and *Pf*DXR by using known inhibitors, fosmidomycin and analogues, to analyse and assess the active site by varying the chain length of the methylene spacer, changing the terminal group and introducing various *N*-benzyl derivatives. The results indicated that although exceptions occur in all cases, i) the two methylene spacer group proved vital for accurate orientation and conformational interactions to occur in the binding cavity, ii) the change of methyl

terminal group to ethyl led to the majority of ligands being excluded from the binding site while the hydroxymethyl resulted, unexpectedly to mostly "reversed" binding as well as formation of further interactions with its hydroxyl group, and iii) The majority of the smaller R groups allowed ligands to bind in the active site, in some instances, irrespective of chain length and terminal group while the larger R group hindered the ligand entrance into active site.

The analysis of the theoretical Ki values calculated confirms the molecular modelling data. The enzyme-ligand relationship in these docking studies is not straight forward. The presence of certain groups enables better binding and interaction even when factors that are supposed to exclude these exist. It is therefore important that further analysis of this data is conducted so that trends based on all factors are determined which could lead to novel "reverse" fosmidomycin-based lead compound and the inclusion of more terminal groups that contain interacting groups such as the hydroxymethyl.

Analysis of the docking studies resulted in **2a_H**, **2a_OH**, **2a_SH**, **2a_NH$_2$**, **2a_Cl** and an additional **2a_NO$_2$** to be taken further into synthesis. The synthesis kept the R^1 group constant as well as the methylene spacer while varying R^2. The 3-nitrobenzyl in the α-aryl-substituent was introduced in order to evaluate the effect of a strongly electron withdrawing group effect on electron density. The dichloride substituted analogues were found to be high in inhibition[193] and thus **2a_Cl** was synthesised as a dichlorobenzyl compound. **2a_H** had a calculated average Ki of 1.16 μM across all 5 proteins, **2a_OH** had 0.42 μM, **2a_SH** had 0.18 μM, **2a_NH$_2$** had 3.65 μM and **2a_Cl** had 8.97 μM.

2.2. Synthesis of *N*-benzyl substituted phosphoramidates

2.2.1. *N*-Benzyl substituted phosphoramidate derivatives

The *Ec*DXR and *Pf*DXR crystal structure docking studies with the known inhibitor fosmidomycin and DXP revealed critical amino acid residues in the active site of DXR that are essential for effective binding as well as inhibition in the case of fosmidomycin. Docking studies have illustrated the presence of three additional binding pockets,[176] which we exploit in the synthesis of novel lead compounds. The previous research groups introduced the α-aryl-substituent which according to docking studies occupies the newly identified pockets thus strengthening the binding and providing bases for increased inhibition.

The structure-activity studies of fosmidomycin and FR9000089 revealed the importance of the tri-methylene spacer, the phosphonate group and a metal binding moiety such as nitrogen or oxygen groups in the potential ligands. This was also observed during the molecular modelling of the *N*-benzyl substituted phosphoramidate derivatives, where the increase in the length of the hydrophobic patch reduced entry into binding site and oxygen and nitrogen groups were seen co-ordinating to the divalent metal cation in the DXR active site. The *N*-benzyl substituted phosphoramidate derivatives **34a-f** are fosmidomycin analogues which conserve the essential phosphonate and hydroxamate functional groups in fosmidomycin but include the substituted benzyl group designed to occupy an additional binding pocket.

In this section, attention is focused on the multi-step synthesis of such compounds (**34a-f**; Scheme 1). Some of the compounds have been prepared previously[176,177] but additional material was required for bioassay purposes; others (**34e-f)** are new. These latter compounds contain the 3-nitrobenzyl group as the α-aryl-substituent to permit evaluation of the effect of a strongly electron-withdrawing group on the electron density and binding of the phosphonate, since 3,4-dichlorobenzyl analogues scaffolds have been shown to increase inhibition of *Pf*DXR.[193]

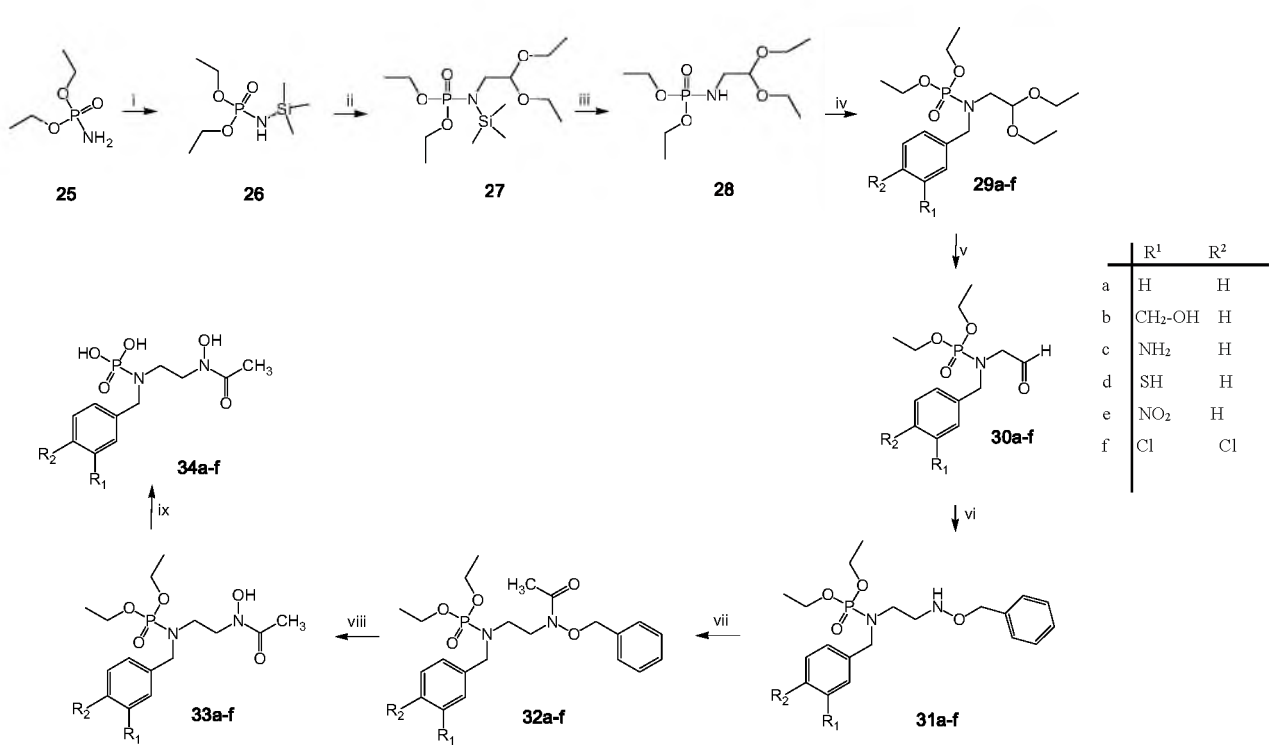

Scheme 1. Synthesis of *N*-benzyl substituted phosphoramidic derivatives.

Reagents and conditions; i) Hexamethyldisilizane, benzene, 80^0C ii) NaH, benzene, rt, bromoacetaldehyde diethyl acetal, TBAB, 80^0C, 4 h iii) EtOH, 80^0C, 1h iv) NaH, THF, benzyl halide, rt, 24 h v) 2M HCl, rt, 24 h vi) *O*-benzylhydroxylamine, MeOH, 40^0C, 3 h then $NaBH_3CN$, MeOH, conc. HCl, 1 h, $NaBH_3CN$, 1 h vii) acetyl chloride, triethylamine, DCM, 0^0C, N_2, 24 h viii) Pd/c, dry MeOH, H_2, 18 h then ix) TMSBr, DCM, 0^0C, DCM, H_2O, 24 h.

The first three steps in the synthesis of *N*-benzyl substituted phosphoramidic derivatives **25-28** are illustrated in scheme 2. Using a method reported by Zwierzak *et* al.,[193] diethyl phosphoramidate **25** was converted into the silylated derivative **26** in 98 % yield. The silylated amine was then deprotonated using sodium hydride and reacted with bromoacetaldehyde diethyl acetal; removal of the TMS group was effected in the presence of the catalyst (TBAB) in ethanol to afford the intermediate **28** in 92 % yield.

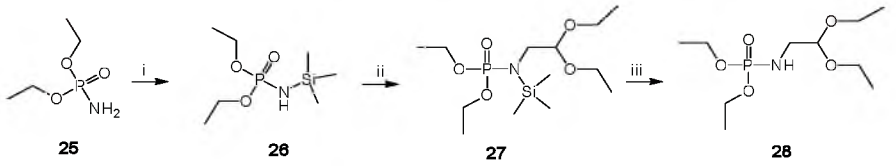

Scheme 2. The protection of diethyl phosphoramidate during the preparation of the diethyl acetal.
Reagents and conditions: i) Hexamethyldisilizane, benzene, 80^0C ii) NaH, benzene, rt, bromoacetaldehyde diethyl acetal, TBAB, 80^0C, 4 h iii) EtOH, 80^0C, 1h.

Figure 32 illustrates the ^{1}H NMR spectrum of the silylated derivative **26** with the silyl methyl groups resonating as a 9 proton singlet at 0.10 ppm, the methyl and methylene protons of diethyl acetal moiety resonating at 1.20 ppm and 3.91 ppm, respectively and the amine proton at 2.72 ppm. This product was found to be highly hygroscopic, and therefore needed to be taken immediately to the next step or stored in an air-tight container.

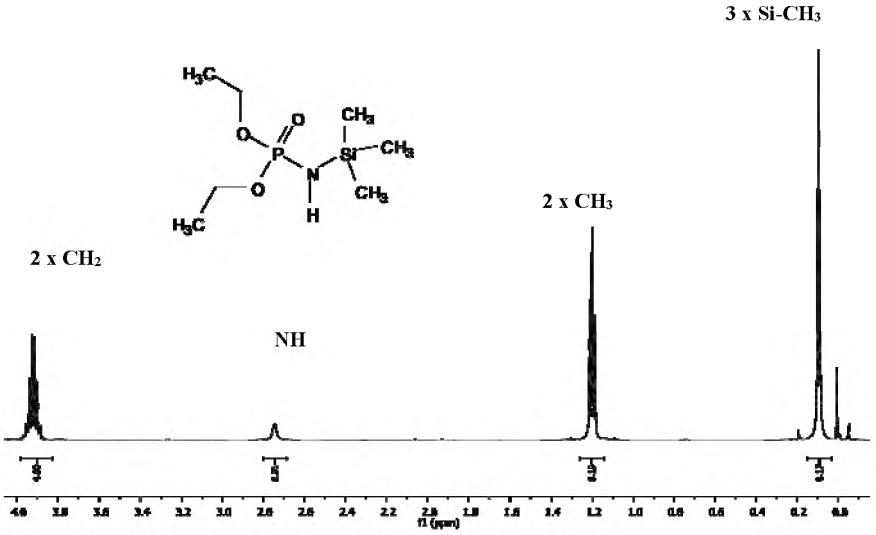

Figure 32. 600 MHz ^{1}H NMR spectrum of compound **26** in $CDCl_3$.

In the ^{13}C NMR spectrum of compound **28** (Figure 33), the phosphonate and acetal methyl carbons resonate at *ca*. 15 ppm, the amide methylene carbon at 31 ppm, the diethyl ether methylene carbons at 65.25 ppm and the phosphonate ester methylene carbons at 102 ppm.

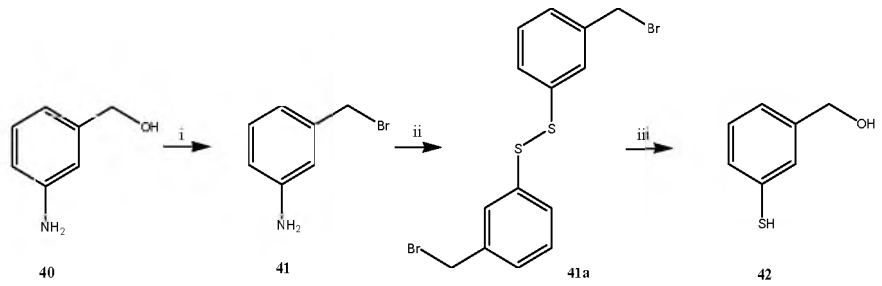

Scheme 3. Preparation of amino and mercapto benzyl halides.

Reagents and conditions: i) PBr_3, DCM, 0^0C, 1 h then rt 25 h ii) H_2O, HCl, $NaNO_2$, Na_2S_2, 0^0, 1 h iii) $NaBH_4$, 0^0 then rt, 1h.

In the next step in Scheme 1, (step iv), the synthesis involves the introduction of the various benzyl substituents to afford the tertiary phosphoramides **29a-f**. The benzyl halides of **29c-d** were not commercially available and were therefore synthesised according to Scheme 3. The synthesis of 3-aminobenzyl bromide **41** involved the reaction of 3-aminobenzyl alcohol with phosphorous tribromide; subsequent treatment of the white product with 1 equivalent of potassium hydroxide afforded compound **41** in 77 % yield. Compound **41** was in turn used in the synthesis of **42**; thus 3-aminobenzyl bromide **41** was reacted with sodium nitrite resulting in a diazonium salt which was treated with sodium disulphide to produce a disulphide intermediate **41a** which was then reduced using sodium borohydride in THF to yield the 3-mercaptobenzyl bromide in 65% yield. The percent yields obtained from Scheme 1 are shown in Table 4.

Table 4. Percentage yields obtained for the synthesis of *N*-benzyl phosphoramidate derivatives **25-29 (a-f)** in the synthetic route **Scheme 1**.

Ar-R	Percentage yield (%)
2	98
4	92
5a	57
5b	35
5c	50
5d	65
5e	20
5f	31

Figures 34 and 35 illustrate the ^{1}H NMR spectra of compounds **41** and **42**, respectively. In Figure 34, the amine protons are observed to resonate at *ca.* 5 ppm, the methylene protons at 4.35 ppm and the four aromatic protons between 6 and 7 ppm. Figure 35 illustrates the mercapto proton signal at 3.65 ppm, the methylene signal at 4.61 ppm and the four aromatic proton signals resonate in the range 6.60 – 7.22 pp

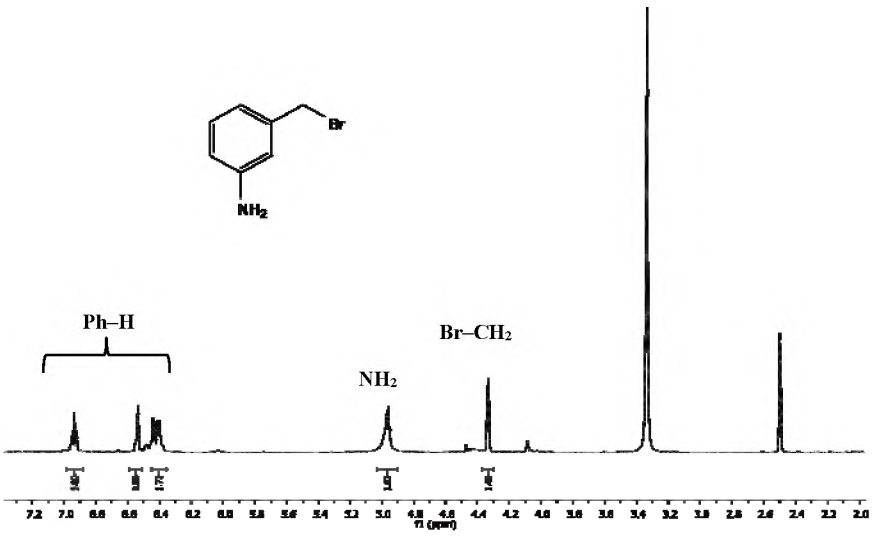

Figure 34. 600 MHz ^{1}H NMR spectrum of compound **41** in DMSO-d_6.

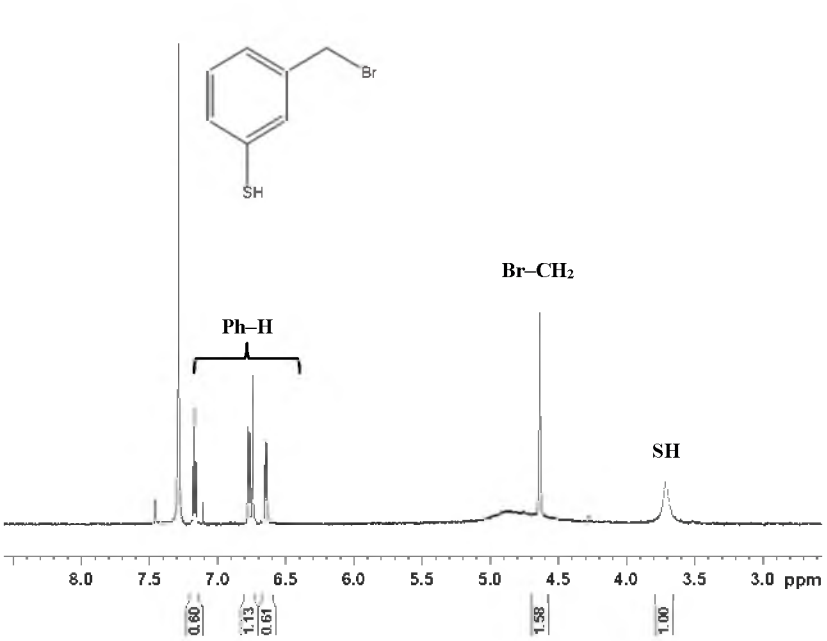

Figure 35. 600 MHz ^{1}H NMR spectrum of compound **42** in $CDCl_3$.

In the next step (step iv) of the synthesis the various benzyl halides were attached to thye nitrogen of the phosphoramidate moiety. The introduction of an *N*-benzyl group, rather than a *N*-benzyl group, was done to avoid generating a chiral centre and consequent problems with asymmetry. The NH group in compound **28** was deprotonated with sodium hydride then reacted with the corresponding benzyl halides **29a-f** with yields of 20–65 %. The yields were low but time didn't permit for optimisation.

Due to the hygroscopic nature and ready decomposition of the silyl derivative **26**, it was essential that benzylation be conducted immediately. Various techniques were attempted to combat the decomposition of compound **26**, and its synthesis had to be repeated several times; this step should ideally be a one-pot reaction yielding the intermediate **28** to minimise decomposition.

Figure 36 illustrates the ^{13}C NMR spectrum of the *N*-benzylated compound **29d** with the aromatic carbons resonating downfield at *ca.* 128 ppm. The benzylic carbon resonates at 47.15 ppm and the methylene and acetal carbons at *ca.* 63 ppm and 103 ppm, respectively, while the signals corresponding to the methyl groups appear at *ca.* 16 ppm.

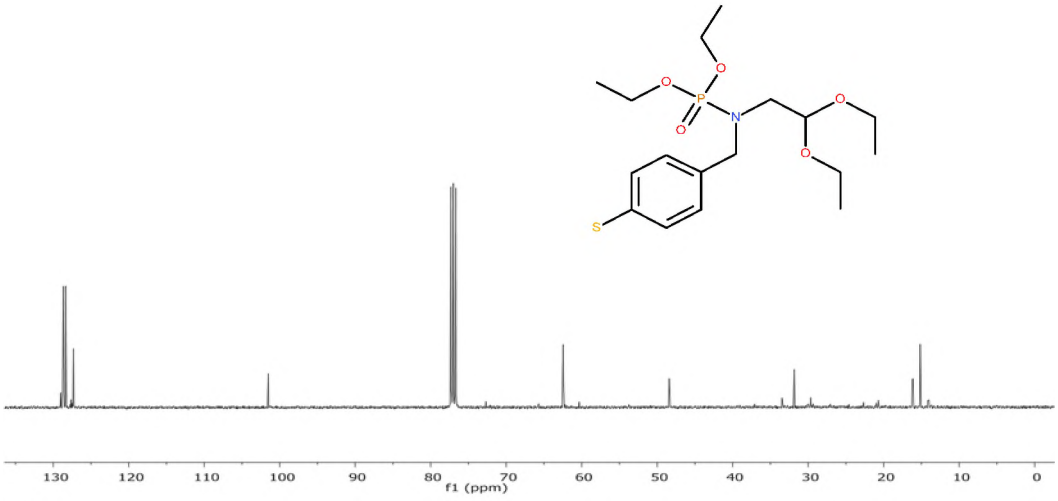

Figure 36. 400MHz ^{13}C NMR spectrum of compound **29d** in $CDCl_3$.

Figure 37 illustrates the ^{1}H NMR spectrum of compound **29a** with the aromatic protons of the benzyl group resonating between 7.33 ppm and 7.48 ppm, while the signal corresponding to the benzylic protons appears at ca. 4.5 ppm. The phosphonate methylene protons resonate as pair of multiplets at *ca.* 3.6 ppm and the methyl protons below 1.5 ppm.

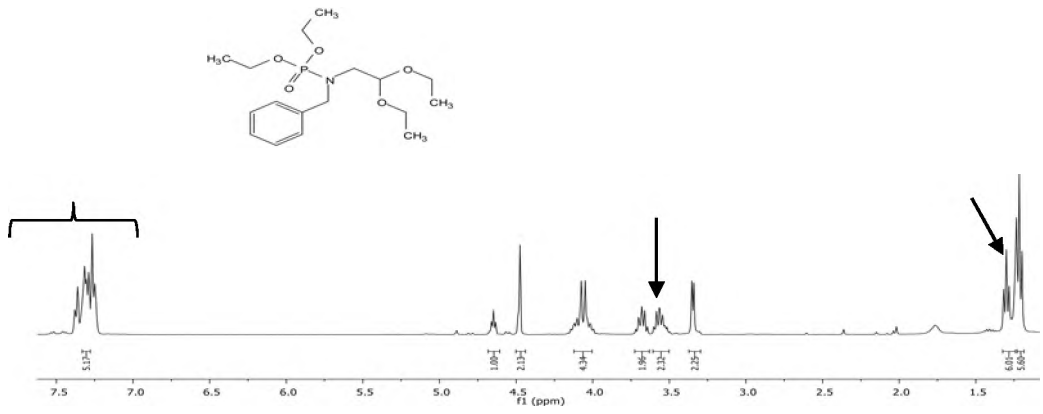

Figure 37. 600 MHz ^{1}H NMR spectrum of compound **29a** in $CDCl_3$.

The benzyl substituent introduces a bulky hydrophobic group to take advantage of the third binding pocket available in the DXR binding cavity and permits substitution without introducing the problem of chirality. The acetal protecting group was removed by acid-catalysed hydrolysis to afford each of the aldehydes **30a-f**.

The NMR spectra of all compounds confirms the presence of an aldehyde which can be seen in the ^{1}H NMR spectrum of compound of **30e** (Figure 38) from which the diethyl acetal signals are absent and the aldehyde proton signal present at 9.55 ppm. The methylene protons adjacent to the aldehyde group resonate at 3.82 ppm, while the signal at 4.25 ppm corresponds to the benzylic methylene protons. The phosphonate ethyl ester signals resonate, characteristically, at 1.26 ppm and 4.13 ppm. The signals in the aromatic region integrate, as expected, for the four aromatic protons.

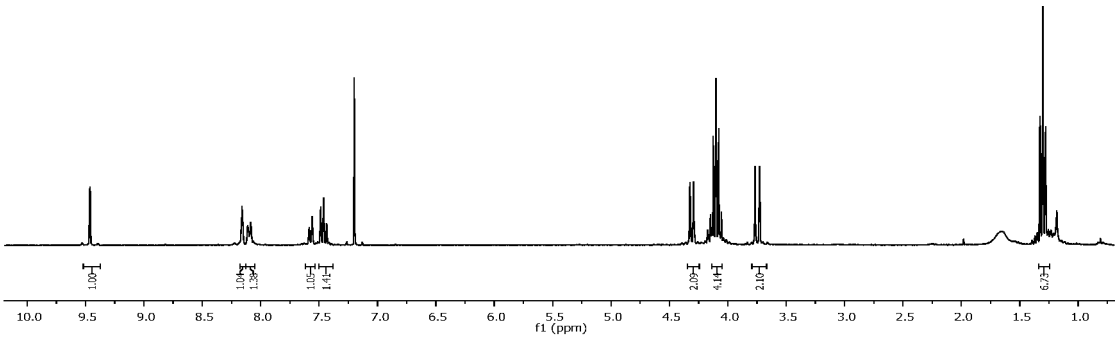

Figure 38. 600MHz ^{1}H NMR spectrum of compound **30e** in $CDCl_3$.

Figure 39 illustrates the HRMS data for the aldehyde **30f** with a pseudo-molecular ion (MH^+) peak at *m/z* 354.042 corresponding to the elemental composition $C_{13}H_{19}NO_4PCl_2$.

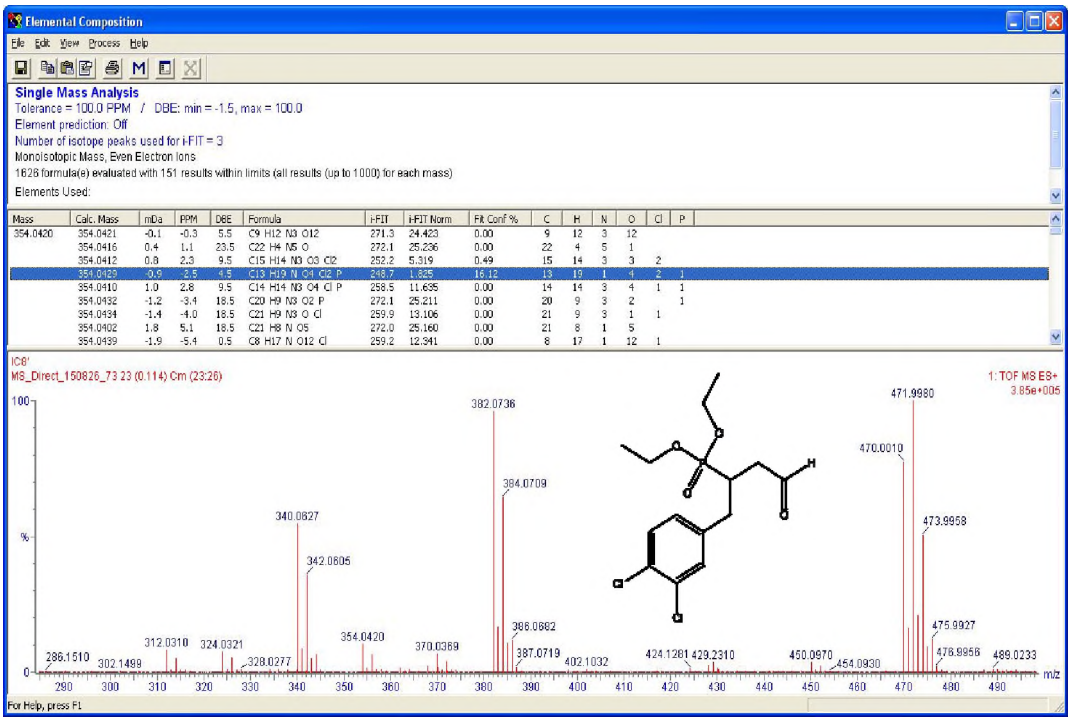

Figure 39. HRMS data for compound **30f.**

The next step involved reductive amination of the aldehydes **30a-f** using *O*-benzylhydroxylamine and sodium cyanoborohydride were used to furnish, via an oxime intermediate, the *O*-benzyl-protected amines **31a-f** (Scheme 4). Acetylation of compounds **31a-f** was achieved by using acetyl chloride in the presence of triethylamine, to obtain the *O*-benzyl-protected acetyl derivatives **32a-f**. The *O*-benzyl-protection allows for the selective acetylation of the second nitrogen which through reduction will yield the hydroxamate moiety which is essential for co-ordination to the divalent metal ion.

Figure 40 illustrates the HRMS data of the benzyloxyamino derivativeprotected **32e**, with a pseudo-molecular ion (MH^+) peak at *m/z* 438.1792 corresponding to the elemental composition $C_{20}H_{29}N_3O_6P$, while Figure 41 illustrates the 1H NMR spectrum of compound **32c**.

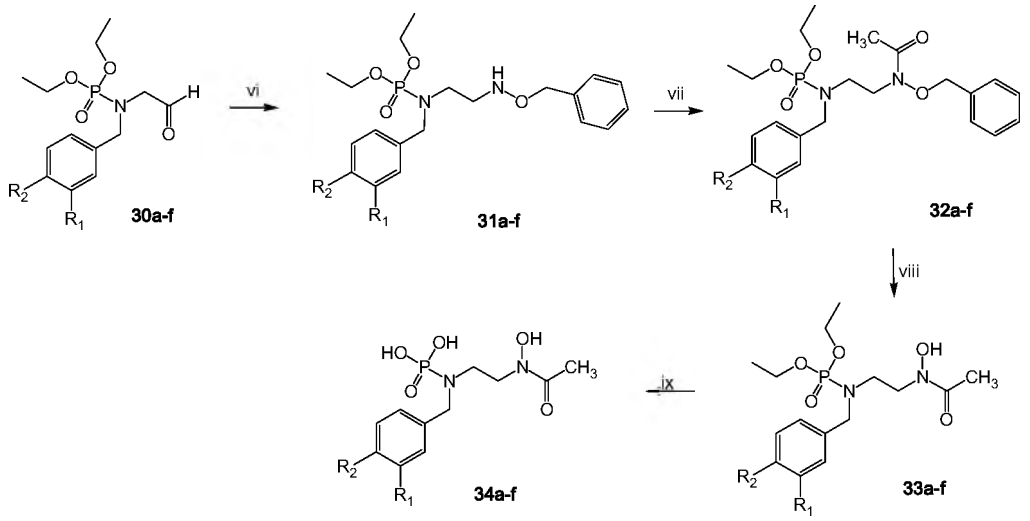

Scheme 4: Synthesis of *N*-benzyl-substituted phosphoramidic acid derivatives.
Reagents and conditions: vi) *O*-benzylhydroxylamine in MeOH, 40^{0}C, 3 h and then $NaCNBH_3$, MeOH, HCl, r.t., 1 h vii) acetyl chloride, DCM, Et_3N, r.t., 24 h, N_2 viii) H_2, Pd/C, MeOH ix) TMSBr, DCM, 0^{0}C, 1 h and then H_2O, r.t., overnight.

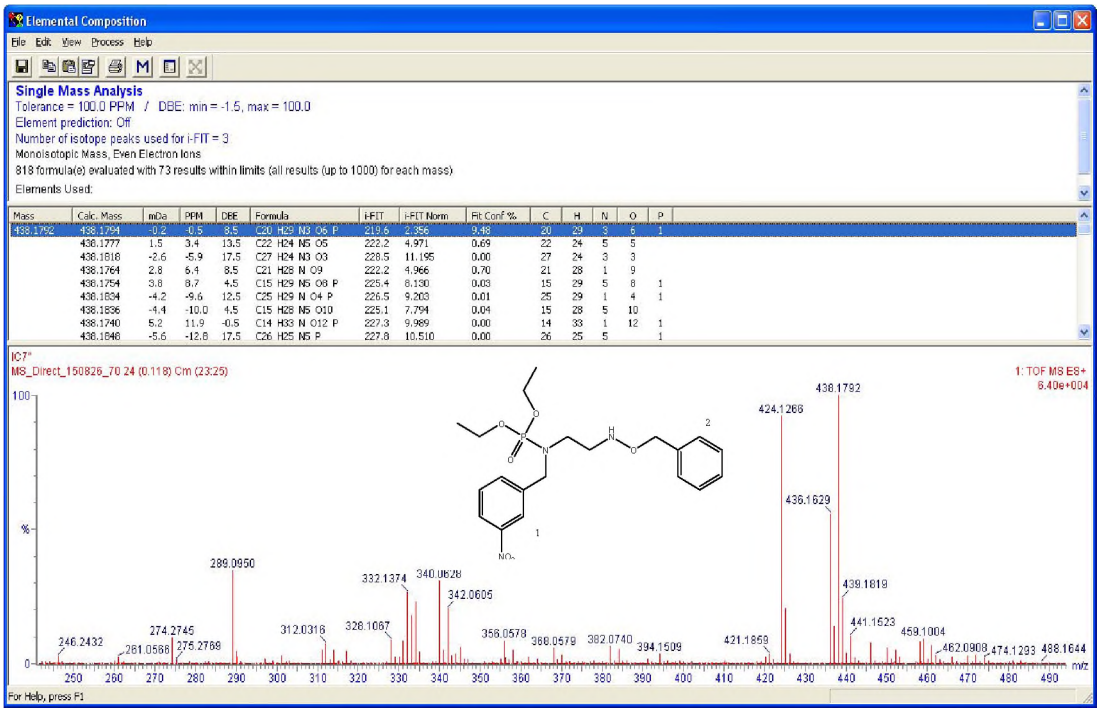

Figure 40. HRMS data for compound **31e**.

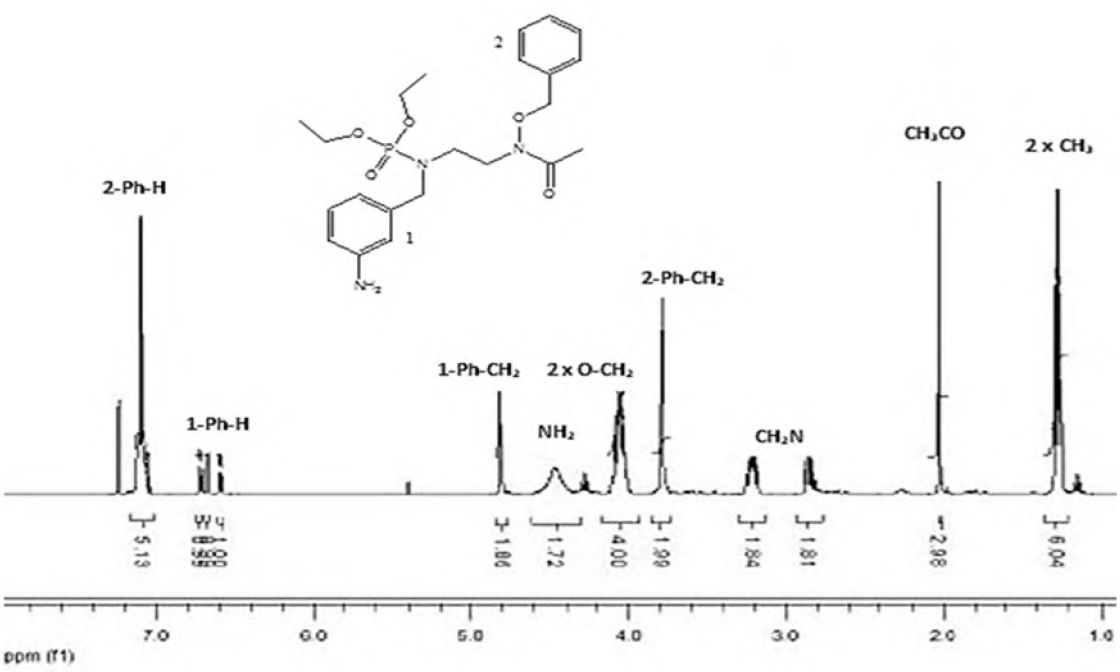

Figure 41. 400MHz NMR of compound **32c** in $CDCl_3$.

The final two steps in the overall synthesis of the target compounds **34** involved removal of the *O*-benzyl protecting group and hydrolysis of the diethyl phosphoramidate ester groups (Scheme 5). The *O*-benzyl protecting group was removed from the intermediates **32** by catalytic hydrogenolysis using 10% Pd/C in methanol to yield the corresponding hydroxamate derivatives **33**. Treatment of these derivatives with TMSBr, followed by hydrolysis, yielded the corresponding phosphoramidic acids **34**. (It is, of course, possible that the diethyl ester intermediates **33a-f** could, themselves, serve as ester pro-drugs, affording the corresponding phosphoramidic acids **34a-f**, through *in vivo* hydrolysis by esterases.) Unfortunately, the yields obtained for the intermediates **32e** and **32f** were too low to continue to compounds **33e** and **33f** and **34e** and **34f**, and time did not permit repetition of the preceding seven steps to generate more of the intermediate compounds. Consequently, the final two steps were completed using compounds **32a-d**. Small but sufficient quantities of compounds **33a-d** and **34a-d** were isolated to permit their characterization.

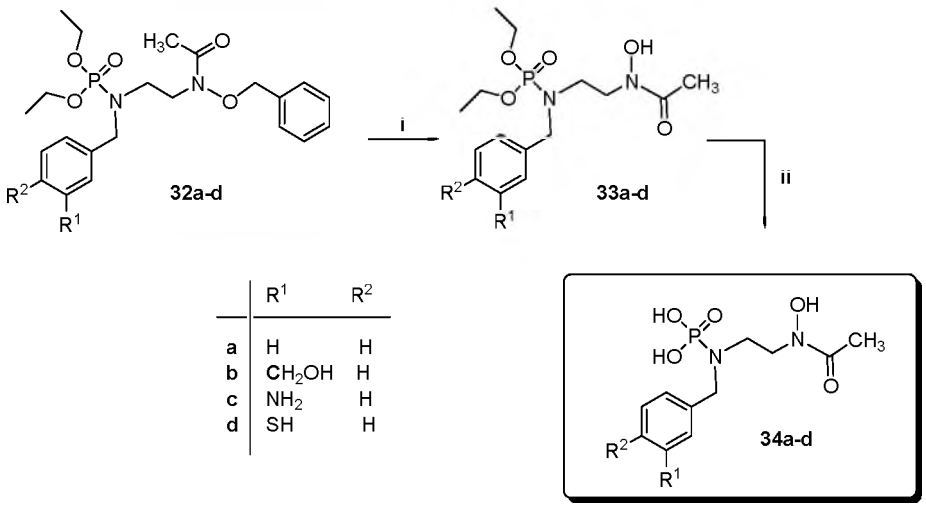

	R^1	R^2
a	H	H
b	CH_2OH	H
c	NH_2	H
d	SH	H

Scheme 5. (Steps viii-ix in overall synthetic sequence)
Reagents and conditions: i) H_2, Pd-C, MeOH; ii) TMSBr, DCM; then H_2O.

Figure 42 illustrates the ^1H NMR spectrum of compound **34d** in D_2O, while Figure 43 illustrates the DEPT135 spectrum of compound **34a**.

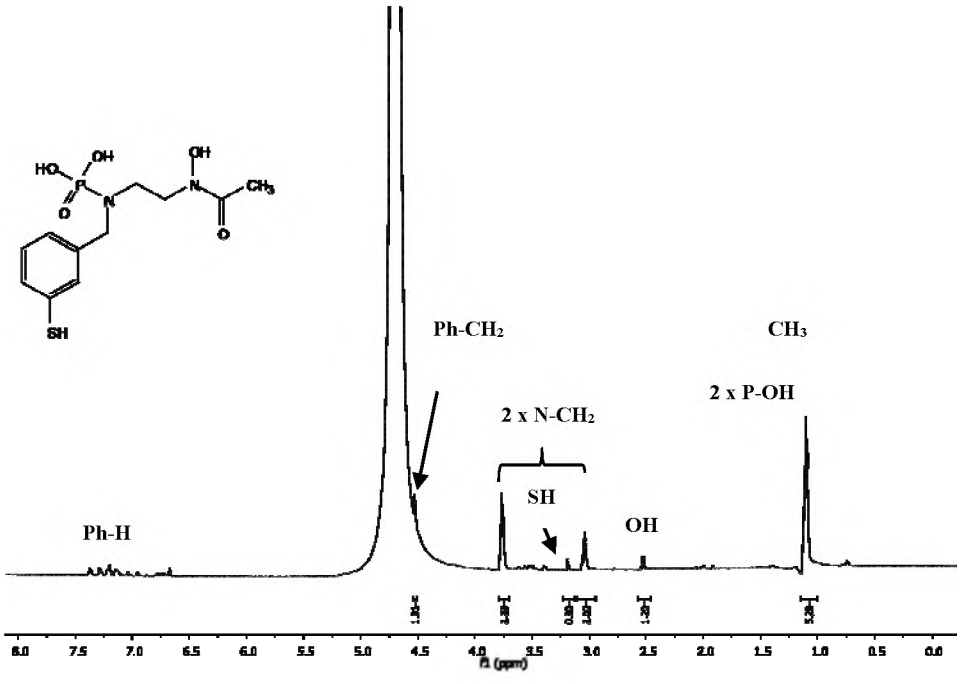

Figure 42. ^1H NMR of compound **34d** in D_2O.

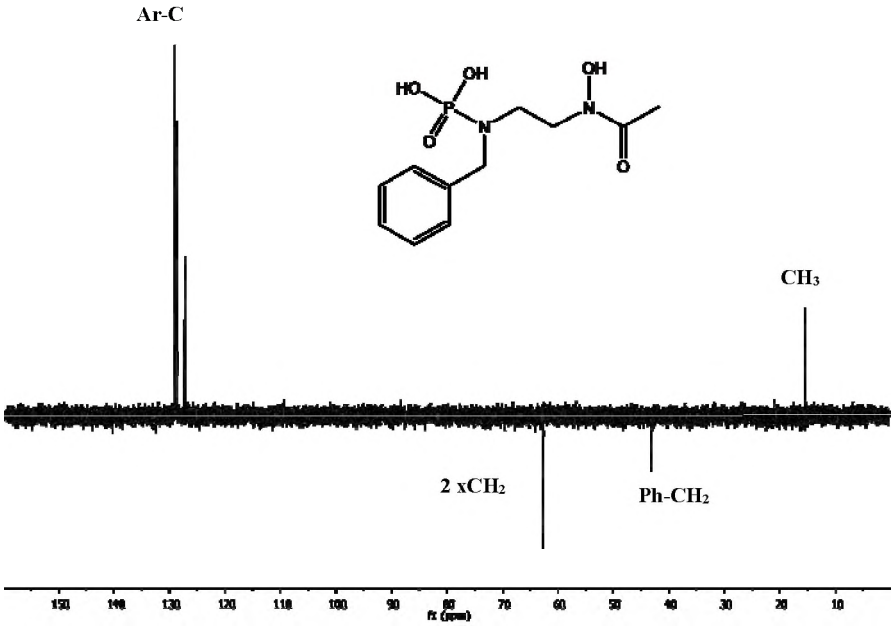

Figure 43. DEPT135 NMR of compound **34a** in D_20.

Compounds **34e** and **f** were not fully characterised at this stage as the yield in the previous synthetic step was very low. The yields for compounds **10a-d** were also low but some 2-D NMR experiments and bioassays could be conducted. Optimisation of the reaction conditions for all compounds would lead to higher yields. The molecular modelling data revealed that the DXR binding cavity is flexible and, consequently, structurally diverse compounds can fit into the binding site. Further analysis of the data will reveal the types of ligands that can bind as well as functional groups available in the ligands that can enhance attachment to the binding cavity.

2.3. Enzyme inhibition studies

The target enzyme DXR is involved in the pathway whereby DOXP is converted to MEP through intramolecular conversion with co-factor NADPH which performs the subsequent reduction.[157,158] The bioassays involved the spectroscopic measurement of the conversion of NADPH to NADP of enzyme (*Pf*DXR) with known inhibitor compared to where there is one of the synthesised ligands bound at the active site of the enzyme. Cytotoxicity studies were also conducted for each of the ligands compared to a known inhibitor that has a high toxicity towards *Pf*DXR enzyme. Cytotoxicity is a measure of drug-induced cell death, where the concentration is gradually increased and the cell viability is measured until at higher concentrations cell death usually occurs.[188] Cytotoxicity (using Hela cells) and PLDH assays were conducted using 20mM solutions in DMSO of the synthesised compounds in triplicate.[190,191]

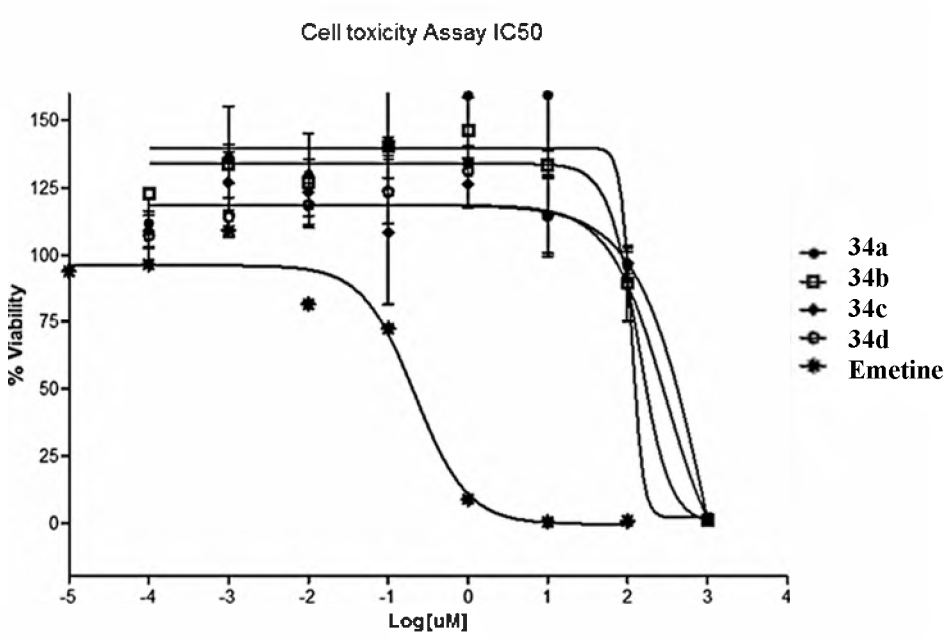

Figure 44. The cytotoxicity IC_{50} values of known inhibitor, emetine and synthesised ligands illustrating percentage viability at increased concentrations of inhibitor.

The cytotoxicity screening of the ligands; **34a**, **34b**, **34c** and **34d** was conducted using emetine, a natural alkaloid with an anti-protozoal properties,[192] as a standard. The results illustrated in Figure 44 reveal that none of the ligands are cytotoxic < 100 μM compared with emetine which exhibits high toxicity at much lower concentrations.

For each of the assays the IC_{50} value was determined to establish the ligand concentration at which 50% inhibition is observed.[189] As shown in Figure 45, chloroquine has an IC_{50} value of < 0.1 μM while the synthesised ligands; **34a**, **34b**, **34c** and **34d** have values > 100 μM.

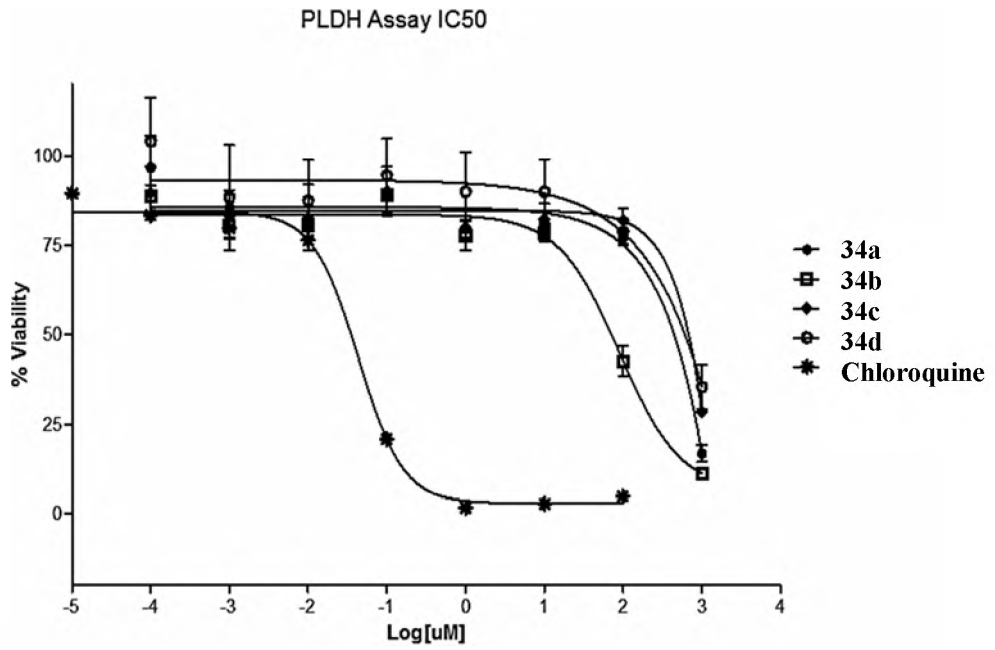

Figure 45. The IC_{50} values for inhibition assay of *Pf*DXR enzyme by ligands; **34a**, **34b**, **34c** and **34d** compared to known inhibitor chloroquine, illustrating percentage viability of cell and increasing concentrations of ligand.

2.4. Conclusions

The aims indicated in this research was to evaluate the DXR enzyme active site by introducing variation in the structure of fosmidomycin analogues which would allow for the determination of the binding site flexibility, affinity as well as structural limitations that the site dictates for activity to occur. Our research project consisted of 3 phases; phase 1 was the computational study of analogues on DXR enzyme, phase 2 was the synthesis of certain analogues that conserved groups essential for activity and finally, phase 3 entailed the use of bioassay to observe inhibition exhibited by these analogues.

The *in silico* studies conducted with both *Ec*DXR and *Pf*DRX on the *N*-benzyl phosphoramidate derivatives reveal high selection for the 2 methylene spacer and methyl terminal group, although exceptions occur. This is an observable trend throughout all proteins. A series of novel *N*-benzyl phosphoramidate derivatives were successfully synthesised. The *N*-benzyl derivatives were then used in bioassay against chloroquine and showed low inhibition and toxicity. The additional derivatives, the 3-nitro and 3,4-dichloro analogue were obtained in low yield and there was not sufficient time to adjust synthetic techniques for these compounds.

While it was unfortunate that the analogues' inhibitory activity was significantly lower than that of the known inhibitor fosmidomycin and chloroquine, these new compounds provide greater insight and depth to our studies in this area.

Future research in this area is being focused on the following:

i) Completion of the synthesis of the 3-nitro- and 3,4-dichlorobenzyl ligands (**34e** and **34f** respectively)

ii) Preparation of larger quantities of all the ligands **34a-f** for bioassay purposes– particularly for *Pf*DXR inhibition assays; and

iii) Optimization of the synthesis and evaluation of a range of furan derivatives as conformationally constrained DOXP analogues.

3. Experimental

3.1. Synthetic Methodology

General

Synthesis and purification

Starting materials were obtained from Sigma-Aldrich and used without purification. THF and benzene distilled from sodium wire and benzophenone under nitrogen. DCM and DMF were dried in calcium hydride and distilled under nitrogen. Normal phase thin layer chromatography plates were used for purification and viewed under UV light (254 nm). Flash chromatography was conducted using silica gel 60 (70-230 mesh) for normal phase.

Analysis and Characterisation

NMR spectra was performed on Bruker 400 and 600 MHz spectrometers (T =298 K) and was calibrated on the residual protonated solvent signals (for $CDCl_3$: δ_H = 7.26 ppm; δ_C = 77.00 ppm). High resolution mass spectroscopy was performed on a waters API Q-TOF Ultima spectrometer,[193] using ionisation mode.

3.1.1. The Synthesis of *N*-benzyl substituted phosphoramidate derivatives.

Diethyl *N*-(trimethylsilyl)phosphoramidate 26

A solution of diethyl phosphoramidate (5.0 g, 33 mmol) **25** in benzene (10 ml) was made up under Ar gas. Through a septum, hexamethyldisilizane (4.1 ml, 20 mmol) was added while stirring. The resulting mixture was heated under reflux in an oil bath at 80 ^{0}C for 3 hours. The excess solvent was then removed under reduced pressure at 60^{0}C for an hour to yield diethyl *N*-(trimethylsilyl) phosphoramidate **26**, a brown oil which formed highly hygroscopic cream-coloured crystals when cool (4.4524 g, 98%). δ_H/ppm (600 MHz; $CDCl_3$) 0.10 (9H, s, 3 x CH_3Si), 1.20 (6H, t, *J* = 7.2 Hz, 2 x CH_3), 2.79 (1H, s, NH) and 3.85 – 4.00 (4H, m, 2 x O-CH_2); δ_C/ppm (600 MHz; $CDCl_3$) 0.6 (d, *J*P–C = 2.4 Hz, 3 x CH_3Si), 16.2 (d, *J*P–C = 7.3 Hz, 2 x CH_3) and 61.9 (d, *J*P–C = 5.3 Hz, 2 x O-CH_2).

Diethyl *N*-(2,2-diethoxyethyl) phosphoramidate 28

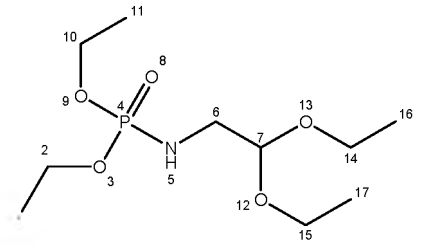

To a stirred solution of sodium hydride (60 % dispersed in mineral oil; 1.07 g, 26.8 mmol) in dry benzene (10 ml) was added through an addition funnel, a solution of diethyl *N*-(trimethylsilyl)phosphoramidate (5.0 g, 22 mmol) **26** in dry benzene (30 ml) slowly over 30 min under N_2 gas. Bromoacetaldehydediethyl acetal (3.3 ml, 22 mmol) and tetrabutylammonium bromide (0.71 g, 22 mmol) were then added to the stirred solution and the resulting mixture was refluxed at 80^0C for 4 hours. EtOH (18 ml) was then added drop-wise and the mixture was further refluxed for another 1 hour. After cooling, EtOAc (100 ml) was added and the organic solution was washed with water (2 x 20 ml). The aqueous layers were combined and extracted with EtOAc (3 x 10 ml), the organic layers were then combined and dried with anhydr. $MgSO_4$ and the solvent evaporated *in vacuo* 30^0C-40^0C, yielding diethyl *N*-(2,2-diethoxyethyl) phosphoramidate **28**, a dark brown oil (5.6798 g, 92 %). δ_H/ppm (600 MHz; $CDCl_3$) 1.16 (6H, t, *J* = 7.2 Hz, 2 x OCH_2CH_3), 1.25 (6H, t, *J* = 7.2 Hz, 2 x $POCH_2CH_3$), 3.94 (1H, s, NH), 3.29 (2H, d, *J* = 5.2 Hz, CH_2N), 3.51 and 3.62 (4H, m, 2 x O–CH_2), 4.00 (4H, m, 2 x PO–CH_2) and 4.59 (1H, t, *J* = 5.4 Hz, CH); δ_C/ppm (600 MHz; $CDCl_3$) 15.0 (2 x OCH_2CH_3)), 15.5 (d, *J*P–C = 6.5 Hz, 2 x $POCH_2CH_3$)), 31.9 (CH_2N), 61.8 (d, *J*P–C = 5.8 Hz, 2 x O–CH_2), 62.5 (2 x PO–CH_2) and 101.1 (C-H).

Diethyl *N*-benzyl-*N*- (2,2-diethoxyethyl) phosphoramidate 29a

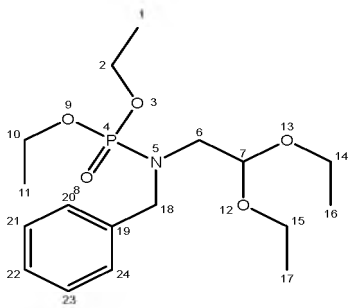

To a stirred solution of diethyl *N*-(2,2-diethoxyethyl) phosphoramidate (1 g, 37 mmol) **28** in dry THF (20 ml) under N_2 gas, NaH (60 % dispersion in mineral oil; 0.20 g, 74 mmol) was added in small portions to permit controlled evolution of hydrogen gas. A solution of benzyl bromide (0.44 ml, 3.7 mmol) in dry THF (5 ml) was added and the resulting solution was stirred at room temperature (~25^0C) for ca. 24 hours. The solvent was evaporated *in vacuo* and the residue extracted with EtOAc (2 x 25 ml). The organic layer was sequentially washed with saturated aq. $NaHCO_3$ (2 x 50 ml), water (2 x 50 ml) and brine (2 x 50 ml). The aqueous washings were then extracted with EtOAc (2 x 25 ml) and the combined organic layers were dried using anhydr. $MgSO_4$. The solvent was evaporated *in vacuo* and the crude product chromatographed on silica gel [elution hexane: EtOAc (4:1)] to yield Diethyl *N*-benzyl-*N*-(2,2-diethoxyethyl) phosphoramidate **29a**, a yellow oil (0.735 g, 56.98 %). δ_H/ppm (600 MHz; $CDCl_3$) 1.18 (6H, t, *J* = 6.8 Hz, 2 x OCH_2CH_3), 1.27 (6H, t, *J* = 7.2 Hz, 2 x $POCH_2CH_3$), 3.32 (2H, d, *J* = 5.6 Hz, CH_2N), 3.51 and 3.64 (4H, m, 2 x O–CH_2), 3.85 (2H, s, Ph-CH_2), 4.03 (4H, m, 2 x PO–CH_2), 4.61 (1H, t, *J* = 5.2 Hz, CH) and 7.29 – 7.37 (5H, m, Ar-H); δ_C/ppm (600 MHz; $CDCl_3$) 15.1 (2 x O CH_2CH_3), 16.1 (d, J_{P-C} = 7.2 Hz, 2 x $POCH_2CH_3$), 31.8 (CH_2N), 52.7 (3-CH_2), 62.4 (d, J_{P-C} = 5.5 Hz, 2 x OCH_2CH_3), 62.7 (2 x $POCH_2CH_3$), 101.4 (C-7), 127.3 (C-22), 128.3 (C-20 and C-24), 128.6 (C-21 and C-23) and 137.4 (C-19).

Diethyl *N*-(2,2-diethoxyethyl)-*N*-[4-(hydroxymethyl) benzyl] phosphoramidate 29b

The procedure for the synthesis of Diethyl *N*-benzyl-*N*-(2,2-diethoxyethyl) phosphoramidate **29a** was employed using NaH (60 % dispersion in mineral oil; 0.20 g, 7.4 mmol), diethyl *N*-(2,2-diethoxyethyl) phosphoramidate (1.00 g, 3.7 mmol) **28** in dry THF (20 mL) and 4-(chloromethyl)benzyl alcohol (0.58 g, 3.7 mmol) in dry THF (5 mL). The solvent was evaporated *in vacuo* and the crude chromatographed on silica gel [elution hexane: EtOAc (4:1)] yielding diethyl *N*-(2,2-diethoxyethyl)-*N*-[4-(hydroxymethyl)]benzyl) phosphoramidate **29b**, a yellow oil (0.4727 g, 35.01 %). δ_H/ppm (600 MHz; $CDCl_3$) 1.16 (6H, t, *J* = 7.2 Hz, 2 x OCH_2CH_3), 1.28 (6H, t, *J* = 6.8 Hz, 2 x $POCH_2CH_3$), 2.13 (1H, s, OH), 3.27 (2H, d, *J* = 5.2 Hz, CH_2N), 3.48 and 3.61 (4H, m, 2 x OCH_2), 3.82 (2H, s, $PhCH_2$), 4.05 (4H, m, 2 x $POCH_2$), 4.47

(1H, t, J = 5.2 Hz, CH), 4.82 (2H, s, CH_2OH) and 7.02 – 7.10 (4H, m, Ar-H); δ_C/ppm (600 MHz; $CDCl_3$) 15.2 (2 x OCH_2CH_3), 16.2 (d, J_{P-C} = 7.2 Hz, 2 x $POCH_2CH_3$), 33.6 (CH_2N), 53.5 (Ph-CH_2), 62.1 (d, J_{P-C} = 6.6 Hz, 2 x O–CH_2), 62.5 (2 x PO–CH_2), 64.2 (CH_2OH), 101.5 (C-7), 127.4 (C-20 and C-24, 128.7 (C-21 and C-23), 136.1 (C-19) and 139.7 (C-22).

Diethyl *N*-(3-aminobenzyl)-*N*-(2,2-diethoxyethyl) phosphoramidate 29c

i) 3-Aminobenzyl bromide 41

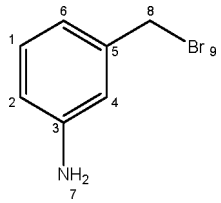

Phosphorous tribromide (0.62 ml, 6.5 mmol) was added drop-wise to a stirred solution of 3-aminobenzyl alcohol (0.80 g, 6.5 mmol) in dry DCM (10 ml) under N_2 at 0^0C and the resulting mixture was stirred for an hour. The mixture was allowed to warm to room temperature and stirred for a further 24 hours. After the addition of sat. aq. $NaHCO_3$ (30 ml) and DCM (30 ml) the organic layer was separated and the aqueous layer was extracted with diethyl ether (3 x 20 ml). Organic layers were combined, dried over $MgSO_4$ and filtered. The solvent was evaporated *in vacuo* and crude weighed. A 1:1 solution of KOH was prepared, the crude was dissolved in water (10 ml) and the KOH solution added drop-wise at 0^0 C for an hour. The organic layer was extracted with EtOAc (2 x 10 ml) and dried over $MgSO_4$. Yielding 3-aminobenzyl bromide **41**, a yellow oil (1.5629g, 77%). δ_H/ppm (400 MHz; DMSO) 4.95 (2H, s, NH_2), 4.35 (2H, s, CH_2Br) and 6.35 - 7.00 (4H, m, Ar- H); δ_C/ppm (400 MHz; DMSO) 36.6 (CH_2Br), 115.5 (C-2), 116.4 (C-4), 119.9 (C-6), 129.0 (C-5), 138.0 (C-1) and 147.5 (C-3).

ii) Diethyl *N*-(3-aminobenzyl)-*N*-(2,2-diethoxyethyl)phosphoramidate 29c

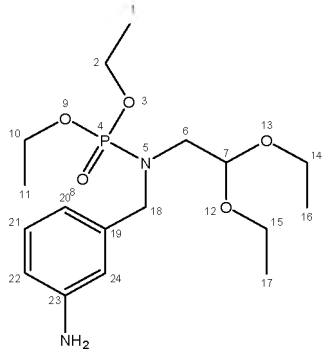

The procedure for the synthesis of diethyl *N*-benzyl-*N*-(2,2-diethoxyethyl)phosphoramidate **29a** was employed using NaH (60 % dispersion in mineral oil; 0.20 g, 7.4 mmol), diethyl *N*-(2,2-diethoxyethyl) phosphoramidate (1.00 g, 3.7 mmol) **28** in dry THF (20 mL) and 3-aminobenzyl bromide (0.69 g, 3.7 mmol) in dry THF (5 mL). The solvent was evaporated *in vacuo* and the crude product chromatographed on silica gel [elution hexane: EtOAc (4:1)], yielding diethyl *N*-(3-aminobenzyl)-*N*-(2,2-diethoxyethyl)phosphoramidate **29c**, a yellow oil (0.69 g, 49.8%). δ_H/ppm (600 MHz; $CDCl_3$) 1.18 (6H, t, *J* = 7.2 Hz, OCH_2CH_3), 1.30 (6H, t, *J* = 6.8 Hz, 2 x $POCH_2CH_3$), 2.87 (2H, d, *J* = 5.6 Hz, CH_2N), 3.47 and 3.62 (4H, m, 2 x OCH_2), 3.83 (2H, s, Ph-CH_2), 3.91 (2H, s, NH_2), 4.07 (4H, m, 2 x $POCH_2$), 4.48 (1H, t, *J* = 5.2 Hz, CH) and 6.31 – 6.87 (4H, m, Ar-H); δ_C/ppm (600 MHz; $CDCl_3$) 14.9 (2 x OCH_2CH_3), 15.9 (d, J_{P-C} = 7.0 Hz, 2 x $POCH_2CH_3$), 31.6 (CH_2N), 53.3 (Ph-CH_2), 62.1 (d, J_{P-C} = 5.4 Hz, 2 x $POCH_2$), 62.2 (2 x OCH_2), 101.4 (C-7), 127.4 (C-20 and C-24), 128.7 (C-21 and C-23), 136.1 (C-19) and 139.7 (C-22).

Diethyl *N*-(2,2-diethoxyethyl)-*N*-(3-mercaptobenzyl)phosphoramidate 29d

i) 3-Merceptobenzyl bromide 42

A solution of sodium nitrite (0.32 g, 4.6 mmol) in water (2 ml) was slowly added to a mixture of 3-aminobenzyl bromide (0.50 g, 2.7 mmol) in water (4 ml) and conc. HCl (1 ml) at -5 – 0 ^{0}C. The mixture was stirred for 1 hour with the temperature kept below 0 ^{0}C.

A solution of sodium sulfide (1.20 g, 4.97 mmol) and sulfur (0.16 g, 5.0 mmol) in water (15 ml) was then added drop-wise during 1 hour to the cold solution of the diazonium salt and the resulting mixture was stirred at 0 ^{0}C for 1 hour. After completion, the mixture was acidified (pH 2.5) and extracted with EtOAc (3 x 15 ml). The organic extracts were washed with 20% Na2CO3 (2 x 20 ml), water (2 x 20ml) and brine (2 x 20ml) and dried with $MgSO_4$. The solvent was removed *in vacuo* and used in the following step without further purification.

In another flask, sodium borohydride (0.12 g, 32 mmol) in THF (3 ml) was added to the disulphide solution (0.25 g, 0.8 mmol) in THF (3 ml) under N_2 at 0 ^{0}C. After the addition, the mixture was allowed to warm to room temperature and stirred for an hour. The reaction was then quenched with water (6 ml), acidified (pH 2.5) with 2M HCl and extracted with EtOAc (3 x 10 ml).

The organic extracts were combined, washed sequentially with 20% Na_2CO_3 (3 x 10 ml), water (3 x 10 ml) and brine (3 x 10 ml) and dried with $MgSO_4$. The solvent was removed *in vacuo* and the residue purified by chromatography on silica [elution with hexane: EtOAc (4:1)] to yield 3-mercaptobenzyl bromide **42** as yellow crystals (0.78g, 65%). δ_H/ppm (400 MHz; $CDCl_3$) 3.65 (1H, s, SH), 4.65 (2H, s, CH_2Br), and 6.60 - 7.46 (4H, m, Ar-H); δ_C/ppm (400 MHz; $CDCl_3$) 36.4 (CH_2Br), 125.8 (C-2), 126.4 C-6), 128.3 (C-5), 130.0 (C-4), 130.2 (C-3) and 137.6 (C-1).

ii) **Diethyl *N*-(2,2-diethoxyethyl)-*N*-(3-mercaptobenzyl)phosphoramidate 29d**

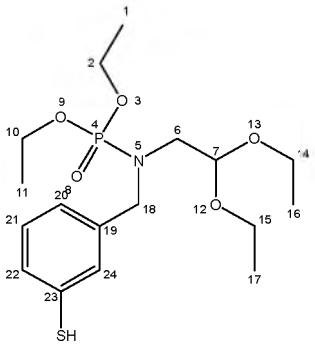

The procedure for the synthesis of diethyl *N*-benzyl-*N*- (2,2-diethoxyethyl) phosphoramidate **29a** was employed using NaH (60 % dispersion in mineral oil; 0.20 g, 7.4 mmol), diethyl *N*-(2,2-diethoxyethyl)phosphoramidate (1.00 g, 3.7 mmol) **28** in dry THF (20 mL) and 3-sulfanylbenzyl bromide (0.75 g, 3.7 mmol) in dry THF (5 mL). The solvent was evaporated *in vacuo* and the crude chromatographed on silica gel [elution hexane: EtOAc (3:2)] to yield diethyl *N*-(2,2-diethoxyethyl)-*N*-(3-mercaptobenzyl)phosphoramidate **29d**, a yellow oil (0.57g, 65%). δ_H/ppm (600 MHz; $CDCl_3$) 1.20 (6H, t, *J* = 7.2 Hz, 2 x OCH_2CH_3), 1.29 (6H, t, *J* = 6.8 Hz, 2 x $POCH_2CH_3$), 2.96 (1H, s, SH), 3.34 (2H, d, *J* = 5.2 Hz, CH_2N), 3.53 and 3.66 (4H, m, 2 x OCH_2), 3.84 (2H, s, Ph-CH_2), 4.05 (4H, m, 2 x $POCH_2$), 4.63 (1H, t, *J* = 5.6 Hz, CH) and 6.89 – 7.01 (4H, m, Ar-H); δ_C/ppm (600 MHz; $CDCl_3$) 15.5 (2 x OCH_2CH_3), 16.5 (d, J_{P-C} = 7.1 Hz, 2 x $POCH_2CH_3$), 32.2 (CH_2N), 49.7 (d, J_{P-C} = 7.0 Hz, 2 x $POCH_2$), 62.8 (2 x OCH_2), 101.0 (CH), 126.8 (C-7), 124.7 (C-20), 125.5 (C-24), 127.4 (C-22), 129.0 (C-21), 130.0 (C-23), 137.1 (C-19).

Diethyl *N*-(2,2-diethoxyethyl)-*N*-(3-nitrobenzyl) phosphoramidate 29e

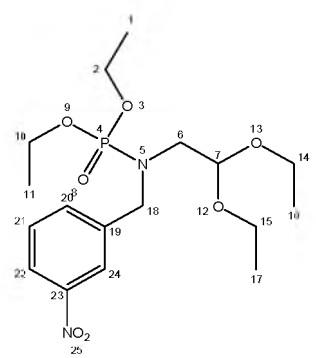

The procedure for the synthesis of diethyl *N*-benzyl-*N*-(2,2-diethoxyethyl)phosphoramidate **29a** was employed using NaH (60 % dispersion in mineral oil; 0.20 g, 7.4 mmol), diethyl *N*-(2,2-diethoxyethyl) phosphoramidate (1.00 g, 3.7 mmol) **28** in dry THF (20 mL) and 3-nitrobenzyl bromide (0.814 g, 3.7 mmol) in dry THF (5 mL). The solvent was evaporated *in vacuo* and the crude chromatographed on silica gel [elution hexane: EtOAc (4:1)] to yield diethyl *N*-(2,2-diethoxyethyl)-*N*-(3-nitrobenzyl)phosphoramidate **29e**, a dark green oil (0.302 g, 20.2%). δ_H/ppm (600 MHz; $CDCl_3$) 1.11 (6H, t, *J* = 6.8 Hz, 2 x OCH_2CH_3), 1.12 (6H, t, *J* = 7.2 Hz, 2 x P OCH_2CH_3), 2.85 (2H, d, *J* = 5.6 Hz, CH_2N), 3.41 (4H, m, 2 x OCH_2), 3.81 (2H, s, Ph-

CH_2), 4.07 (4H, m, 2 x $POCH_2$), 4.43 (1H, t, *J* = 5.2 Hz, CH) and 7.32 – 8.07 (4H, m, Ar-H); δ_C/ppm (600 MHz; $CDCl_3$) 15.5 (2 x OCH_2CH_3), 14.5 (d, J_{P-C} = 7.2 Hz, 2 x $POCH_2CH_3$), 44.5 (CH_2N), 69.5 (Ph-CH_2), 61.4 (d, J_{P-C} = 5.5 Hz, 2 x $POCH_2$), 60.7 (2 x OCH_2), 100.2 (CH), 120.4 (C-7), 124.8 (C-20), 126.7 (C-21), 128.0 (C-22), 129.1 (C-24), 130.0 (C-19), 137.7 (C-23).

Diethyl *N*-(3,4 dichlorobenzyl)-*N*-(2,2-diethoxyethyl)phosphoramidate 29f

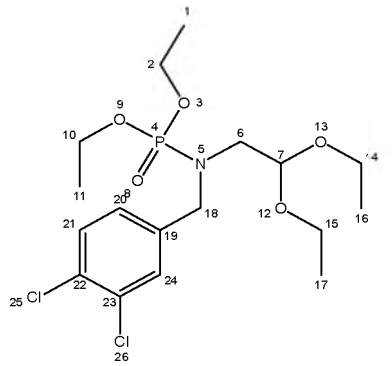

The procedure for the synthesis of diethyl *N*-benzyl-*N*- (2,2-diethoxyethyl) phosphoramidate **29a** was employed using NaH (60 % dispersion in mineral oil; 0.20 g, 7.4 mmol), diethyl *N*-(2,2-diethoxyethyl)phosphoramidate (1.00 g, 3.7 mmol) **28** in dry THF (20 mL) and 3, 4 dichlorobenzyl chloride (0.51 ml, 37 mmol) in dry THF (5 ml). The solvent was evaporated *in vacuo* and the crude chromatographed on silica gel [elution hexane: EtOAc (4:1)] to yield diethyl *N*-(3,4 dichlorobenzyl)-*N*-(2,2-diethoxyethyl)phosphoramidate **29f**, a yellow oil (0.488g, 30.7%). δ_H/ppm (600 MHz; $CDCl_3$) 1.25 (6H, t, *J* = 6.8 Hz, 2 x OCH_2CH_3), 1.31 (6H, t, *J* = 7.2 Hz, 2 x $POCH_2CH_3$), 3.31 (2H, d, *J* = 5.6 Hz, CH_2N), 3.61 (4H, m, 2 x OCH_2), 4.01 (2H, s, Ph-CH_2), 4.17 (4H, m, 2 x $POCH_2$), 4.58 (1H, t, *J* = 5.2 Hz, CH) and 7.02 – 7.55 (3H, m, Ar-H); δ_C/ppm (600 MHz; $CDCl_3$) 15.5 (2 x OCH_2CH_3), 14.5 (d, J_{P-C} = 7.2 Hz, 2 x $POCH_2CH_3$), 44.6 (CH_2N), 69.0 (Ph-CH_2), 61.4 (d, J_{P-C} = 5.5 Hz, 2 x $POCH_2$), 60.1 (2 x OCH_2), 100.2 (CH), 127.0 (C-7), (C-19), (C-20), (C-21), (C24), (C-22), 136.4 (C-23).

Diethyl *N*-benzyl-*N*-(2-oxoethyl)phosphoramidate 30a

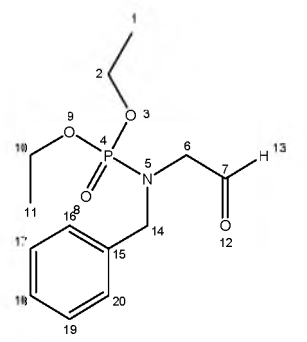

Diethyl *N*-benzyl-*N*-(2,2diethoxyethyl) phosphoramidate (0.5 g, 1.4 mmol) **29a** and 2M HCl (4 ml) were stirred at room temperature for approximately 24 hours. After completion the reaction mixture was added to $CHCl_3$ (20 ml) and the organic phase was washed with water (3 x 20 ml). The aqueous washings were combined and extracted with $CHCl_3$ (30 ml). The combined organic extracts were sequentially washed with saturated aq. $NaHCO_3$ (3 x 20 ml) and brine (3 x 20 ml) and then dried with anhydr. $MgSO_4$. The solvent was evaporated *in vacuo* and the residue chromatographed on silica gel (4:1) to yield diethyl *N*-benzyl-*N*-(2-oxoethyl)phosphoramidate **30a**, a yellow oil (0.35g, 70%). δ_H/ppm (600 MHz; $CDCl_3$) 1.33 (6H, t, *J* = 6.8 Hz, 2 x $POCH_2CH_3$), 3.74 (2H, d, *J* = 6.0 Hz, CH_2CO), 3.83 (2H, s, Ph-CH_2), 4.12 (4H, m, 2 x OCH_2), 7.31 – 7.37 (5H, m, Ar-H) and 9.82 (1H, s, CHO); δ_C/ppm (600 MHz; $CDCl_3$) 16.2 (d, J_{P-C} = 5.9 Hz, 2 x $POCH_2CH_3$), 51.9 (d, J_{P-C} = 6.0 Hz, CH_2CO), 62.4 (d, J_{P-C} = 6.5 Hz, 2 x OCH_2), 67.6 (Ph–CH_2), 127.6 (C-18), 128.0 (C-16 and C-20), 128.1 (C-17 and C-19), 137.7 (C-15) and 175.2 (C=O).

Diethyl *N*-[4-(hydroxymethyl)benzyl]-*N*-(2-oxoethyl)phosphoramidate 30b

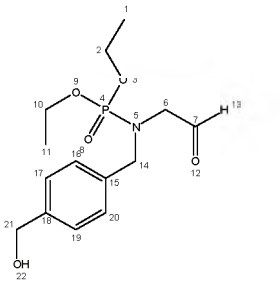

The procedure described for the synthesis of diethyl *N*-benzyl-*N*-(2-oxoethyl)-phosphoramidate **30a** was employed using diethyl *N*-(2,2-diethoxyethyl)-*N*-[4-(hydroxymethyl)benzyl]phosphoramidate (0.5 g, 1.3 mmol) **29b** and 2M HCl (4 ml). After work up, the solvent was removed *in vacuo* and the residue chromatographed on silica gel (4:1) to yield diethyl *N*-[4-(hydroxymethyl)benzyl]-*N*-(2-oxoethyl)phosphoramidate **30b**, a yellow oil (0.36g, 72%). δ_H/ppm (600 MHz; $CDCl_3$) 1.36 (6H, t, *J* = 7.2 Hz, 2 x CH_3), 2.03 (1H, s, OH), 3.72 (2H, d, *J* = 5.2 Hz, CH_2CO), 3.82 (2H, s, $PhCH_2$), 4.18 (4H, m, 2 x OCH_2), 4.82 (2H, s, CH_2OH), 7.09 – 7.17 (4H, m, Ar-H) and 9.81 (1H, s, CHO); δ_C/ppm (600 MHz; $CDCl_3$) 16.3 (d, *J*P–C = 5.8 Hz, 2 x CH_3), 48.9 (d, J_{P-C} = 5.9 Hz, *C*H_2CO), 63.0 (d, J_{P-C} = 6.3 Hz, 2 x OCH_2), 64.9 (CH_2OH), 67.2 (Ph-CH_2), 127.1 (C-20 and C-16), 128.2 (C-17 and C-19), 135.8 (C-15), 139.8 (C-18) and 172.8 (C=O).

Diethyl *N*-(3-aminobenzyl)-*N*-(2-oxoethyl) phosphoramidate 30c

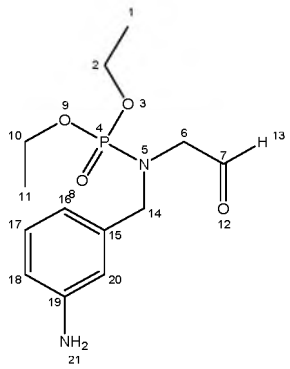

The procedure described for the synthesis of diethyl *N*-benzyl-*N*-(2-oxoethyl)-phosphoramidate **30a** was employed using diethyl *N*-(3-aminobenzyl)-*N*-(2,2diethoxyethyl)-phosphoramidate (0.5 g, 1.3 mmol) **29c** and 2M HCl (4 ml). After work up, the solvent was removed *in vacuo* and the residue chromatographed on silica gel (4:1) to yield diethyl *N*-(3-aminobenzyl)-*N*-(2-oxoethyl)phosphoramidate **30c**, a yellow oil (0.37g, 74%). δ_H/ppm (600 MHz; $CDCl_3$) 1.35 (6H, t, *J* = 6.8 Hz, 2 x CH_3), 3.24 (2H, s, NH_2), 3.71 (2H, d, *J* = 5.2 Hz, CH_2CO), 3.83 (2H, s, Ph-CH_2), 4.17 (4H, m, 2 x OCH_2), 7.00 – 7.47 (4H, m, Ar-H) and 9.81 (1H, s, CHO); δ_C/ppm (600 MHz; $CDCl_3$) 16.3 (d, J_{P-C} = 6.0 Hz, 2 x CH_3), 52.8 (d, J_{P-C} = 4.9 Hz, *C*H_2CO), 61.7

(d, J_{P-C} = 6.4 Hz, 2 x OCH_2), 68.3 (Ph-CH_2), 114.0 (C-18), 114.9 (C-20), 118.3 (C- 18), 129.8 (C-17), 137.7 (C-15), 147.8 (C-19) and 174.8 (C=O).

Diethyl *N*-(3-mercaptobenzyl)-*N*-(2-oxoethyl)phosphoramidate 30d

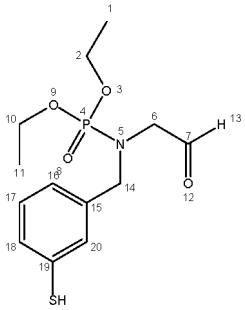

The procedure described for the synthesis of diethyl *N*-benzyl-*N*-(2-oxoethyl)-phosphoramidate **30a** was employed using diethyl *N*-(3-mercaptobenzyl)-*N*-(2,2diethoxyethyl)phosphoramidate (0.5 g, 1.3 mmol) **29d** and 2M HCl (4 ml). After work up, the solvent was removed *in vacuo* and the residue chromatographed on silica gel (4:1) to yield diethyl *N*-(3-mercaptobenzyl)-*N*-(2-oxoethyl)phosphoramidate **30d**, a yellow oil (0.37g, 74%). δ_H/ppm (600 MHz; $CDCl_3$) 1.36 (6H, t, *J* = 7.2 Hz, 2 x CH_3), 2.77 (1H, s, SH), 3.53 (2H, d, *J* = 6.0 Hz, CH_2CO), 3.79 (2H, s, Ph-CH_2), 4.12 (4H, m, 2 x O-CH_2), 6.86 – 7.40 (4H, m, Ar-H) and 9.87 (1H, s, CHO); δ_C/ppm (600 MHz; $CDCl_3$) 16.4 (d, J_{P-C} = 6.0 Hz, 2 x CH_3), 52.7 (d, J_{P-C} = 4.7 Hz, CH_2CO), 61.4 (d, J_{P-C} = 6.4 Hz, 2 x OCH_2), 68.6 (Ph-CH_2), 124.6 (C-16), 126.2 (C-20), 127.8 (C-18), 128.3 (C-17), 130.4 (C-19), 137.7 (C-15) and 173.2 (C=O).

Diethyl *N*-(3-nitrobenzyl)-*N*-(2-oxoethyl) phosphoramidate 30e

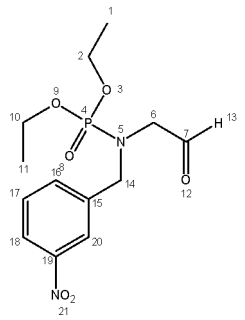

The procedure described for the synthesis of diethyl *N*-benzyl-*N*-(2-oxoethyl)-phosphoramidate **30a** was employed using Diethyl *N*-(3-nitrobenzyl)-*N*-(2,2-diethoxyethyl)-phosphoramidate (0.3 g, 0.91 mmol) **29e** and 2M HCl (2.5 ml). After work up, the solvent was removed *in vacuo* and the residue chromatographed on silica gel (4:1) to yield diethyl *N*-(3-nitrobenzyl)-*N*-(2-oxoethyl) phosphoramidate **30e**, a green oil (0.25g, 83%). δ_H/ppm (600 MHz; $CDCl_3$) 1.11 (6H, t, *J* = 6.8 Hz, 2 x CH_3),3.65 (2H, d, *J* = 6.0 Hz, CH_2CO), 3.81 (2H, s, Ph-CH_2),4.07 (4H, m, 2 x OCH_2), 7.30-8.07 (4H, m, Ar-H) and 9.72 (1H, s, CHO); δ_C/ppm (600 MHz; $CDCl_3$) 14.4 (d, J_{P-C} = 5.9 Hz, 2 x CH_3), 52.0 (d, J_{P-C} = 6.0 Hz, *C*H_2CO), 60.02(d, J_{P-C} = 6.5 Hz, 2 x OCH_2), 68.5 (Ph–CH_2), 142.6-146.5 (Ar-C), 200.0 (C=O).

Diethyl *N*-(3,4 dichlorobenzyl)-*N*-(2-oxoethyl)phosphoramidate 30f

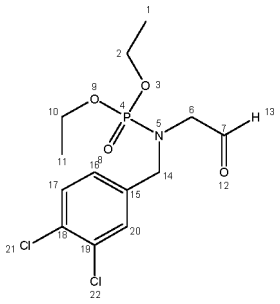

The procedure described for the synthesis of diethyl *N*-benzyl-*N*-(2-oxoethyl)-phosphoramidate **30a** was employed using diethyl *N*-(3,4-dichlorobenzyl)-*N*-(2,2diethoxyethyl)phosphoramidate (0.4 g, 1.13 mmol) **29f** and 2M HCl (3.2 ml). After work up, the solvent was removed *in vacuo* and the residue chromatographed on silica gel (4:1) to yield diethyl *N*-(3,4 dichlorobenzyl)-*N*-(2-oxoethyl) phosphoramidate **30f**, a yellow oil (0.30g, 75%). δ_H/ppm (600 MHz; $CDCl_3$) 1.11 (6H, t, *J* = 6.8 Hz, 2 x CH_3), 3.55 (2H, d, *J* = 6.0 Hz, CH_2CO), 3.82 (2H, s, Ph-CH_2), 4.07 (4H, m, 2 x O–CH_2), 6.80-7.09 (3H, m, Ar-H) and 9.72 (1H, s, CHO); δ_C/ppm (600 MHz; $CDCl_3$) 14.4 (d, J_{P-C} = 5.9 Hz, 2 x CH_3), 52.1 (d, J_{P-C} = 6.0 Hz, *C*H_2CO), 60.0 (d, J_{P-C} = 6.5 Hz, 2 x O–CH_2), 68.3 (Ph–CH_2), 127.6-133.2 (Ar-C), 199.5 (C=O).

Diethyl *N*-benzyl-*N*-[2-(benzyloxyamino)ethyl]phosphoramidate 31a

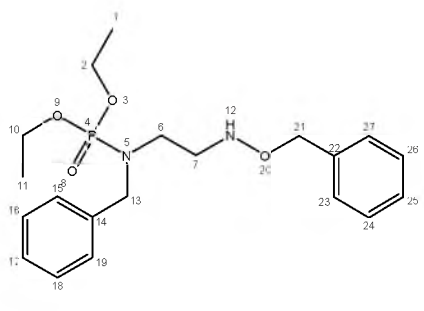

To a stirred solution of diethyl *N*-benzyl-*N*-(2-oxoethyl)phosphoramidate (0.30 g, 1.05 mmol) **30a** in MeOH (5 mL) was added a solution of *O*-benzylhydroxylamine (0.15 g, 1.29 mmol) in MeOH (8 mL). The reaction mixture was heated at 40^0C for 3 hours, cooled to room temperature and diluted with MeOH (50 mL). After the addition of sodium cyanoborohydride (0.20 g, 3.1 mmol), conc. HCl (1.2 mL) was added dropwise over a period of 30 min and the mixture was stirred for 1 hour. Sodium cyanoborohydride (0.075 g, 1.05 mmol) was again added and the mixture was stirred for 1 hour. The solvent was removed under reduced pressure, the residue dissolved in MeOH (30 mL) and then treated with ice-water (50 mL). The pH of the resulting mixture was adjusted to pH 10 with an aq. KOH solution and extracted with DCM (3 x 20 mL). The combined organic layers were washed with 10 % $NaHCO_3$ (50 mL) and brine (50 mL) and then dried (anhydr. $MgSO_4$). The solvent was evaporated *in vacuo* and the residual oil was purified by flash chromatography on silica gel [elution with hexane-EtOAc (3:1)] to yield diethyl *N*-benzyl-*N*-[2-(benzyloxyamino)ethyl]-phosphoramidate **31a**, a yellow oil (0.20 g 50 %). δ_H/ppm (600 MHz; $CDCl_3$) 1.32 (6H, t, J = 7.2 Hz, 2 x CH_3), 2.89 (4H, m, NCH_2), 3.82 (2H, s, Ph-CH_2), 4.10 (4H, m, 2 x OCH_2), 4.74 (2H, s, OCH_2Ph), 5.23 (1H, s, NH) and 7.29 – 7.37 (10H, m, Ar-H); δ_C/ppm (600 MHz; $CDCl_3$) 16.5 (d, $J_{P–C}$ = 6.0 Hz, 2 x CH_3), 36.7 (d, $J_{P–C}$ = 4.5 Hz, NCH_2), 52.1 (d, $J_{P–C}$ = 16.7 Hz, NCH_2), 61.5 (d, $J_{P–C}$ = 6.4 Hz, 2 x $POCH_2$), 67.3 (Ph-CH_2), 68.3 (OCH_2Ph), 113.9 (C-17), 114.9 (C-19), 118.3 (C15), 126.9 (C-23 and C-27), 127.8 (C-25), 128.3 (C-24 and C-26), 129.3 (C-16), 136.7 (C-14), 137.7 (C-22) and 148.3 (C-18).

Diethyl *N*-[2-(benzyloxyamino)ethyl]-*N*-(hydroxymethyl)benzyl]phosphoramidate 31b

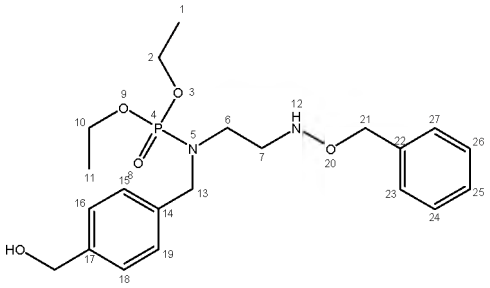

The procedure described for the synthesis of diethyl *N*-benzyl-*N*-[2-(benzyloxyamino)ethyl]-phosphoramidate **31a** was employed, using diethyl *N*-[4-(hydroxymethyl)benzyl]-*N*-(2oxoethyl phosphoramidate (0.32 g, 1.0 mmol) **30b**, *O*-benzylhydroxylamine (0.16 g, 1.28 mmol) in MeOH (10 mL), sodium cyanoborohydride (0.18 g, 2.90 mmol), conc. HCl (1.2 mL) and a further portion of sodium cyanoborohydride (0.061 g, 0.92 mmol). After work-up, the solvent was evaporated *in vacuo* and the remaining oil was purified by flash chromatography on silica gel [elution with hexane-EtOAc (3:1)] to yield diethyl *N*-[2-(benzyloxyamino)ethyl]-N-[4(hydroxymethyl)benzyl]phosphoramidate **31b**, a yellow oil (0.22 g, 53 %). δ_H/ppm (600 MHz; $CDCl_3$) 1.29 (6H, t, J = 7.2 Hz, 2 x CH_3), 2.87 (4H, m, NCH_2), 3.80 (2H, s, Ph-CH_2), 4.07 (4H, m, 2 x $POCH_2$), 4.77 (2H, s, OCH_2Ph), 4.86 (2H, s, CH_2OH), 7.33 – 7.42 (9H, m, Ar-H), 7.97 (1H, s, OH) and 8.11 (1H, s, NH); δ_C/ppm (600 MHz; $CDCl_3$) 16.3 (d, J_{P-C} = 6.0 Hz, 2 x CH_3), 36.4 (d, J_{P-C} = 4.8 Hz, N-CH_2), 52.0 (d, J_{P-C} = 16.4 Hz, N-CH_2), 61.3 (d, J_{P-C} = 6.5 Hz, 2 x $POCH_2$), 64.7 (CH_2OH), 67.2 (OCH_2Ph), 69.2 (Ph-CH_2), 127.7 (C-19 and C-15), 127.8 (C-23 and C-27), 128.2 (C-25), 128.3 (C-18 and C-16), 128.3 (C-24 and C-26), 137.4 (C-14), 137.8 (C-22) and 138.3 (C-17).

Diethyl *N*-(3-aminobenzyl)-*N*-[2-(benzyloxyamino)ethyl]phosphoramidate 31c

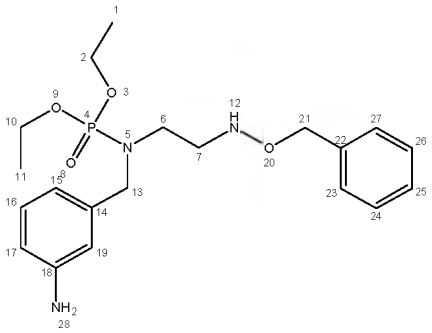

The procedure described for the synthesis of diethyl *N*-benzyl-*N*-[2-(benzyloxyamino)ethyl]=phosphoramidate **31a** was employed, using diethyl *N*-(3-aminobenzyl)-*N*-(2oxoethyl)phosphoramidate (0.34 g, 1.16 mmol) **30c**, *O*-benzyl-hydroxylamine (0.17 g, 1.39 mmol) in MeOH (10 mL), sodium cyanoborohydride (0.22 g, 3.46 mmol), conc. HCl (1.2 mL) and a further portion of sodium cyanoborohydride (0.070 g, 1.01 mmol). After work-up, the solvent was evaporated *in vacuo* and the remaining oil was purified by flash chromatography on silica gel [elution with hexane-EtOAc (3:1)] to yield diethyl *N*-(3-aminobenzyl)-*N*-[2(benzyloxyamino)ethyl]phosphoramidate **31c**, a yellow oil (0.25 g, 57 %). δ_H/ppm (600 MHz; $CDCl_3$) 1.22 (6H, t, *J* = 6.0 Hz, 2 x CH_3), 2.95 (4H, m, N-CH_2), 3.59 (2H, s, OCH_2Ph), 4.03 (4H, m, 2 x $POCH_2$), 4.62 (2H, s, Ph-CH_2), 5.55 (2H, s, NH_2), 6.59 – 6.87 (4H, m, Ar-H), 7.28-7.37 (5H, m, Ar-H) and 8.40 (1H, s, NH); δ_C/ppm (600 MHz; $CDCl_3$) 16.4 (d, *J*P–C = 6.0 Hz, 2 x CH_3), 36.5 (d, J_{P-C} = 4.8 Hz, N-CH_2), 52.0 (d, J_{P-C} = 16.7 Hz, N-CH_2), 61.5 (d, J_{P-C} = 6.5 Hz, 2 x $POCH_2$), 67.4 (Ph-CH_2), 69.9 (OCH_2Ph), 113.9 (C-17), 114.9 (C-19), 118.3 (C-15), 126.9 (C-23 and C-27), 127.8 (C-25), 128.3 (C-24 and C-26), 129.3 (C-16), 136.7 (C-14), 137.7 (C-22) and 148.3 (C-18).

Diethyl *N*-[2-(benzyloxyamino)ethyl]-*N*-(3-mercaptobenzyl)phosphoramidate 31d

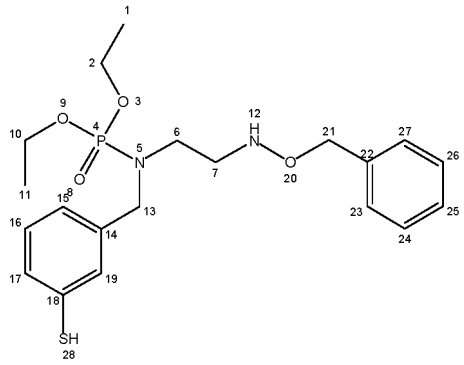

The procedure described for the synthesis of diethyl *N*-benzyl-*N*-[2-(benzyloxyamino)ethyl]-phosphoramidate **31a** was employed, using diethyl *N*-(3-mercaptobenzyl)-*N*-(2oxoethyl) phosphoramidate (0.34 g, 1.08 mmol) **30d**, *O*-benzylhydroxylamine (0.108 g, 0.85 mmol) in MeOH (10 mL), sodium cyanoborohydride (0.21 g, 3.3 mmol), conc. HCl (1.2 mL) and a further portion of sodium cyanoborohydride (0.070 g, 1.005 mmol). After work-up, the solvent was evaporated *in vacuo* and the remaining oil was purified by flash chromatography on silica gel [elution with hexane-EtOAc (3:1)] to yield diethyl *N*-[2-(benzyloxyamino)ethyl]-*N*-(3-mercaptobenzyl)phosphoramidate **31d**, a yellow oil (0.24 g, 55 %). δ_H/ppm (600 MHz; $CDCl_3$) 1.28 (6H, t, J = 7.2 Hz, 2 x CH_3), 2.61 (4H, m, N-CH_2), 3.38 (1H, s, SH), 3.61 (2H, s, Ph-CH_2), 4.04 (4H, m, 2 x $POCH_2$), 4.81 (2H, s, OCH_2Ph), 6.75 - 7.18 (4H, m, Ar-H), 7.31 - 7.35 (5H, m, Ar-H) and 8.18 (1H, s, NH); δ_C/ppm (600 MHz; $CDCl_3$) 16.4 (d, J_{P-C} = 6.0 Hz, 2 x CH_3), 36.8 (d, J_{P-C} = 4.8 Hz, N-CH_2), 52.1 (d, J_{P-C} = 16.7 Hz, N-CH_2), 61.5 (d, J_{P-C} = 6.5 Hz, 2 x $POCH_2$), 66.7 (OCH_2Ph), 71.2 (Ph-CH_2), 124.6 (C-15), 125.9 (C-19), 127.6 (C-17), 127.9 (C-23 and C-27), 128.0 (C-25), 128.3 (C-16), 128.4 (C-24 and C-26), 130.6 (C-18) and 137.8 (C-14) and 138.0 (C-22).

Diethyl *N*-[2-(benzyloxyamino)ethyl]-*N*-(3-nitrobenzyl)phosphoramidate 31e

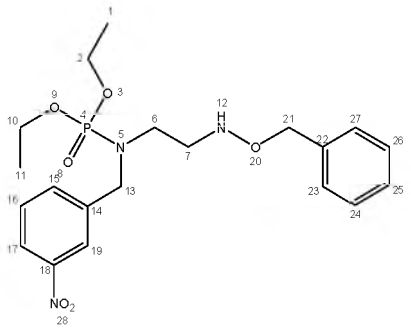

The procedure described for the synthesis of diethyl *N*-benzyl-N-[2-(benzyloxyamino)ethyl]-phosphoramidate **31a** was employed, using diethyl *N*-(3-nitrobenzyl)-N-(2-oxoethyl) phosphoramidate (0.25 g, 0.57 mmol) **30e**, *O*-benzylhydroxylamine in MeOH (10 mL), sodium cyanoborohydride, conc. HCl (mL) and a further portion of sodium cyanoborohydride. After work-up, the solvent was evaporated *in vacuo* and the remaining oil was purified by flash chromatography [on silica gel; elution with hexane-EtOAc (3:1)] to yield diethyl *N*-[2-(benzyloxyamino)ethyl]-N-(3-nitrobenzyl)phosphoramidate, a light green oil (0.14 g, 56 %) **31e**. δ_H/ppm (600 MHz; $CDCl_3$) 1.11 (6H, t, J = 7.2 Hz, 2 x CH_3), 2.03 (1H, s, NH), 2.77-2.81 (4H, m, N-CH_2), 3.82 (2H, s, Ph-CH_2), 4.10 (4H, m, 2 x $POCH_2$), 4.74 (2H, s, OCH_2Ph) and 7.91 – 8.01 (10H, m, Ar-H); δ_C/ppm (600 MHz; $CDCl_3$) 14.5 (d, J_{P-C} = 6.0 Hz, 2 x CH_3), 37.7 (d, J_{P-C} = 4.5 Hz, N-CH_2), 51.2 (d, J_{P-C} = 16.7 Hz, N-CH_2), 60.0 (d, J_{P-C} = 6.4 Hz, 2 x $POCH_2$), 68.9 (Ph-CH_2), 77.3 (OCH_2Ph), 120.9-156.4 (11 x Ar-C).

Diethyl *N*-[2-(benzyloxyamino)ethyl-*N*-(3,4-dichlorobenzyl)phosphoramidate 31f

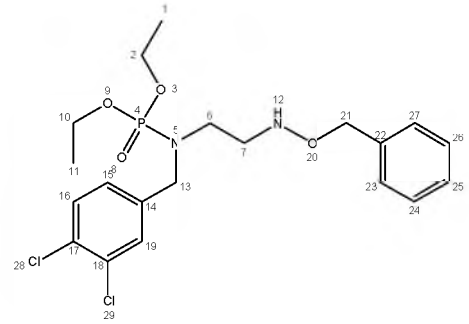

The procedure described for the synthesis of diethyl *N*-benzyl-*N*-[2-(benzyloxyamino)ethyl]-phosphoramidate **31a** was employed, using diethyl *N*-(3,4-dichlorobenzyl)-*N*-(2oxoethyl)-phosphoramidate (0.30 g, 0.65 mmol) **30f**, *O*-benzylhydroxylamine in MeOH (10 mL), sodium cyanoborohydride, conc. HCl (1.2 mL) and a further portion of sodium cyanoborohydride. After work-up, the solvent was evaporated *in vacuo* and the remaining oil was purified by flash chromatography [on silica gel; elution with hexane-EtOAc (3:1)] to yield diethyl *N*-[2-(benzyloxyamino)ethyl]-*N*-(3,4-dichlorobenzyl)phosphoramidate, a yellow oil (0.20 g, 67 %) **31f**. δ_H/ppm (600 MHz; $CDCl_3$) 1.12 (6H, t, *J* = 7.2 Hz, 2 x CH_3), 2.0 (1H, s, NH), 2.77-2.81 (4H, m, N-CH_2), 3.81 (2H, s, Ph-CH_2), 4.07 (4H, m, 2 x $POCH_2$), 4.79 (2H, s, OCH_2Ph) and 6.88 – 7.19 (8H, m, Ar-H); δ_C/ppm (600 MHz; CDCl3) 14.5 (d, J_{P-C} = 6.0 Hz, 2 x CH_3), 37.7 (d, J_{P-C} = 4.5 Hz, N-CH_2), 51.2 (d, J_{P-C} = 16.7 Hz, N-CH_2), 60.0 (d, J_{P-C} = 6.4 Hz, 2 x $POCH_2$), 68.4 (Ph-CH_2), 77.0 (OCH_2Ph), 127.2-141.4 (11 x Ar-C).

Diethyl *N*-benzyl-2-[*N*-(benzyloxy)acetamido]ethylphosphoramidate 32a

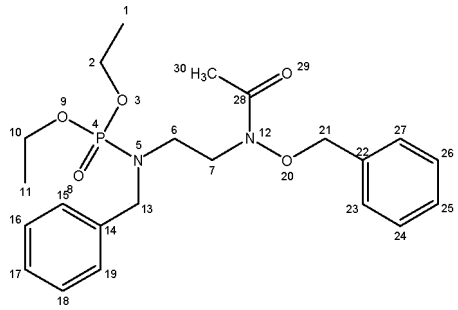

Acetyl chloride (0.12 mL, 1.3 mmol) was added dropwise to a stirred solution of diethyl *N* benzyl-N-[2-(benzyloxyamino)ethyl]phosphoramidate (0.25 g, 0.64 mmol) **31a** and triethylamine (0.13 mL, 0.96 mmol) in DCM (10 mL) under N_2 at 0 ^oC. The mixture was stirred at 0 ^0C for 1 hour, allowed to warm to room temperature and then stirred for ca. 24 hours. The solvent was removed under reduced pressure and the residual oil dissolved in diethyl ether (20 mL). The ethereal solution was washed sequentially with aq. K_2CO_3 solution, 0.5M-HCl and water. The organic solution was dried over anhydr. $MgSO_4$, the solvent removed *in vacuo* and the residue purified by flash chromatography [on silica gel;

elution with hexane-EtOAc (7:3)] to yield diethyl *N*-benzyl-2-[N-benzyloxy)acetamido]ethyl-phosphoramidate **32a**, a yellow oil (0.17 g, 80 %). δ_H/ppm (600 MHz; $CDCl_3$) 1.29 (6H, t, *J* = 7.2 Hz, 2 x CH_3), 2.00 (3H, s, CH_3CO), 2.71 (2H, m, N-CH_2), 3.01 (2H, t, *J* = 6.4 Hz, N-CH_2), 3.67 (2H, s, Ph-CH_2), 4.08 (4H, m, 2 x $POCH_2$), 4.77 (2H, s, OCH_2Ph) and 7.27 - 7.39 (9H, m, Ar-H); δ_C/ppm (600 MHz; $CDCl_3$) 16.4 (d, J_{P-C} = 5.9 Hz, 2 x PO-CH_3), 23.7 (CH_3CO), 35.4 (d, J_{P-C} = 5.4 Hz, NCH_2), 52.6 (d, J_{P-C} = 16.8 Hz, NCH_2), 62.5 (d, J_{P-C} = 6.7 Hz, 2 x $POCH_2$), 66.8 (Ph-CH_2), 68.7 (OCH_2Ph), 124.8 (C-17), 124.9 (C-25), 127.5 (C-19 and C-15), 127.8 (C-23 and C-27), 128.5 (C-18 and C-16), 128.7 (C-24 and C-26), 138.3 (C-14), 138.4 (C-22) and 171.6 (C=O).

Diethyl-2-[*N*-(benzyloxy)acetamido]-*N*-[4(hydroxymethyl)benzyl]ethylphosphoramidate 32b

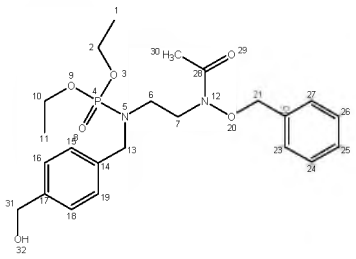

The procedure described for the synthesis of diethyl *N*-benzyl-2-[N-benzyloxy)acetamido]ethylphosphoramidate **32a** was employed, using diethyl *N*-[2-(benzyloxyamino)ethyl]-N-[4(hydroxymethyl)benzyl]phosphoramidate **31b** (0.25 g, 0.59 mmol), acetyl chloride (0.12 mL, 1.3 mmol) and triethylamine (0.12 mL, 0.89 mmol) in DCM (10 mL). The solvent was evaporated *in vacuo* and the residue was purified by flash chromatography on silica gel; elution with hexane-EtOAc (7:3) to yield diethyl 2-[(*N*-benzyloxy)acetamido]-*N*-[4(hydroxymethyl)benzyl]ethyl phosphoramidate, a yellow oil (0.12 g, 60 %) **32b**. δ_H/ppm (600 MHz; $CDCl_3$) 1.32 (6H, t, *J* = 7.2 Hz, 2 x CH_3), 2.04 (3H, s, CH_3CO), 2.32 (2H, m, N-CH_2), 2.76 (2H, t, *J* = 6.0 Hz, N-CH_2), 3.71 (2H, s, Ph-CH_2), 4.11 (4H, m, 2 x PO-CH_2), 4.79 (2H, s, Ph-CH_2), 4.84 (2H, s, CH_2OH), 7.22 - 7.43 (9H, m, Ar-H) and 8.22 (1H, s, OH); δ_C/ppm (600 MHz; $CDCl_3$) 16.4 (d, J_{P-C} = 5.9 Hz, 2 x CH_3), 23.0 (CH_3CO), 36.8 (d, J_{P-C} = 4.1 Hz, N-CH_2), 52.8 (d, J_{P-C} = 16.6 Hz, N-CH_2), 62.3 (d, J_{P-C} = 6.6 Hz, 2 x $POCH_2$), 65.9 (CH_2OH), 66.6

(Ph-CH_2), 68.7 (OCH_2Ph), 126.3 (C-19 and C-15), 126.4 (C-23 and C-27), 126.8 (C-25), 127.0 (C-18 and C-16), 127.7 (C-24 and C-26), 137.2 (C-14), 137.4 (C-22), 140.2 (C-17) and 171.1 (C=O).

Diethyl *N*-(3-aminobenzyl)-2-[(*N*-benzyloxy)acetamido]ethylphosphoramidate 32c

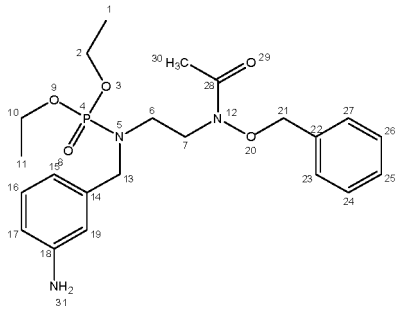

The procedure described for the synthesis of diethyl *N*-benzyl-2-[*N*-benzyloxy)acetamido]ethylphosphoramidate **32a** was employed, using diethyl *N*-[2-(benzyloxyamino)ethyl]-*N*-(3mercaptobenzyl)phosphoramidate **31c** (0.28 g, 0.68 mmol), acetyl chloride (0.13 mL, 1.4 mmol) and triethylamine (0.14 mL, 1.0 mmol) in DCM (10 mL). The solvent was evaporated *in vacuo* and the residue was purified by flash chromatography [on silica gel; elution with hexane-EtOAc (7:3)] to yield diethyl *N*-(3-aminobenzyl)-2-[(*N*-benzyloxy)acetamido]ethylphosphoramidate, a yellow oil **32c** (0.11 g, 55 %). δ_H/ppm (600 MHz; $CDCl_3$) 1.30 (6H, t, *J* = 7.2 Hz, 2 x CH_3), 2.02 (3H, s, CH_3CO), 2.81 (2H, m, N-CH_2), 3.23 (2H, t, *J* = 4.4 Hz, N-CH_2), 3.79 (2H, s, Ph-CH_2), 4.08 (4H, m, 2 x $POCH_2$), 4.52 (2H, s, NH_2), 4.81 (2H, s, Ph-CH_2), 6.63 - 6.78 (4H, m, Ar-H) and 7.16 - 7.19 (5H, m Ar-H); δ_C/ppm (600 MHz; $CDCl_3$) 16.4 (d, J_{P-C} = 6.6 Hz, 2 x CH_3), 23.8 (CH_3CO), 36.7 (d, J_{P-C} = 4.7 Hz, NCH_2), 52.1 (d, J_{P-C} = 16.7 Hz, N-CH_2), 61.4 (d, J_{P-C} = 6.5 Hz, 2 x $POCH_2$), 68.4 (Ph-CH_2), 69.8 (OCH_2Ph), 114.1 (C-17), 114.8 (C-19), 118.6 (C-15), 126.5 (C-23 and C-27), 127.8 (C-25), 128.3 (C-24 and C-26), 129.8 (C-16), 137.3 (C-14), 137.7 (C-22), 147.9 (C-18) and 170.8 (C=O).

Diethyl 2-[(*N*-benzyloxy)acetamido]-*N*-(3-mercaptobenzyl)ethylphosphoramidate 32d

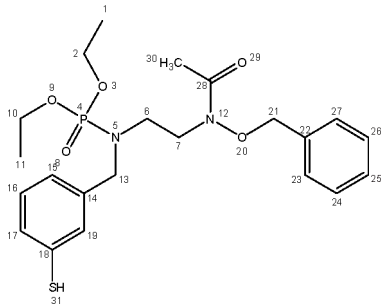

The procedure described for the synthesis of diethyl *N*-benzyl-2-[*N*-benzyloxy)acetamido]ethylphosphoramidate **32a** was employed, using diethyl *N*-[2-(benzyloxyamino)ethyl]-*N*-(3mercaptobenzyl)phosphoramidate **31d** (0.27 g, 0.64 mmol), acetyl chloride (0.12 mL, 1.3 mmol) and triethylamine (0.12 mL, 0.88 mmol) in DCM (10 mL). The solvent was evaporated *in vacuo* and the residue was purified by flash chromatography [on silica gel; elution with hexane-EtOAc (7:3)] to yield diethyl 2-[(*N*-benzyloxy)acetamido]-*N*-(3-mercaptobenzyl)ethylphosphoramidate **32d**, a yellow oil (0.1 g, 50 %). δ_H/ppm (600 MHz; $CDCl_3$) 1.36 (6H, t, *J* = 7.2 Hz, 2 x CH_3), 2.20 (3H, s, CH_3CO), 2.79 (2H, m, N-CH_2), 3.25 (2H, t, *J* = 5.6 Hz, N-CH_2), 3.83 (2H, s, Ph-CH_2), 4.19 (4H, m, 2 x PO-CH_2), 4.71 (2H, s, Ph-CH_2), 6.21 (1H, s, SH), 6.63 - 7.29 (4H, m, Ar-H) and 7.42 - 7.50 (5H, m, Ar-H); δ_C/ppm (600 MHz; $CDCl_3$) 16.4 (d, J_{P-C} = 5.9 Hz, 2 x CH_3), 24.2 (CH_3CO), 36.7 (d, J_{P-C} = 4.8 Hz, NCH_2), 52.9 (d, J_{P-C} = 16.8 Hz, N-CH_2), 61.6 (d, J_{P-C} = 6.5 Hz, 2 x $POCH_2$), 68.1 (Ph-CH_2), 70.8 (OCH_2Ph), 124.7 (C-15), 126.0 (C-19), 126.2 (C-17), 126.8 (C-23 and C-27), 128.7 (C-25), 129.1 (C-16), 129.4 (C-24 and C-26), 130.3 (C-18), 138.5 (C-14), 138.8 (C-16) and 167.3 (C=O).

Diethyl *N*-benzyl-2-[*N*-(3-nitrobenzyl)acetamido]ethylphosphoramidate 32e

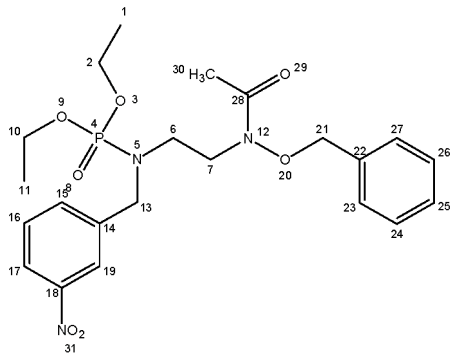

The procedure described for the synthesis of diethyl *N*-benzyl-2-[N-benzyloxy)acetamido]ethylphosphoramidate **32a** was employed, using diethyl *N*-[2-(benzyloxyamino)ethyl]-*N*-(3-nitrobenzyl)phosphoramidate (0.27 g, 0.64 mmol) **31e**, acetyl chloride (0.12 mL, 1.3 mmol) and triethylamine (0.12 mL, 0.88 mmol) in DCM (10 mL). The solvent was evaporated *in vacuo* and the residue was purified by flash chromatography [on silica gel; elution with hexane-EtOAc (7:3)] to yield diethyl *N*-benzyl-2-[*N*-(3-nitrobenzyl)acetamido]ethylphosphoramidate **32e**, a light green oil (5.3 mg, 3.8 %). δ_H/ppm (600 MHz; $CDCl_3$) 1.10 (6H, t, *J* = 7.2 Hz, 2 x CH_3), 2.02 (3H, s, CH_3CO), 2.81 (2H, m, N-CH_2), 3.32 (2H, t, *J* = 6.4 Hz, N-CH_2), 3.81 (2H, s, Ph-CH_2), 4.07 (4H, m, 2 x $POCH_2$), 4.79 (2H, s, OCH_2Ph) and 7.19 – 8.07 (9H, m, Ar-H); δ_C/ppm (600 MHz; $CDCl_3$) 14.4 (d, J_{P-C} = 5.9 Hz, 2 x CH_3), 17.4 (CH_3CO), 35.0 (d, J_{P-C} = 5.4 Hz, NCH_2), 68.6 (d, J_{P-C} = 16.8 Hz, N-CH_2), 60.0 (d, J_{P-C} = 6.7 Hz, 2 x $POCH_2$), 66.8 (Ph-CH_2), 74.3 (OCH_2Ph), 120.8-146.9 (2 x Ar-C), 164.6 (C=O).

Diethyl *N*-benzyloxy-2-[*N*-(3,4- dichlorobenzyl)acetamido]ethylphosphoramidate 32f

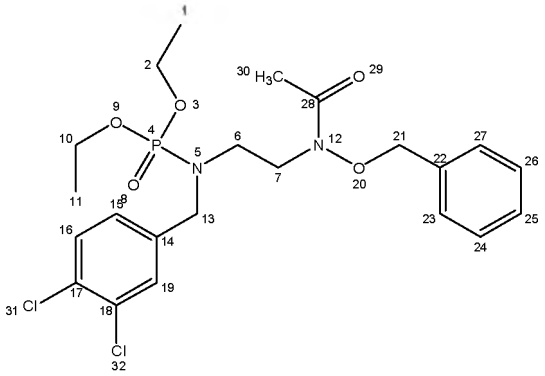

The procedure described for the synthesis of diethyl N-benzyl-2-[N-benzyloxy)-acetamido]ethylphosphoramidate **32a** was employed, using diethyl *N*-[2-(benzyloxyamino)-ethyl]-*N*-(3,4 dichlorobenzyl)phosphoramidate **31f** (0.27 g, 0.64 mmol), acetyl chloride (0.12 mL, 1.3 mmol) and triethylamine (0.12 mL, 0.88 mmol) in DCM (10 mL). The solvent was evaporated *in vacuo* and the residue was purified by flash chromatography [on silica gel; elution with hexane-EtOAc (7:3)] to yield Diethyl *N*-benzyloxy-2-[*N*-(3,4-dichlorobenzyl)-acetamido]ethylphosphoramidate **32f**, a yellow oil (5.8 mg, 2.9 %). δ_H/ppm (600 MHz; $CDCl_3$) 1.11 (6H, t, *J* = 7.2 Hz, 2 x CH_3), 2.02 (3H, s, CH_3CO), 2.81 (2H, m, N-CH_2), 3.32 (2H, t, *J* = 6.4 Hz, N-CH_2), 3.81 (2H, s, Ph-CH_2), 4.07 (4H, m, 2 x $POCH_2$), 4.79 (2H, s, OCH_2Ph) and 6.88 - 7.19 (8H, m, Ar-H); δ_C/ppm (600 MHz; $CDCl_3$) 14.5 (d, J_{P-C} = 5.9 Hz, 2 x CH_3), 17.7 (CH_3CO), 35.0 (d, J_{P-C} = 5.4 Hz, NCH_2), 49.2 (d, J_{P-C} = 16.8 Hz, NCH_2), 60.5 (d, J_{P-C} = 6.7 Hz, 2 x $POCH_2$), 68.4 (Ph-CH_2), 74.3 (OCH_2Ph), 127.2-141.9 (2 x Ar-C), 164.2 (C=O).

Diethyl *N*-benzyl-2-(*N*-hydroxyacetamido)ethylphosphoramidate 33a

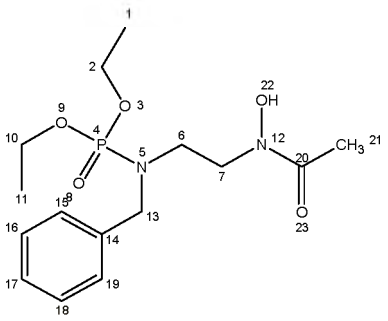

A solution of diethyl *N*-benzyl-2-[N-benzyloxy)acetamido]ethylphosphoramidate **32a** (0.20 g, 0.46 mmol) in dry MeOH (2 mL) was added to a solution of Pd/C (10 %, 0.35 g) in dry MeOH (10 mL) under an H_2-atmosphere and the mixture was stirred at room temperature for 18 hours. The reaction mixture was then filtered through a celite pad, the filtrate was evaporated *in vacuo* and the residue purified by flash chromatography [on silica gel; elution with hexane-EtOAc (3:1)] to yield diethyl *N*-benzyl-2-(*N*-hydroxyacetamido)ethyl-phosphoramidate **33a**, a clear oil (80 mg, 80 %). δ_H/ppm (600 MHz; $CDCl_3$) 1.28 (6H, t, *J* = 7.2 Hz, 2 x CH_3), 1.83 (1H, s, N-OH), 2.08 (3H, s, CH_3CO), 2.89 (2H, m, N-CH_2), 3.21 (2H, t, *J* = 6.0 Hz, N-CH_2), 3.79 (2H, s, Ph-CH_2), 4.17 (4H, m, 2 x $POCH_2$) and 7.32 - 7.45 (5H, m, Ar-H); δ_C/ppm (600 MHz; $CDCl_3$) 16.1 (d, J_{P-C} = 7.2 Hz, 2 x CH_3), 20.8 (CH_3CO), 35.8 (d, J_{P-C} = 5.0 Hz, N-CH_2), 53.6 (d, J_{P-C} = 16.5 Hz, N-CH_2), 62.3 (d, J_{P-C} = 5.6 Hz, 2 x $POCH_2$), 67.5 (Ph-CH_2), 127.3 (C-17), 128.3 (C-19 and C-15), 128.6 (C-18 and C-16), 137.4 (C-14 and 167.5 (C=O).

Diethyl-2-(*N*-hydroxyacetamido)-*N*-[4-(hydroxymethyl)benzyl]ethylphosphoramidate 33b

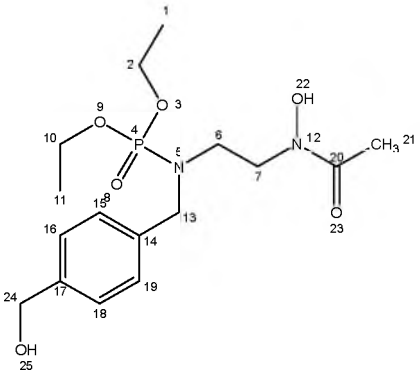

The procedure described for the synthesis of diethyl *N*-benzyl-2-(*N*-hydroxyacetamido)ethyl-phosphoramidate **33a** was employed, using diethyl-2-[(*N*-benzyloxy)acetamido]-*N*-[4(hydroxymethyl)benzyl]ethylphosphoramidate **32b** (0.20 g, 0.43 mmol) in MeOH (2 mL) and Pd/C (10 %, 0.33 g) in MeOH (10 mL). The solvent was evaporated *in vacuo* and the residue was purified by flash chromatography [on silica gel; elution with hexane-EtOAc (3:1)] to yield diethyl 2-(*N*-hydroxyacetamido)-*N*-[4-(hydroxymethyl)benzyl]ethylphosphoramidate **33b** (82 mg, 82 %). δ_H/ppm (600 MHz; $CDCl_3$) 1.32 (6H, t, *J* = 7.2 Hz, 2 x CH_3), 1.91 (1H, s, N-OH), 2.12 (3H, s, CH_3CO), 2.80 (2H, m, N-CH_2), 3.38 (2H, t, *J* = 6.4 Hz, N-CH_2), 3.85 (2H, s, Ph-

CH_2), 4.12 (4H, m, 2 x $POCH_2$), 5.10 (2H, s, CH_2OH), 7.25 - 7.30 (4H, m, Ar-H) and 8.02 (1H, s, CH_2OH); δ_C/ppm (600 MHz; $CDCl_3$) 16.3 (d, J_{P-C} = 6.1 Hz, 2 x CH_3), 23.4 (CH_3CO), 37.4 (d, J_{P-C} = 5.2 91 Hz, N-CH_2), 52.5 (d, J_{P-C} = 16.5 Hz, N-CH_2), 63.6 (d, J_{P-C} = 5.8 Hz, 2 x $POCH_2$), 66.4 (CH_2OH), 68.8 (Ph-CH_2), 123.4 (C-19 and C-15), 123.7 (C-18 and C-16), 136.6 (C-14), 138.3 (C-17) and 170.1 (C=O).

Diethyl *N*-(3-aminobenzyl)-2-(*N*-hydroxyacetamido]ethylphosphoramidate 33c

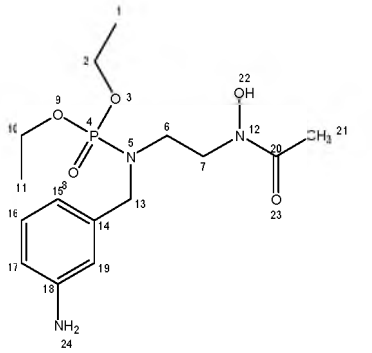

The procedure described for the synthesis of diethyl *N*-benzyl-2-(*N*-hydroxyacetamido)ethyl-phosphoramidate **33a** was employed, using diethyl *N*-(3-aminobenzyl)-2-[(*N*-benzyloxy)acetamido]ethylphosphoramidate **32c** (0.20 g, 0.44 mmol) in MeOH (2 mL) and Pd/C (10 %, 0.33 g) in MeOH (10 mL). The solvent was evaporated *in vacuo* and the residue was purified by flash chromatography [on silica gel; elution with hexane-EtOAc (3:1)] to yield diethyl *N*-(3-aminobenzyl)-2-(*N*-hydroxyacetamido]ethylphosphoramidate **33c** (70 mg, 70 %). δ_H/ppm (600 MHz; $CDCl_3$) 1.29 (6H, t, *J* = 6.8 Hz, 2 x CH_3), 2.14 (3H, s, CH_3CO), 2.69 (2H, m, N-CH_2), 3.26 (2H, t, *J* = 6.8 Hz, N-CH_2), 3.81 (2H, s, Ph-CH_2), 4.09 (4H, m, 2 x $POCH_2$), 4.78 (2H, s, NH_2), 5.68 (1H, s, OH) and 6.59 - 7.16 (4H, m, Ar-H); δ_C/ppm (600 MHz; CDCl3) 16.3 (d, J_{P-C} = 6.2 Hz, 2 x CH_3), 21.5 (CH_3CO), 36.4 (d, J_{P-C} = 4.7 Hz, N-CH_2), 53.2 (d, J_{P-C} = 16.4 Hz, N-CH_2), 62.2 (d, J_{P-C} = 6.5 Hz, 2 x $POCH_2$), 68.3 (Ph-CH_2), 114.0 (C-17), 114.7 (C-19), 118.6 (C-15), 129.6 (C-16), 136.7 (C-14), 148.2 (C-18) and 166.6 (C=O).

Diethyl 2-(*N*-hydroxyacetamido)-*N*-(3-mercaptobenzyl)ethylphosphoramidate 33d

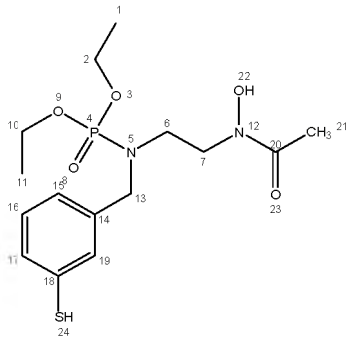

The procedure described for the synthesis of diethyl *N*-benzyl-2-(*N*-hydroxyacetamido)ethyl-phosphoramidate **33a** was employed, using diethyl 2-[(*N*-benzyloxy)acetamido]-*N*-(3-mercaptobenzyl)ethylphosphoramidate **32d** (0.20 g, 0.43 mmol) in MeOH (2 mL) and Pd/C (10 %, 0.33 g) in MeOH (10 mL). The solvent was evaporated *in vacuo* and the residue was purified by flash chromatography [on silica gel; elution with hexane-EtOAc (3:1)] to yield diethyl 2-(*N*-hydroxyacetamido)-*N*-(3-mercaptobenzyl)ethylphosphoramidate **33d** (71 mg, 71 %). δ_H/ppm (600 MHz; $CDCl_3$) 1.30 (6H, t, *J* = 6.8 Hz, 2 x CH_3), 1.87 (1H, s, OH), 2.12 (3H, s, CH_3CO), 2.71 (2H, m, N-CH_2), 3.08 (1H, s, SH), 3.29 (2H, t, *J* = 6.8 Hz, N-CH_2), 3.83 (2H, s, Ph-CH_2), 4.09 (4H, m, 2 x $POCH_2$) and 6.61 - 7.18 (4H, m, Ar-H); δ_C/ppm (600 MHz; $CDCl_3$) 16.4 (d, J_{P-C} = 6.0 Hz, 2 x CH_3), 22.4 (CH_3CO), 36.4 (d, J_{P-C} = 4.8 Hz, N-CH_2), 48.7 (d, J_{P-C} = 16.5 Hz, N-CH_2), 61.5 (d, J_{P-C} = 6.5 Hz, 2 x $POCH_2$), 66.6 (Ph-CH_2), 124.2 (C-15), 125.0 (C-19), 127.8 (C-17), 128.3 (C-16), 129.6 (C-18), 137.2 (C-14) and 163.0 (C=O).

***N*-Benzyl-2-(*N*-hydroxyacetamido)ethylphosphoramidic acid 34a**

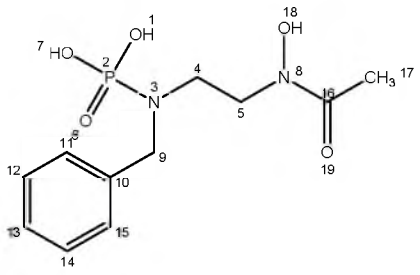

Trimethylsilyl bromide (0.15 mL, 1.0 mmol) was added drop-wise to diethyl *N*-benzyl-2-(*N*-hydroxyacetamido)ethylphosphoramidate **33a** (0.12 g, 0.34 mmol) in DCM (5 mL) under N_2 at 0 ^{0}C and the mixture was stirred for 1 hour. The mixture was allowed to warm to room temperature, water was added (1 mL) and the resulting mixture was stirred overnight. After completion, the solvent was removed *in vacuo* and the residue chromatographed [preparative layer chromatography on silca; elution with hexane-EtOAc-MeOH (1:1:1)] to yield *N*-benzyl-2-(*N*-hydroxyacetamido)ethylphosphoramidic acid **34a** (50 mg, 63 %). δ_H/ppm (600 MHz; D_2O) 2.09 (3H, s, CH_3CO), 2.79 (2H, m, N-CH_2), 3.34 (2H, t, *J* = 6.4 Hz, N-CH_2), 3.83 (2H, s, Ph-CH_2), 5.25 (1H, s, N-OH), 7.29 - 7.37 (5H, m, Ar-H) and 8.15 (2H, s, 2 x OH); δ_C/ppm (600 MHz; D_2O) 20.7 (CH_3), 42.6 (d, J_{P-C} = 4.7 Hz, N-CH_2), 52.3 (d, J_{P-C} = 16.9 Hz, N-CH_2), 67.2 (Ph-CH_2), 126.4 (C-14), 128.6 (C-11 and C-15), 129.4 (C-13 and C-15), 139.4 (C-10) and 171.5 (C=O).

2-(*N*-Hydroxyacetamido)-*N*-[4-(hydroxymethyl)benzyl]ethylphosphoramidic acid 34b

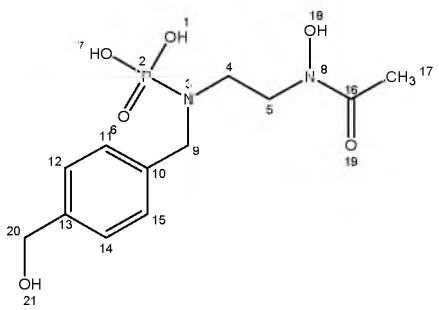

The procedure described for the synthesis of *N*-benzyl-2-(*N*-hydroxyacetamido)ethyl-phosphoramidic acid **34a** was employed, using diethyl 2-(*N*-hydroxyacetamido)-*N*-[4-(hydroxymethyl)benzyl]ethylphosphoramidate **33b** (0.12 g, 0.31 mmol) and TMSBr (0.12 mL, 0.93 mmol) in DCM (5 mL). The solvent was removed *in vacuo* and the residue chromatographed [preparative layer chromatography on silca; elution with hexane-EtOAc-MeOH (1:1:0.5)] to yield 2-(*N*-hydroxyacetamido)-*N*-[4-(hydroxymethyl)benzyl]ethyl-phosphoramidic acid **34b** (53 mg, 65 %). δ_H/ppm (600 MHz; D_2O) 1.76 (1H, s, CH_2OH), 2.07 (3H, s, CH_3CO), 2.75 (2H, m, N-CH_2), 3.27 (2H, t, *J* = 6.0 Hz, N-CH_2), 3.82 (2H, s, Ph-CH_2), 4.78

(2H, s, CH_2OH), 6.67 (1H, s, N-OH), 7.09 - 7.24 (4H, m, Ar-H) and 8.92 (2H, s, 2 x OH); δ_C/ppm (600 MHz; D_2O) 20.3 (CH_3), 37.5 (d, *J*P–C = 5.1 Hz, N-CH_2), 51.8 (d, *J*P–C = 16.6 Hz, N-CH_2), 65.7 (CH_2OH), 68.4 (Ph-CH_2), 126.2 (C-14 and C-12), 128.3 (C-15 and C-11), 136.5 (C-10), 139.2 (C-13) and 166.3 (C=O).

_N_-(3-Aminobenzyl)-2-(_N_-hydroxyacetamido)ethylphosphoramidic acid 34c

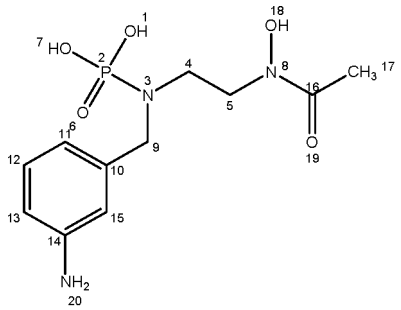

The procedure described for the synthesis of diethyl *N*-benzyl-2-(*N*-hydroxyacetamido)ethyl-phosphoramidic acid **34a** was employed, using diethyl *N*-(3-aminobenzyl)-2-(*N*-hydroxy-acetamido)ethylphosphoramidate **33c** (0.10 g, 0.27 mmol) and TMSBr (0.10 mL, 0.81 mmol) in DCM (5 mL). The solvent was removed *in vacuo* and the residue chromatographed [preparative layer chromatography on silca; elution with hexane-EtOAc-MeOH (1:1:0.5)] to yield *N*-(3-aminobenzyl)-2-(*N*-hydroxyacetamido)ethylphosphoramidic acid **34c** (40 mg, 57 %). δ_H/ppm (600 MHz; D_2O) 2.08 (3H, s, CH_3CO), 2.81 (2H, m, N-CH_2), 3.28 (2H, t, *J* = 6.0 Hz, N-CH_2), 3.60 (2H, s, Ph-CH_2), 4.66 (1H, s, N-OH), 5.48 (2H, s, NH_2), 7.00 (2H, s, 2 x OH) and 7.10 - 7.29 (4H, m, Ar-H); δ_C/ppm (600 MHz; D_2O) 19.8 (CH_3), 36.7 (d, $J_{P–C}$ = 4.9 Hz, N-CH_2), 53.0 (d, $J_{P–C}$ = 16.5 Hz, N-CH_2), 68.1 (Ph-CH_2), 113.9 (C-13), 114.7 (C-15), 117.8 (C-11), 128.4 (C-12), 138.3 (C-10), 146.5 (C-14) and 166.8 (C=0).

2-(*N*-Hydroxyacetamido)-*N*-(3-mercaptobenzyl)ethylphosphoramidic acid 34d

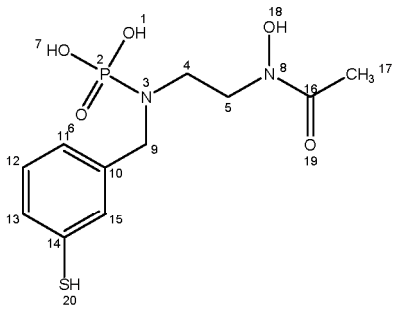

The procedure described for the synthesis of diethyl *N*-benzyl-2-(*N*-hydroxyacetamido)ethyl-phosphoramidic acid **34a** was employed, using diethyl 2-(*N*-hydroxyacetamido)-*N*-(3-mercaptobenzyl)ethylphosphoramidate **33d** (0.12 g, 0.31 mmol) and TMSBr (0.13 mL, 92 mmol) in DCM (5 mL). The solvent was removed *in vacuo* and the residue chromatographed [preparative layer chromatography; elution with hexane-EtOAc-MeOH (1:1:1)] to yield 2-(*N*-hydroxyacetamido)-*N*-(3-mercaptobenzyl)ethylphosphoramidic acid **34d** (48 mg, 68 %). δ_H/ppm (600 MHz; D_2O) 2.09 (3H, s, CH_3CO), 2.68 (2H, m, N-CH_2), 2.80 (1H, s, SH), 3.33 (2H, t, J = 6.0 Hz, N-CH_2), 3.84 (2H, s, Ph-CH_2) and 6.85 – 7.37 (4H, m, Ar-H); δ_C/ppm (600 MHz; D_2O) 22.4 (CH_3), 40.6 (d, J_{P-C} = 4.8 Hz, N-CH_2), 52.7 (d, J_{P-C} = 16.5 Hz, N-CH_2), 68.2 (Ph-CH_2), 119.2 (C-11), 123.1 (C-15), 126.6 (C-13), 129.4 (C-12), 130.2 (C-14), 138.5 (C-10) and 162.1 (C=0).

3.2. Docking Studies

The ligand structures (**2–4, a–c** and R-group) were constructed using Discovery Studio Visualiser,[178] each with two water molecules near the phosphonate group. An *in vacuo* global energy was located for each of the ligands using conformational lowest Energy_dlgfn in autodock tools.[179] The lowest energy conformers were then subjected to geometry optimisation in Gaussian. The crystal structure of the proteins (**1Q0L**, **1Q0Q**, **2EGH**, **3AU8**, **3AU9** and **3AUA**) were obtained from a Protein Data Bank.[163] The protein structures were dehydrated, while the divalent cation (Mg^{2+}) and co-factor NADPH were retained and the template ligand removed then re-docked along with the constructed ligands.

The geometry optimised and energy minimised ligands were imported into AutoDock 4.2 experiments using putty. All possible conformations of the ligands were allowed with flexible residues assigned to the protein active site (Ser270, Ser306, Asn311, Lys312 and Glu315) to allow uniform binding of ligands.

4. References

1. Cox F.E.G, History of human parasitology, *Clin. Microbiol. Rev.*, **2002**, 15, 606.

2. Brightman C, Malaria: a deadly vector-borne disease, *Trends in urology and men's health*, **2012**, March/April, 37.

3. Cater R and Mendis K.N, Evolutionary and historical aspects of the burden of malaria, *Clin. Microbiol. Rev.*, **2002**, 15, 564.

4. Ghosh A, Edwards M.J and Jacobs-Lorena M, The journey of the malaria parasite in the mosquito: Hopes for the new century, *Parasitol. Today*, **2000**, 16, 196.

5. Medaglini D and Hoeveler A, The European research effort for HIV/AIDS, malaria and tuberculosis, *Vaccine.*, **2003**, 21, 1.

6. Shahinas D, *Targeting Plasmodium falciparum heat shock protein 90 (PfHsp90): A strategy to reverse antimalarial resistance*, **2012**, PhD Thesis, University of Toronto.

7. Cook G.C and Webb A.J, Perception of malaria transmission before Ross' discovery in 1897, *Postgrad Med. J.*, **2000**, 76, 738.

8. Sterner C.S, *A brief history of miasmic theory*, **2007**, 1.

9. Cox F.E.G, History of the discovery of the malaria parasites and their vectors, *Parasit. Vectors.*, **2010**, 3, 5.

10. Theodorides J, A history of parasitology, *Medical History*, **1966**, 10, 306.

11. Garnham P.C.C, History of Discoveries of Malaria Parasites and their Life Cycles, *History and Philolosophy of the Life Sciences*, **1988**, 10, 93.

12. Cook G.C., Ross R. (1857-1932): 100 years since the demonstration of mosquito transmission of *Plasmodium* spp.-on 20 august 1897, *Trans R. Soc. Trop. Med. Hyg.*, **1997**, 91, 487.

13. Egerton F.N., History of ecological sciences, Part 46: From parasitology to germ theory, *Bulletin of the Ecological Society of America*, **2013**, 94, 136.

14. Foley M. and Tilley L., Quinoline anti-malarials: Mechanism of action and resistance, *Int. J. Parasitol.*, **1997**, 27, 231.

15. Breman J.G., The ears of the hippopotamus: manifestations, determinants and estimates of the malaria burden, *Am. J. Trop. Med. Hyg*, **2001**, 1-11.

16. Winstanley P.A, Chemotherapy for *Falciparum* malaria: The armoury, the problems and the prospects, *Parasitol. Today*, **2000**, 16, 146.

17. Winstanley P., Modern chemotherapeutic options for malaria, *Lancet Infect. Dis.*, **2001**, 1, 242.

18. Oddoux O., Debourgogne, Kantele A., Kocken C.H, Jokiranta T.S., Vedy S., Puyhardy J.M. and Machouart, Identification of the five human Plasmodium species including P. knowlesi by real-time polymerase chain reaction, *Eur. J Clin. Microbio Infec Dis*., **2011**, 30, 597-601.

19. Liu W, Li Y, Learn G. H, Rudicell R. S, Robertson J. D, Keele B. F, Ndjango J-B. N, Sanz C. M, Morgan D. B, Locatelli S, Gonder M. K, Kranzusch P. J, Walsh P. D, Delaporte E, Mpoudi-Ngole E, Georgiev A. V, Muller M. N, Shaw G. M, Peeters M, Sharp P.M, Rayner J. C and Hahn B. H, Origin of the human malaria parasite *Plasmodium falciparum* in gorillas, *Nature*, **2010**, 467, 420-425.

20. Noland G. S, Briones N and Sullivan Jr D. J, The shape and size of hemozoin crystals distinguishes diverse *Plasmodium* species, *Mol. Biochem. Parasitol.*, **2003**, 130, 91-99.

21. Liew K. J. L, Zbynek G. Hu and Peter P. R, Defining species specific genome differences in the malaria parasites, *BMC Genomics*, **2010**, 11, 128.

22. Westernberger S. J, McClean C. M, Chattopadhyay R, Dharia N. V, Carlton J. M, Barnwell J. W, Collins W. E, Hoffman S. L, Zhou Y, Vinetz J. M and Winzeler E. A, A system-based

analysis of Plasmodium vivax lifecycle transcription form human to mosquito, *PloS One*, **2010**, 4, 4.

23. Rayner, J.C, Tran T, Vladimir C, Huber, C S, Barnwell, J.W and Galinski M.R, Dramatic difference between *Plasmodium falciparum* and *Plasmodium vivax* reticulocyte binding-like genes, *Am. J. Trop. Med. Hyg* , **2005**, 76, 666-674.

24. Muller I, Galinski M. R, Baird J. K, Carlton J. M, Kochar D. K, Alonso P. L and Del-Portillo H. A, Key gaps in the knowledge of Plasmodium vivax, a neglected human parasite, *Lancet Infect Dis.*, **2009**, 9, 555-566.

25. Frech C and Chan N, Genome comparison of humans and non-human malaria parasites reveals species subset-specific genes potentially linked to human disease, *PloS One*, **2011**, 10, 1371.

26. Dinko B, Oguike M. C, Larbi J. A, Bousema T and Sutherland C. J, Persistent detaction of *Plasmodium falciparum, P. malariae, P. ovale curtisi and P. ovale wallikeri* after ACT treatment of asymptomatic Ghanaian school-children, *Int. J. Parasitiol. Drugs Drug Resist.*, **2012**, 3, 45-50.

27. Calderaro A, Piccolo G, Gorrini C, Rossi S, Montecchini S, Loretana M.A, Dell C, De Medici F, Chezzi M.C, Arcangeletti C, Cristina M, Accurate identification of the six human Plasmodium spp. causing imported malaria , including Plasmodium ovale wallikeri and Plasmodium knowlesi, *Malaria J.*, **2013**, 12, 321.

28. World Health Organisation, annual report, http://www.who.int/annrep/, **2012** and **2013**,

29. Ward and Boulton, a prioritized research agenda to expedite the discovery of new anti-malarial drugs, *Malaria J.*, **2013**, 12, 395.

30. Olliaro and Taylor, Antimalarial compounds: from bench to bedside, *J. Exp. Biol.*, **2003**, 21, 206.

31. Gardner, M.J, Hall N, Fung E, White O, Berriman M, Hyman R.W, Carlton J.M, Pain A, Nelson K.E, Bowman S, Paulsen I.T, James K, Eisen J, Rutherford A, Salzberg K, Craig SL, Kyes A, Chan S, Nene M, Shallom V, Suh S.J, Peterson B, Angiuoli J, Pertea S, Allen M, Selengut J, Haft J, Mather D, Vaidya M.W, Martin A.B, Fairlamb D.M, Fraunholz A.H, Roos M.J, Ralph D.S, McFadden S.A, Cummings G.I, Subramanian L.M, Mungall G.M,Venter C, Carucci J.C, Hoffman D.J, Newbold S.L, Davis C, Fraser R.W, Barrell C.M, Bart, Genome sequence of the human malaria parasite *Plasmodium falciparum*, nature, **2002**, 6906, 419.

32. Sachs and Malaney, The economic and social burden of malaria, *Nature*, 2002, 415, 680-685.

33. Slutsker L and Kachur S.P, Its time to rethink tactics in the fight against malaria, *Biomed. Central*, **2013**, 12, 140.

34. Whitty C.J.M, Rowland M, Sanderson F and Mutabingwa T.K, Malaria, *BMJ*, **2002**, 325, 1221–1224.

35. Hay S.I, Guerra C.A, Tatem A.J, Noor A.M and Snow R.W, The global distribution are risk of malaria: past, present and future, *Lancet Infect. Dis*., **2004**, 4, 327–336.

36. Eshar S, Dahan-Pasternak N, Weiner A, Dzikowski R, High resolution 3D perspective of Plasmodium biology: advancing into a new era, *Trends Parasitol.*, **2011**, 12, 27.

37. Kaiser K, Camargo N and Kappe H.I, Transformation of sporozoites into early exoerythrocytic malaria parasite does not require host cells, *J. Exp. Med.*, **2003**, 197, 1045.

38. Delves M, Plouffe D, Scheurer C, Meister S, Wittlin S, Winzeler E.A, Sinden R.E and Leroy D, The activities of current antimalarial drugs on the lifecycle stages of *Plasmodium:* A comparative study with humans and rodent parasites, *PloS Medicine*, **2012**, 9, 1-11.

39. Frevert U, Sneaking in through the back entrance: the biology of malaria liver stages, *Trends Parasitol.*, **2004**, 20, 1471-4922.

40. Moon S, Lee S, Kim H, Freitas-Junior L.H, Kang M, Ayong L and Hansen M.A.E, An image analysis algorithm for malaria parasite stage classification and viability quantification, *PloS One*, **2013**, 8, 1.

41. Farrow R.E, Green J, Katsimitsoulia Z, Taylor W.R, Holder A.A and Molloy J.E, The mechanism of erythrocyte invasion by malaria parasite, *Plasmodium falciparum*, *Semin. Cell Dev. Biol.*, **2011**, 22, 953-960.

42. Prudencio M, Mota M.M and Mendes A.M, A toolbox to study liver stage malaria, *Trends Parasitol.*, **2011**, 27, 565574.

43. Miller L.H, Baruch D.I and Doumbo O.K, The pathogenic basis of malaria, *Nature*, **2002**, 415, 673-679.

44. Derbyshire E.R, Mota M.M and Clardy J, The Next Opportunity in Anti-Malaria Drug Discovery: The Liver Stage, *PloS Pathogens*, **2011**, 9, 7.

45. Ziegler H.L, Franzyk H, Sairafianpour M, Tabatabai M, Tehrani M.D, Bagherzadeh K, Hagerstrand H, Staerk D and Jaroszewski J.W, Erythrocyte membrane modifying agents and the inhibition of *Plasmodium falciparum* growth: structure-activity relationships for betulinic acid anolgues, *Bioorg Med. Chem.*, **2004**, 12, 119–127.

46. Glenister F.K, Coppel R.L, Cowman A.F, Mohandas N and Cooke B.M, Contribution of parasite protein to altered mechanical properties of malaria-infected red blood cells, *Blood*, **2002**, 99, 1060-3.

47. Eshar S, Dahan-Pasternak N, Weiner A and Dzikowski R, High resolution 3D perspective of *Plasmodium* biology: advancing into a new era, *Trends Parasitol.*, **2011**, 27, 1471-4922.

48. Schlitzer M, Anti-malarial drugs–What is in use and what is in the pipeline, *Arch. Pharm. Chem. Life Sci.*, **2008**, 341, 149–163.

49. Gaur D and Chitnis C.E, Molecular interactions and signalling mechanisms during erythrocyte invasion by malaria parasites, *Curr. Opin. Microbiol.*, **2011**, 14, 422-428.

50. Baum J, Maier A.G, Good R.T, Simpson K.M and Cowman A.F, Invasion of *P. falciparum* merozoites suggests a hierarchy of molecular interactions, *PLos Pathol.*, **2005**, 1, 37.

51. Tilley L, Dixon M. W. and Kirk K, The *Plasmodium Falciparum* infected red-blood cells, *Int. J. Biochem. Cell Biol.*, **2011**, 43, 839-842.

52. Eksi S, Suri A and Williamson K.C, Sex and stage-specific reporter gene expression in *Plasmodium Falciparum, Mol. Biochem. Parasitol.*, **2008**, 160, 3–8.

53. Angrisano F, Riglar D. T, Sturm A, Volz J. C, Delves M. J, Zuccala E. S, Turnbull L, Dekiwadia C, Olshina M. A, Marapana D. S, Wong W, Mollard V, Bradin C. H, Tonkin C. J, Gunning P. W, Ralph S. A, Whitchurch C. B, Sinden R. E, Cowman A. F, McFadden G. I and Baum J, Spatial localisation of actin filaments across developmental stages of the malaria parasite, *PLoS One*, **2012**, 7, 2.

54. Baton and Ranford-Cartwright, Spreading the seeds of million-murdering death: metamorphosis of malaria in the mosquito, *Trends Parasitol.*, **2005**, 21, 573-80.

55. Kuehn A and Pradel G, The Coming-Out of Malaria Gametocytes, *Journal of Biomedicine and Biotechnology*, **2009**, 10.

56. Drakeley C, Sutherland C, Bousema T, Sauerwein R.W and Targett G.A.T, The epidemiology of *Plasmodium Falciparum* gametocytes: weapons of mass dispersion, *Trends Parasitol.*, **2006**, 22, 425–430.

57. Dinglasan R.R, Disruption of *Plasmodium falciparum* development by antibodies against a conserved mosquito gut antigen, *Proc. Nat. Acad. Sci. USA*, **2007**, 104, 13416-13466.

58. Winzeler E.A, Malaria research in the post-genomic era, *Nature*, **2008**, 455, 751-756.

59. Russell T.L, Beebe N.W, Cooper R.D, Lobo N.F and Burkot T.R, Successful malaria elimination strategies require interventions that target changing vector behaviours, *Malaria J.*, **2013**, 12, 56.

60. Wigglesworth V.B, *The principles of insect physiology*, Methuen & Co Ltd, **1976**, 25–53.

61. Russell T.L, Govella N.J, Azizi S, Drakeley C.J, Kachur S.P and Killeen G.F, Increased proportions of outdoor feeding among residual malaria vector populations following increased use of insecticide-treated nets in rural Tanzania, *Malaria J.*, **2011**, 10, 80.

62. Bruce-Chwatt L, Mosquitoes, malaria and war; then and now, *Journal of the Royal Army Medical Corps*, **1985**, 131, 85-99.

63. O`Shaughnessy P, Parachuting cats and crushed eggs. The controversy over the use of DDT to control malaria, *Journal of the Royal Army Medical Corps*, **2008**, 98, 1940-8.

64. Desowitz R.S and Miller L.H, A perspective on malaria vaccines, *Bull World Health Organ.*, **2002**, 58, 897–908.

65. Guerin P.J, Olliaro P, Nosten F, Druilhe P, Laxminarayan R, Binka F, Kilama W.L, Ford N and White N.J, Malaria : current status of control , diagnosis , treatment , and a proposed agenda for research and development, *Lancet Infect. Dis.*, **2002**, 2, 564-573.

66. Gregory and Mayfield, Applied Microbiology and Biotechnology, **2014.**

67. Turusov V, Rakitsky V and Tomatis L, Dichlorodiphenyltrichloroethane (DDT): Ubiquity, Persistence, and Risks, *Environ. Health Perspect.*, **2002**, 110, 125-128.

68. Zitko V, Chlorinated Pesticides: Aldrin, DDT, Endrin, Dieldrin, Mirex, *The Handbook of environmental chemistry*, **2003**, 3, 70-76.

69. Pedercini M, Movilla Blanco S and Kopainsky B, Application of the malaria management model to the analysis of costs and benefits of DDT versus non-DDT malaria control, *PloS One*, **2011**, 6, e27771.

70. Bouwman H, van den Berg H and Kylin, H, DDT and malaria prevention: addressing the paradox, *Environ Health Perspect.*, **2011**, 119, 744-7.

71. Zubrin R, The truth about DDT and *silent* springs, New atlantis, **2012**.

72. Fidock D.A, Rosenthal P.J, Croft S.L, Brun R, Nwaka S and Einstein A, Antimalarial drug discovery: efficiency models for compound screening, *Nature*, **2004**, 3, 509-518.

73. Ridley R.G, Medical need, scientific opportunity and the drive for antimalarial drugs, *Nature*, **2002**, 41, 5686-5693.

74. Cooper R.A, Fidock D.A, Nomura T, Talley A.K, Dzekunov S.M, Ferdig M.T, Ursos L.B.M, Sidhu A.B.S, Naude B, Deitsch K.W, Su X, Wooton J.C, Roepe P.D and Wellems T.E, Mutations in the Falciparum digestive vacuole transmembrane protein PfCRT and eveidence of their role in chloroquine resistance, *Mol. Cell.*, **2000**, 6, 861-871.

75. Ehlgen F, Pham J.S, Koning-ward T, De Cowman A.F and Ralph S.A, Investigation of the *Plasmodium falciparum* Food Vacuole through Inducible Expression of the Chloroquine Resistance Transporter (PfCRT), *PLoS One*, **2012**, 7, 38781.

76. Sullivan Jr D.J, Gluzman I.Y, Russell D.G and Goldberg D.E, On the molecular mechanism of chloroquin's antimalarial action, *Proc. Nat. Acad. Sci. USA*, **1996**, 93, 11865-70.

77. Rosenthal P, Cysteine proteases of malaria parasites, *Int. J. Parasitol.*, **2003**, 34, 1489-99.

78. Marella A, Tanwar O.P, Saha R, Ali M.R, Srivastava S, Akhter M, Shaquiquzzaman M and Alam M.M, Quinoline: A versatile heterocyclic, *Saudi Pharm. J.*, **2012**, 1319–0164.

79. Ridley R.G, Introduction: Antimalaria drug resistance: ramifications, explanations and challenges, *Microbes Infect.*, **2002**, 4, 155-156.

80. Achan J, Talisuna A.O, Erhart A, Yeka A, Tibenderana J.K, Baliraine F.N, Rosenthal P.J and Alessandro U.D, Quinine , an old anti-malarial drug in a modern world : role in the treatment

of malaria, *Malaria J.*, **2011**, 10, 144.

81. Beteck R.M, Smit F.J, Haynes R.K and N'Da D.D, Recent progress in the development of anti-malarial quinolones, *Malaria J.*, **2014**, 13, 339.

82. Foley M and Tilley L, Quinoline Antimalarials: Mechanisms of Action and Resistance, *Int J. Parasitol.*, **1997**, 27, 234-240.

83. Newton P and White N, MALARIA: New Developments in Treatment and Prevention, *Ann. Rev. Med.*, **1999**, 50, 179-92.

84. Wellems T.E, How chloroquine works, *Nature*, **1992**, 355, 108–109.

85. Egan T.J, Recent advances in understanding the mechanism of hemozoin (malaria pigment) formation, *J. Inorg. Biochem.*, **2008**, 102, 1288-1299.

86. MacIntosh M.T, Vaid A, Hosgood H.D, Vijay J, Bhattacharya A, Sahani M.H, Baevova P, Joiner K.A and Sharma P, Traffic to the malaria parasite food vacuole: A novel pathway involving a phosphatidylinositol 3-phosphate-binding protein, *J. Biol. Chem.*, **2007**, 282, 11499–11508.

87. Alam A, Serine Proteases of Malaria Parasite *Plasmodium falciparum*: Potential as Antimalarial Drug Targets, *Interdisciplinary Perspectives on Infectious Diseases*, **2014**, 7.

88. Singh A and Rosenthal P, Selection of cysteine protease inhibitor-resistant malaria parasites is accompanied by amplification of falcipain genes and alteration in inhibitor transport, *J. Biol. Chem.*, **2004**, 279, 35236-41.

89. Glushakova S, Mazar J, Hohmann-marriott M.F and Hama E, malaria parasites from infected erythrocytes, *Cell. Microbiol.*, **2009**, 11, 95-105.

90. Ades V, Safety, pharmacokinetics and efficacy of artemisinins in pregnancy, *Infect. Dis. Rep.*, **2011**, 3, e8.

91. Faurant C, From bark to weed: The history of artemisinin, *Parasite*, **2011**, 18, 215-218.

92. Haynes R and Krishna S, Artemisinins: activities and actions, *Microbes Infect.*, **2004**, 14, 1339-46.

93. Krishna S, Uhlemann A.C and Haynes R.K, Artemisinins: mechanisms of action and potential for resistance, *Drug. Resist. Updat.*, **2004**, 4-5, 233-44.

94. Bray P.G, Neill S.A and Ward P.M.O, Quinolines and Artemisinin: Chemistry, Biology and History, *Malaria: Drugs, Disease and Post-genomic Biology*. Springer-Verlag Berlin Heidelberg, **2005**, 1, 3-38.

95. Li J and Zhou B, Biological actions of artemisinin: insight from medical Chemistry studies, *Molecules*, **2010**, 15, 1378-97.

96. Woodrow C.J, Haynes,R K and Krishna S, Artemisinins, *Postgrad. Med. J.*, **2004**, 81, 71-8.

97. Bray P.G, Eckstein-Ludwig U, Webb R, Van Geothem I.D, East J.M, Lee A.G, Kimura M, O'Neill P.M, Ward S.A and Krishna S, Artemisinin target the SERCA of *Plasmodium falciparum*, *Nature*, **2003**, 424, 957-961.

98. O'Neill P.M and Posner G.H, A medical chemistry perspective on artemisinin and related endoperoxides, *J. Med. Chem.*, **2004**, 47, 2945-2964.

99. Kumar S, Kumari R and Pandey R, New insight-guided approaches to detect, cure, prevent and eliminate malaria, Springer-Verlag Berlin Heidelberg, **2014.**

100. Starzengruber P, Swoboda P, Fuehrer H-P, Khan W, Hofecker V, Siedl A, Fally M, Graf O, Teja-Isavadharm P, Haque R, Ringwald P and Noedl H, Current status of artemisinin-resistant falciparum malaria in South Asia: a randomized controlled artesunate monotherapy trial in Bangladesh, *PloS One*, **2012**, 7, e52236.

101. Dellicour S, Hall S, Chandramohan D and Greenwood B, The safety of artemisinins during pregnancy: a pressing question, *Malaria J.*, **2007**, 6, 15.

102. Salcedo-Sora J.E, Ochong E, Beveridge S, Johnson D, Nzila A, Biagini G, Stocks P, O'Neill P.M, Krishna S, Bray P.G and Ward S, *J. Biol. Chem.*, **2011**, 286, 44659-68.

103. Rathod P.K, Khatri A, Hubbert T and Milhous W.K, Selective activity of 5-fluororotic acid against *Plasmodium falciparum in vitro*, *Antimicrob. Agents. Chemother.*, **1989**, 33, 1090-1094.

104. Zhang Y and Meshnick S, Inhibition of *Plasmodium falciparum* Dihydropteroate Synthetase and Growth In Vitro by Sulfa Drugs, *Antimicrob. Agents. Chemother.*, **1991**, 35, 267-271.

105. Nzila A, Ward S.A, Marsh K, Sims P.F and Hyde J.E, Comparative folate metabolism in human and malaria parasites (part II): activities as yet untargeted or specific to Plasmodium, *Trends parasitol.*, **2005**, 21, 292-298.

106. Rawat P, Goyal S, Dhaliwal N and Kumar S, Therapeutic Drug Targets for Antimalarial Drug Discovery Table I: Targets for antimalarial chemotherapy, *International Journal of Research in Pharmaceutical and Biomedical Sciences*, **2013**, 4, 1055-1059.

107. Royer R, Deck L.M, Campos N.M, Hunsaker L.A and Vander D.L, Biologically Active Derivatives of Gossypol: Synthesis and Antimalarial Activities of Peri-Acylated Gossylic Nitriles, *J. Med. Chem.*, **1986**, 29, 1799-1801.

108. Cassera M.B, Zhang Y, Hazleton K.Z and Vern L.S, Purine and Pyrimidine Pathways as Targets in *Plasmodium falciparum*, *Curr. Top. Med. Chem.*, **2011**, 11, 2130-2115.

109. Hatherley R, Blatch G.L and Bishop O.T, *Plasmodium falciparum* Hsp70-x: a heat shock protein at the host-parasite interface, *Journal of Biomolecular Structure and Dynamics*,

2013, 37-41.

110. Shahinas D, Targeting *Plasmodium falciparum* heat shock protein 90 (pfhsp90): a strategy to reverse antimalarial resistance, PhD Thesis, Department of Laboratory Medicine and Pathobiology University of Toronto **2012.**

111. Painter H.J, Morrisey J.M, Mather M.W and Vaidya A.B, Specific role of mitochondrial electron transport in blood-stage *Plasmodium falciparum*, *Nature*, **2007**, 446, 88-91.

112. Van Dooren G.G, Stimmler L.M and McFadden Geoffrey I, Metabolic maps and functions of the Plasmodium mitochondrion, *FEMS Microbiol. Rev.*, **2005**, 30, 596-630.

113. Nixon G, Moss D.M, Shone A.E, Lalloo D.G, Fisher N, O'Neill P.M, Ward S and Biagini G, Antimalarial pharmacology and therapeutics of atovaquone *J. Antimicrob. Chemother.*, **2013**, 68, 977-85.

114. Mather M.W, Darrouzet E, Valkova-Valchanova M, Cooley J.W, McIntosh M.T, Daldal F and Vaidya A.B, Uncovering the molecular mode of action of the antimalarial drug atovaquone using a bacterial system, *J. Biol. Chem.*, **2005**, 280, 27458-65.

115. Baggish A and Hill D, MINIREVIEW Antiparasitic Agent Atovaquone, *Antimicrob. Agents. Chemother.*, **2002**, 46, 1163-1173.

116. Nayak S.K, Mallik S.B, Kanaujia S.P, Sekar K, Ranganathan K. R, Ananthalakshmi V, Jeyaraman G, Saralaya S. S, Rao K.S, Shridhara K, Nagarajan K and Row T.N.G, Crystal structures and binding studies of atovaquone and its derivatives with cytochrome bc1: a molecular basis for drug design, *Cryst. Eng. Comm.*, **2013**, 15, 4871.

117. Cordel H, Cailhol J, Matheron S, Bloch M, Godineau N, Consigny P-H, Gros H, Campa, P, Bourée P, Fain O, Ralaimazava Pascal and Bouchaud Olivier, Atovaquone-proguanil in the

treatment of imported uncomplicated *Plasmodium falciparum* malaria: a prospective observational study of 553 cases, *Malaria J.*, **2013**, 12, 399.

118. Harvey L, Arnold B, Zipursky S.L, Matsudaira P, Baltimore D, and Darnell J, Molecular biology, W.H Freeman and company, **2000.**

119. Krugliak M, Feder R, Zolotarev V.Y, Gaidukov L and Dagan A, Antimalarial Activities of Dermaseptin S4 Derivatives, *Antimicrob. Agents. Chemother*., **2000**, 44, 2442-2451.

120. Narla Mohandas and Xiuli An, Malaria and humanred blood cells, *Med. Microbiol. Immunol*, **2012**, 593–598.

121. Roggero R, Zufferey R, Minca M, Richier E, Calas M, Vial H and Mamoun C.B, Unraveling the Mode of Action of the Antimalarial Choline Analog G25 in *Plasmodium falciparum* and Saccharomyces cerevisiae, *Antimicrob. Agents. Chemother.*, **2004**, 48, 2816-2824.

122. Calas M, Ancelin M.L, Portefaix P, Piquet G, Cordina G, Vidal-Sailhan V and Vial H, Antimalarial Activity of Compounds Interfering with *Plasmodium falciparum* Phospholipid Metabolism : Comparison between Mono- and Bisquaternary, *J. Med. Chem*., **2000**, 43, 505-516.

123. Vera M, Yaun Z, Ramsubir S and Bokavic M, Choline transport for phospholipid synthesis, *Exp. Biol. Med.*, **2006**, 231, 490–504.

124. Padmanaban G, Nagaraj V.A and Rangarajan P.N, Drugs and drug targets against malaria, *Current Science Bangalore*, **2007**, 92, 1545-1555.

125. Kalanon M and McFadden GI, Malaria, *Plasmodium Falciparum* and its apicoplast, Biochem Soc Trans, **2010**, 3, 775–82.

126. Botte C, Dubar F, McFadden G.I and Marechal E.B.C, *Plasmodium falciparum* apicoplast drugs: targets or off-targets, *Chem. Rev.*, **2012**, 112, 1269–1283.

127. Waller R.F, Keeling P.J, Donald R.G, Striepen B, Handman E, Lang-Unnasch N, Cowman A.F, Besra G.S, Roos D.S, and McFadden G.I, Nuclear-encoded proteins target to the plastid in Toxoplasma gondii and *Plasmodium falciparum*, *Proc. Natl. Acad. Sci. U. S. A*, **1998**, 95, 12352–12357.

128. Lim L and McFardden G, The evolution, metabolism and functions of the apicoplast, *Philos. Trans. R. Soc. Lond. B. Biol. Sci.*, **2010**, 365, 749-63.

129. van Dooren G and Striepen B, The algal past and parasite present of the apicoplast, *Ann. Rev. Microbiol.*, **2013**, 67, 271-89.

130. Carlton J.M, Adams J.H, Silva J.C, Bidwell S.L, Lorenzi H, Caler E, Crabtree J, Angiuoli S.V, Merino E.F, Amedeo P, Cheng Q, Coulson R.M.R, Crabb B.S, del Portillo H.A, Essien K, Feldblyum T.V, Fernandez-Becerra C, Gilson P.R, Gueye A.H, Guo X, Kang'a S, Kooij T.W.A, Korsinczky M, Meyer E.V.S, Nene V, Paulsen I, White O, Ralph S.A, Ren Q, Sargeant T.J, Salzberg S.L, Stoeckert C.J, Sullivan S.A, Yamamoto M.M, Hoffman S.L, Wortman J.R, Gardner M.J, Galinski M.R, Barnwell J.W and Fraser-Liggett C.M, Comparative genomics of the neglected human malaria parasite *Plasmodium vivax*, *Nature*, **2008**, 455, 757–763.

131. Ekland E.H, Schneider J and Fidock D, Identifying apicoplast-targeting antimalarials using high-throughput compatible approaches, *FASEB J.*, **2011**, 25, 3583-93.

132. Hyde J.E, Drug-resistant malaria, *Trends Parasitol.*, **2005**, 21, 494–498.

133. Craft J.C., Challenges facing drug development for malaria, *Curr. Opin. Microbiol.*, **2008**, 11, 428–433.

134. Wongsrichanalai C, Pickard A.L, Wernsdorfer W.H and Meshnick S.R, Epidemiology of drug-resistant malaria, *Lancet Infect. Dis*., **2002**, 2, 209-218.

135. Cowman A.F, and Foote S.J, Chemotherapy and drug resistance in malaria. *Int. J. Parasitol.*, **1990**, 20, 503–513.

136. Cowman A.F, and Foote S.J, The mode of action and mechanism of resistance to antimalarial drugs, *Acta Tropica*, **1994**, 56, 157–171.

137. Olliaro P.L, Mode of action and mechanisms of resistance for antimalarial drugs, *Pharmacol Ther.*, **2001**, 89, 207-219.

138. Payne D, Spread of chloroquine resistance in *Plasmodium falciparum*, *Parasitol. Today*, **1987**, 3, 241-245.

139. Wellems T.E and Plowe C.V, Chloroquine-resistant malaria, *J. Infect. Dis.*, **2001**, 184, 770–776.

140. Hastings I.M, The origins of antimalarial drug resistance, *Trends parasitol.*, **2004**, 20, 512-8.

141. Ward S.A, Mechanisms of chloroquine in malarial chemotheraphy, *Trends Pharmacol Sci.*, **1988**, 9, 241–246.

142. Dondrop A.M, Fanello C.I, Hendriksen I.C.E, Gomes E and Seni A, Artesunate versus quinine in the treatment of severe falciparum malaria in African children (AQUAMAT): an open-label, randomised trial, *Lancet*, **2010**, 376, 1647–1657.

143. Lin L, Linka M, Mullin K.A, Weber A.P and McFadden G.I, The carbon and energy sources of the non-photosynthetic plastid in the malaria parasite, *FEBS Lett.*, **2010**, 584, 549–54.

144. Martin V.J.J, Pitera D.J, Withers S.T, Newman J.D and Keasling J.D, Engineering a mevalonate pathway in *Escherichia coli* for production of terpenoids, *Nat. biotechnol.*, **2003**, 21, 796-802.

145. Kuzuyama T, Mevalonate and Non-mevalonate Pathways for the Biosynthesis of Isoprene Units, *Biosci. Biotechnol. Biochem.*, **2002**, 66, 1619-1627.

146. Rauthan M and Pilon M, The mevalonate pathway in *C. elegans*, *Lipids Health Dis.*, **2011**, 10, 243.

147. van der Meer J-Y and Hirsch A.K.H, The isoprenoid-precursor dependence of Plasmodium spp., *Nat. Prod. Rep.*, **2012**, 29, 721-8.

148. Hunter W.N, Bond C.S, Gabrielsen M and Kemp L.E, Structure and reactivity in the non-mevalonate pathway of isoprenoid biosynthesis, *Biochem. Soc. Trans.*, **2003**, 31, 537-542.

149. Lombard J and Moreira D, Origins and early evolution of the mevalonate pathway of isoprenoid biosynthesis in the three domains of life, *Mol. Biol. Evol.*, **2011**, 28, 87-99.

150. Lichtenthaler H.K, Schwender J, Disch A, Rohmer M, Ii I and Karlsruhe D, Biosynthesis of isoprenoids in higher plant chloroplasts proceeds via a mevalonate-independent pathway, *FEBS Lett.*, **1997**, 400, 271-274.

151. Eisenreich W, Schwarz M, Zenk M.H, Bacherl A, Cartayrade A and Arigoni D, The deoxyxylulose phosphate pathway of terpenoid biosynthesis in plants and microorganisms, *Chem. Biol.*, **1998**, 5,.R221-R233.

152. Wanke M, Mep D, Skorupinska-tudek K and Swiezewska E, Isoprenoid biosynthesis via 1-deoxy-D-xylulose 5-phosphate/2-C- methyl-D-erythritol 4-phosphate (DOXP/MEP) pathway, *Acta. Biochemica. Polonica*, **2001**, 48, 663-671.

153. Rohdich F, Kis K, Bacher and Eisenreich W, The non-mevalonate pathway of isoprenoids: genes, enzymes and intermediates, *Curr. Opin. Chem. Biol.*, **2001**, 5, 535–540.

154. Dubey V.H, Bhalla R and Luthra R, An overview of the non-mevalonate pathway for terpenoid biosynthesis in plants, *J.Biosci.*, **2003**, 28, 637-646.

155. Fowler D.J, B.Sc. (Hons) Thesis, Dunelm, GRSC, **2001.**

156. Masini T, Kroezen B.S and Hirsch A.K.H, Druggability of the enzymes of the non-mevalonate-pathway, *Drug Discov. Today*, **2013**, 18, 1256-62.

157. Hsieh M-H and Goodman H.M, The Arabidopsis IspH Homolog Is Involved in the Plastid Non-mevalonate Pathway of Isoprenoid Biosynthesis, *Am. Soc. Plant Biol.*, **2005**, 138, 641-653.

158. Hojo M, Tasaka M and Shikanai T, Physiological requirements of the non-mevalonate pathway for photo-acclimation in Arabidopsis, Plant Biotechnology, 2005, 22(1), 39–45

159. Proteau P.J, 1-Deoxy-D-xylulose 5-phosphate reductoisomerase: an overview, *Bioorg. Chem.*, **2004**, 32, 483-93.

160. Mac Sweeney A, Lange R, Fernandes R.P.M, Schulz H, Dale G.E, Douangamath A, Proteau P.J and Oefner C, The crystal structure of E.coli 1-deoxy-D-xylulose-5-phosphate reductoisomerase in a ternary complex with the antimalarial compound fosmidomycin and NADPH reveals a tight-binding closed enzyme conformation, *J. Mol. Biol.*, **2004**, 345, 115-27.

161. Reuter K, Sanderbrand S, Jomaa H, Wiesner J, Steinbrecher I, Beck E, Hintz M, Klebe G and Stubbs M.T, Crystal structure of 1-deoxy-D-xylulose-5-phosphate reductoisomerase, a crucial enzyme in the non-mevalonate pathway of isoprenoid biosynthesis, *J. Biol. Chem.*, **2002**, 277, 5378-84.

162. Singh N, Cheve G, Avery M.A and McCurdy C.R, Comparative Protein Modeling of 1-Deoxy- D -xylulose-5-phosphate Reductoisomerase Enzyme from *Plasmodium falciparum* : A Potential Target for Antimalarial Drug Discovery, *J. Chem. Inf. Model*, **2006**, 46, 1360-1370.

163. Protein data bank, http://www.pdb.com, accessed **2014.**

164. Kuntz L, Tritsch D, Grosdemange-billiard C, Willem A, Bach, T.J and Rohmer M, Isoprenoid biosynthesis as a target for antibacterial and antiparasitic drugs : phosphonohydroxamic acids as inhibitors of deoxyxylulose phosphate reducto-isomerase, *Biochem. J.*, **2005**, 135, 127-135.

165. Li H, Tian J, Sun W, Qin W and Gao W-Y, Mechanistic insights into 1-deoxy-D-xylulose 5-phosphate reductoisomerase, a key enzyme of the MEP terpenoid biosynthetic pathway, *FEBS J.*, **2013**, 280, 5896-905.

166. Goble J.L, Adendorff M.R, de Beer T.P, Stephens L.L and Blatch G.L, The malarial drug target *Plasmodium falciparum* 1-deoxy-D-xylulose-5-phosphate reductoisomerase (*PfDXR*): development of a 3-D model for identification of novel, structural and functional features and for inhibitor screening, *Protein Pept. Lett.*, **2010**, 17, 109-20.

167. Hale I, O'Neill P.M, Berry N.G, Odom A and Sharma R, The MEP pathway and the development of inhibitors as potential anti-infective agents, *Med. Chem. Comm.*, **2012**, 3, 418.

168. San Jose G, Haymond A, Lundberg L, Pinkham C, Kehn-hall K, Boshoff H.I, Couch D and Dowd C.S, Design of potential bisubstrate inhibitors against Mycobacterium tuberculosis (Mtb) 1-deoxy-D-xylulose 5-phosphate reductoisomerase (Dxr)—evidence of a novel binding mode, *Med. Chem. Comm.*, **2013**, 4, 1099-1104.

169. Reuter K, Sanderbrand S, Jomaa H, Weisner J, Steinbrecher I, Beck E, Hintz M, Klebe G and Stubbs M, Crystal structure of 1-deoxy-D-xylulose 5-phosphate reductoisomerase, a crucial enzyme in the non-mevalonate pathway of isoprenoid biosynthesis. *J. Biol. Chem.*, **2002**, 277, 5378-5384.

170. Lell B, Ruangweerayut R, Wiesner J, Missinou M.A, Schindler A, Hintz M.T.B, Hutchinson D, Jomaa H and Kremsner P.G, Fosmidomycin, a Novel Chemotherapeutic Agent for Malaria, *Antimicrob. Agents Chemother.*, **2014**, 47, 735–738.

171. Zhang B, Watts K.M, Hodge D, Kemp L.M, Hunstad D.A, Hicks L.M and Odom A.R, A Second Target of the Antimalarial and Antibacterial Agent Fosmidomycin Revealed by Cellular Metabolic Profiling, *Biochem.*, **2011**, 50, 3570-3577.

172. Bodill T, Conibear A.C, Mutorwa M.K.M, Goble J.L, Blatch G.L, Lobb K.A, Klein R and Kaye P.T, Exploring DOXP-reductoisomerase binding limits using phosphonated N-aryl and N-heteroarylcarboxamides as DXR inhibitors, *Bioorg. Med. Chem.*, **2013**, 21, 4332-41.

173. Haemers T, Wiesner J, Giebmann D, Hillaer U, Ortmann R, Jomaa H, Link A, Schiltzer M and van Calenbergh S, Synthesis of β- and γ-oxa isosteres of fosmidomycin and FR900098 as antimalarial candidates, bioorganic &medical chemistry, **2007**, 16, 3361–3371.

174. Konzuch S, Umeda T, Held J, Ha S, Bru K, Lienau C, Behrendt C.T, Gra T, Bacher A, Illarionov B, Fischer M, Mordmu B, Tanaka N and Kurz T, Binding Modes of Reverse Fosmidomycin Analogs toward the Antimalarial Target IspC, *Med.Chem.*, **2014**, 57, 8827-8838.

175. Symyx draw 3.2, http://www.symaxdraw.com, accessed **2014.**

176 Conibear A.C, MSc Thesis, Rhodes University, **2010.**

177. Mutorwa M.K.M, PhD Thesis, Rhodes University, **2011.**

178. Accelrys Software Inc, Discovery Studio Modeling Environment, Release 4.0, San Diego: Accelrys Software Inc, **2013**.

179. WinSCP, http://winscp.net, accessed **2014.**

180. Autodock Vina, http://vina.scripps.edu, accessed **2014.**

181. Pechkin A.A., Elchaninov M.M., Lukyanov B.S and Alekseenko Y.S, *Chem. Heterocycl. Compd.*, **2004**, 40, 599-602.

182. Thomas A.D, Asokan J and Asokan C.V, *Tetrahedron*, **2004**, 60, 5069-5076.

183. Rai L.M.K, Musad E.A, Jagadish R.L and Shivakumar K.N, *Synth. Commun.*, **2011**, 41, 953-955.

184. Sarvari H.M and Sharghi H, *Helv. Chim. Acta.*, **2005**, 88, 2282-2287.

185. Bachmann K.A and Lewis J.D, Predicting inhibitory drug-drug interactions and evaluating drug interaction reports using inhibition constants, *Ann. Pharmacother.*, **2005**, 39, 1064-72.

186. Robert A, Copeland D, Lombardo J.G, and Decicco C.P, estimating Ki values for tight binding inhibitors from dose-response plots, *Bioorg. Med. Chem. Lett.*, **2005**, 37, 1947-1952.

187. Haymond A, Johny C, Dowdy T, Schweibenz B, Villarroel K, Young R, Mantooth CJ, Patel T, Bases J, San Jose G, Jackson ER, Dowd CS, Couch RD, Kinetic characterization and allosteric inhibition of the Yersinia pestis 1-deoxy-D-xylulose 5-phosphate reductoisomerase (MEP synthase), *PLoS One*, **2014**, 9, e106242.

188. Buckberry L.D, Cytotoxicity testing using cell lines, *Methods in Biotechnology*, **1999**, 8, 239-252.

189. Burlingham B.T and Widlanski T.S, An Intuitive Look at the Relationship of Ki and IC50: W A More General Use for the Dixon Plot, *J. Chem. Ed.*, **2003**, 80, 214-218.

190. Michelle Isaacs, Bioassay Technician, Chemistry Department, Rhodes University, Grahamstown, **2015.**

191. http://www.sigma-aldrich.com. In vitro toxicology assay kit.

192. Akinboye E.S and Bakare O, Biological Activities of Emetine, *The Open Natural Products Journal*, **2011**, 4, 8-15.

193. Verbrugghen T, Vandurm P, Pouyez J, Maes L, Waiters J and Colenbergh S.V, Alpha-Heteroatom Derivatized Analogues of 3-(Acetylhydroxyamino)propyl Phosphonic Acid (FR900098) as Antimalarials, *Med. Chem.*, **2013**, 15, 376-380.

194. Haemers T, Wiesner J, Van Poecke S, Goeman J, Henschker D, Beck E, Jomaab H and Van Calenbergh S, Synthesis of a-substituted fosmidomycin analogues as highly potent Plasmodium falciparum growth inhibitors, *Bioorg. Med. Chem. Lett.*, **2006**, 16, 1888-1891.

193. Zwierzak A., *Synthesis,* **1982**, 11, 920-922.